Distribution Agreement

In presenting this thesis or dissertation as a partial fulfillment of the requirements for an advanced degree from Emory University, I hereby grant to Emory University and its agents the non-exclusive license to archive, make accessible, and display my thesis or dissertation in whole or in part in all form of media, now or hereafter known, including display on the world wide web. I understand that I may select some access restrictions as part of the online submission of this thesis or dissertation. I retain all ownership rights to the copyright of the thesis or dissertation. I also retain the right to use in future works (such as article or books) all or part of this thesis or dissertation.

Signature:

_____ _____

Alana L. Reed Date

The Senescence-Accelerated Mouse (SAM): A Murine Model of Age-Associated Diastolic Dysfunction

By

Alana L. Reed
B.S., Georgia Institute of Technology, 2003

Advisors:
Samuel C. Dudley, Jr., MD, PhD
Roy L. Sutliff, PhD

An abstract of
A dissertation submitted to the Faculty of the
James T. Laney Graduate School of Graduate Studies of Emory University
in partial fulfillment of the requirements for the degree of
Doctor of Philosophy
in Molecular and Systems Pharmacology
Graduate Division of the Biological and Biomedical Sciences
2011

Abstract

The Senescence-Accelerated Mouse (SAM):
A Murine Model of Age-Associated Diastolic Dysfunction
By
Alana L. Reed

Diastolic heart failure, a form of heart failure in which patients exhibit signs and symptoms of heart failure despite the maintenance of a normal ejection fraction, is a major cause of mortality in the elderly population. It is often preceded by diastolic dysfunction, which is characterized by impaired active relaxation and increased stiffness of the left ventricle. The goal of this dissertation project has been to use a murine model of spontaneous aging, the senescence-accelerated mouse (SAM) model as a model for the investigation of the mechanisms contributing to age-associated diastolic dysfunction. This model is comprised of senescence-prone (SAMP8) mice and senescence-resistant (SAMR1) controls. Using echocardiography and invasive hemodynamics, it was found that by 6 months of age, SAMP8 mice exhibit diastolic dysfunction. Since diastolic dysfunction is characterized by impaired relaxation and left ventricular stiffening, fibrosis was measured. SAMP8 mice showed increased deposition of fibrotic tissue in the interstitial and perivascular areas of the myocardium compared to SAMR1 controls at 6 months of age. Furthermore, gene expression of collagen 1A1, collagen 3A, and fibronectin was increased. Expression of the pro-fibrotic cytokines transforming growth factor-beta (TGF-β) and connective tissue growth factor was increased in the hearts of 6-month-old SAMP8 mice. Cardiac fibroblasts isolated from SAMP8 mice exhibited a decrease in collagen 3A, which is a more elastic form of collagen, in response to TGF-β, suggesting that perhaps the loss of the more elastic isoform of collagen could promote stiffening of the left ventricle. Next, the role of oxidative stress was examined. Increased oxidative stress was found in the blood and vasculature of SAMP8 mice; however, no increase in myocardial superoxide was observed. Increased gene expression of the NADPH oxidases Nox2 and Nox4 as well as antioxidants was observed in the hearts of 6-month-old SAMP8 mice. It is possible that in the heart, antioxidant upregulation at least partially compensates for increased ROS resulting from increased expression of NADPH oxidases. In this dissertation, the SAM model has been established as a model of age-associated diastolic dysfunction, and cardiac fibrosis has been demonstrated as a mechanism of diastolic dysfunction in this complicated pathology.

The Senescence-Accelerated Mouse (SAM): A Murine Model of Age-Associated Diastolic Dysfunction

By

Alana L. Reed
B.S., Georgia Institute of Technology, 2003

Advisors:
Samuel C. Dudley, Jr., MD, PhD
Roy L. Sutliff, PhD

A dissertation submitted to the Faculty of the
James T. Laney Graduate School of Graduate Studies of Emory University
in partial fulfillment of the requirements for the degree of
Doctor of Philosophy
in Molecular and Systems Pharmacology
Graduate Division of the Biological and Biomedical Sciences
2011

TABLE OF CONTENTS

INDEX OF FIGURES

INDEX OF TABLES

LIST OF SYMBOLS AND ABBREVIATIONS

A	Late (atrial) diastolic filling velocity
A'	Mitral annulus velocity during late diastole
ACE	Angiotensin-Converting Enzyme
α-SMA	Alpha Smooth-Muscle Actin
β-MHC	Beta Myosin Heavy Chain
BH_4	Tetrahydrobiopterin
CTGF	Connective Tissue Growth Factor
DHE	Dihydroethidium
DMEM	Dulbecco's Modified Eagle's Medium
DOCA	Deoxycorticosterone Acetate
dP/dt_{max}	Maximal slope of LV pressure rise during systole
dP/dt_{min}	Maximal slope of LV pressure decline during diastole
dP/dt_{EDV}	dP/dt divided by LVEDV
Ea	Arterial Elastance
Ea/Es	Ventricular-vascular coupling ratio
E	Early diastolic filling velocity
E/A	Ratio of early to late diastolic filling velocity
E'	Mitral annulus velocity during early diastole
E'/A'	Ratio of early to late mitral annulus velocity
ECM	Extracellular Matrix
EF	Percent Ejection Fraction
ELISA	Enzyme-linked Immunosorbent Assay
ESR	Electron Spin Resonance
FHC	Familial Hypertrophic Cardiomyopathy

FS	Percent Fractional Shortening
GSH	Glutathione
GSSG	Glutathione Disulfide
GPX	Glutathione Peroxidase
H_2O_2	Hydrogen Peroxide
HPLC	High-Performance Liquid Chromatography
IM	Intimal Medial
IVRT	Isovolumic Relaxation Time
LV	Left Ventricle
LVEDP	LV End-Diastolic Pressure
LVEDV	LV End-Diastolic Volume
LVEDPVR	LV End-Diastolic Pressure-Volume Relationship
LVESP	LV End-Systolic Pressure
LVESV	LV End-Systolic Volume
LVESPVR	LV End-Systolic Pressure-Volume Relationship
MMP	Matrix metalloproteinase
$NO^{\bullet}$	Nitric Oxide
NOS	Nitric Oxide Synthase
Nox	NADPH Oxidase
$O_2^{\bullet -}$	Superoxide
8-oxo-dG	8-oxo-2'-deoxyguanosine
PLB	Phospholamban
PRSW	Preload Recruitable Stoke Work
P/S/A	Penicillin/Streptomycin/Amphotericin B
qRT-PCR	Quantitative Real-Time PCR
RAAS	Renin-Angiotensin-Aldosterone System

ROS	Reactive Oxygen Species
RV	Right Ventricle
RVSP	Right Ventricular Systolic Pressure
SAM	Senescence-Accelerated Mouse
SAMR1	Senescence-Accelerated Resistant Mouse
SAMP8	Senescence-Accelerated Prone Mouse
SERCA2a	Sarcoplasmic Reticulum Calcium ATPase
SOD	Superoxide Dismutase
SR	Sarcoplasmic Reticulum
SV	Stroke Volume
τ	Time constant of pressure decay
TGF-β	Transforming Growth Factor-beta

Chapter 1:

General Introduction

Aging and cardiovascular disease

1.1 Aging: demographics and lifespan

The United States is currently experiencing an unprecedented rise in the population of older adults because of advances in medicine, health promotion and preventive medicine, and an aging baby boomer cohort. While the life expectancy of the average American was just 47 years for someone born in 1900, it has risen to 77 years for those born in 2001. Over the next 25 years, it is expected that the number of Americans over the age of 65 will double, and by 2030 it is projected that there will be 71 million older adults, comprising 20% of the US population (CDC, 2007).

While the increase in lifespan represents a major achievement in medicine and public heath, older age also presents a new set of challenges. There has been a historic shift in the cause of death from infectious diseases to chronic and degenerative illnesses, and this is particularly so for the elderly population. It is estimated that 80% of older adults live with one or more chronic medical conditions such as cardiovascular disease, cancer, stroke, and diabetes. Unfortunately, these conditions are costly: health care for patients over the age of 65 costs approximately five times more than for a person under the age of 65, and nationally, healthcare expenditures are projected to increase by 25% by the year 2030 as a result of the growing demographic of older Americans (CDC, 2007). Not only do chronic diseases increase healthcare costs, they cause pain, and disability, and decreased quality of life. While the public health arena has expended a great deal of effort in educating Americans about the relationship between these chronic diseases and lifestyle factors such as smoking, poor diet, and physical inactivity, there are still many people suffering from these conditions, particularly in the elderly population. A greater understanding of the mechanisms of

aging and how aging impacts cardiovascular health is needed to address the health concerns of this growing demographic segment of our population.

1.2 Mechanisms of aging in mammalian cells

Humans, and, for that matter, all living organisms, age. This is a readily observable and obvious fact, but exactly how and why is a compelling question and one that has been pondered by mankind for centuries. As early as the 1920's, Raymond Pearl, one of the founders of the field of biogerontology, set forth the "rate of living" hypothesis in which he posited that metabolic rate was related to longevity (Pearl, 1928). In 1956, Denham Harman proposed a "free-radical theory" of aging, suggesting that aging is a result of a lifetime of cumulative exposure to reactive oxygen species (ROS) generated as a by-product of normal aerobic metabolism (Harman, 1956). It is widely accepted that aerobic metabolism, and its subsequent production of ROS, contribute to the aging process, but exactly how this occurs is still somewhat mysterious. In 1965, Hayflick et al. found that human diploid fibroblasts would only divide a finite number of times in cell culture before they went into a growth-arrested, senescent phase. At the time it was not known whether this phenomenon was a result of culture conditions or was a property inherent to the cells (Hayflick, 1965). In more recent studies using mouse embryonic fibroblasts, it was found that reducing the percentage of oxygen in which the cells were cultured from 20% to 5% or 3% reduced DNA damage and delayed senescence, providing evidence that aerobic respiration contributed significantly to senescence (Busuttil et al., 2003; Parrinello et al., 2003).

Mitochondrial ROS production

The mitochondria carry out the process of oxidative phosphorylation, a process necessary for the production of ATP, a vital energy source for cells. In doing so, they

produce ROS as a byproduct. While ROS may be deleterious in excess, they are also needed for redox-dependent signaling. In the mitochondrial electron transport chain, sites I and III are the main sources of ROS, more specifically superoxide ($O_2^{\bullet-}$). In the mitochondria and elsewhere, superoxide dismutase (SOD) eliminates $O_2^{\bullet-}$ by converting it to hydrogen peroxide (H_2O_2), which is then converted to water by catalase and glutathione peroxidases (GPX). SOD exists in three different isoforms: SOD1 contains copper and zinc and is located in the cytosol, SOD2 is manganese-dependent and is located in the mitochondrial matrix, and SOD3 is extracellular. These antioxidant enzymes are important because free $O_2^{\bullet-}$ is highly reactive and is capable of damaging proteins (Oliver et al., 1987), lipids (Tappel, 1973), and DNA (Richter et al., 1988). Specifically in mitochondria, $O_2^{\bullet-}$ can react with cytochrome C and interfere with mitochondrial function or damage mitochondrial DNA (Balaban et al., 2005). Oxidative damage to DNA is very common with increasing age and has been suggested as a mechanism of aging. There are approximately 20 known oxidative DNA damage byproducts, and one that has been most frequently measured is 8-oxo-2'-deoxyguanosine (8-oxo-dG) (Fraga et al., 1990). 8-oxo-dG is an oxidatively modified product of deoxyguanosine, which is made up of the purine nucleotide base guanine lined to deoxyribose that forms when deoxyguanosine reacts with $O_2^{\bullet-}$. This DNA adduct is mutagenic because, if left unrepaired, it can cause G:C to T:A transversions (de Souza-Pinto et al., 2001). With increasing age, increased 8-oxo-dG has been found in nuclear DNA from rodent tissues, including liver, heart, brain, kidney, and skeletal muscle, indicative of oxidative DNA damage (Hamilton et al., 2001). It has been postulated that as mitochondria become damaged with advancing age, they produce more ROS, setting up a vicious cycle, and mitochondrial DNA damage has been found in the form of increased 8-oxo-dG in rodents as well, supporting this idea (de Souza-Pinto et al., 2001; Hamilton et al., 2001).

Several mammalian models have shed light on the role of ROS and mitochondrial damage in aging. One strain of long-lived mutant mice were found to have a smaller body size, a lower body temperature, increased antioxidant capacity, and diminished insulin/insulin-like growth factor-1 (IGF-1) signaling (Quarrie and Riabowol, 2004). In another model, haploinsufficiency of the IGF-1 receptor prolonged lifespan and reduced oxidative stress, implicating this pathway in ROS-mediated aging (Holzenberger et al., 2003). Mice with p66shc knocked out live longer and have less oxidative stress as well. p66shc helps regulate the insulin receptor and may also interact with Forkhead activity, resulting in increased expression of antioxidants (Migliaccio et al., 1999; Nemoto and Finkel, 2002; Trinei et al., 2002). Conversely, mice expressing a proofreading-deficient form of mitochondrial DNA polymerase gamma developed more mitochondrial mutations, decreased mitochondrial function, a shorter lifespan, and early onset of many age-related phenotypic changes, further supporting the idea that mitochondrial damage contributes to aging (Trifunovic et al., 2004).

Telomere shortening

A second hypothesis on the mechanisms of aging is that telomere shortening contributes to aging. Telomeres are sections of repetitive non-coding DNA that cap the ends of chromosomes and protect them from degradation. Originally, it was thought that telomere shortening was responsible for aging. Each time a cell divides, the telomeres are shortened slightly, and after many divisions they reach a length that triggers the tumor suppressor protein p53, which initiates growth arrest and cellular senescence (Finkel, 2011). Recent evidence related to cardiovascular aging shows that in elderly men, the rate of shortening of leukocyte telomeres correlates with mortality from cardiovascular disease (Epel et al., 2009). Telomere length has also been correlated

with increased expression of genes related to age-associated inflammation (Blagosklonny et al., 2010).

While the telomere shortening hypothesis and the oxidative stress hypothesis of aging may have originally seemed to be contradictory, new evidence suggests they are interrelated. Sahin et al. have used a mouse model deficient in telomerase, which results in dramatically shortened telomeres (Sahin et al., 2011). While it was expected that highly proliferative tissues showed a high degree of DNA damage, it was unexpected that non-proliferative tissues, such as those found in the heart, also showed a great amount of damage. The gene pathways most affected by the deficit in telomerase were those related to metabolism, mitochondrial function, oxidative phosphorylation, and antioxidant defenses. In these mice, shortened telomeres activated p53, which repressed expression of peroxisome proliferator-activated receptor gamma coactivator 1 alpha and beta (PCG-1α and PCG-1β), which in turn activated downstream signaling pathways that culminated in compromised mitochondrial function. In the heart, reduced mitochondrial number and function could be normalized by reintroducing telomerase (Sahin et al., 2011). Taken together, these data suggest that telomere shortening activates signaling pathways mediated by p53 that result in metabolic and oxidative derangements that contribute to the senescence process. Therefore, both oxidative stress and telomeres are important in the process of aging.

Senescence-associated signaling pathways

Cellular senescence and aging are complex processes, and many different signaling pathways are affected by and contribute to aging. These signaling pathways are often activated by DNA damage or oxidative stress. It is likely that increased ROS, telomere shortening, DNA damage, and activation of signaling pathways that promote senescence are all interrelated. As mentioned in the previous section, the tumor

suppressor protein p53 appears to play a pivotal role in senescence, and it also functions in oncogene signaling pathways. In cultured primary cells, increased expression of the oncogene Ras leads to increased ROS as well as increased expression of p16 and p21, all of which culminates in growth arrest (Serrano et al., 1997). The presence of p53 is important in Ras-mediated senescence; the presence of p53 attenuates Ras-mediated increases in ROS, and the lack of p53 leads to greatly increased ROS (Lee et al., 1999). In another example of the role played by oncogenes in ROS-mediated senescence, overexpression of Akt activates the FoxO proteins, member of the Forkhead transcriptional regulator family, and this leads to growth arrest and senescence (Miyauchi et al., 2004; Murphy, 2006). It has been shown that caloric restriction extends the lifespan in a variety of organisms (Blagosklonny et al., 2010). Recent evidence suggests that caloric restriction in rhesus monkeys decreases aging-related deaths and the development of age-associated diseases such as diabetes, cancer, and cardiovascular disease at the end of a 20-year-long study (Colman et al., 2009). On a molecular level, it was found that caloric restriction increases the expression of sirtuins, which are NAD-dependent protein deacetylases related to the silent information regulator 2 protein (North and Verdin, 2004). Sirtuins serve many cellular functions related to regulation of metabolism, stress resistance, cell proliferation, and apoptosis, all functions involved in the aging process and its associated diseases (Yamamoto et al., 2007). Additionally, in animals that are calorically restricted, caloric restriction, and the ensuing differences in metabolism, is a model for increased longevity. In this caloric restriction model, p53 acts on the target of rapamycin (TOR) pathway, the FoxO pathway, and the hypoxia inducible factor pathways in *C. elegans* and *D. melanogaster* (Blagosklonny et al., 2010). The mammalian TOR (mTOR) pathway is involved in aging in mammals as well. In human and mouse cells, inhibiting

this pathway with rapamycin slows senescence (Demidenko et al., 2009), and administering rapamycin to mice increases their life span (Harrison et al., 2009).

Impact of aging on stem cells and renewal

In all organisms, stem cells are a source of renewed cells that can replace old or damaged cells and aid in tissue repair. The impact of ROS on aging and disease has been discussed in previous sections, and it seems likely that ROS also have a negative effect on progenitor cells, such as hematopoietic stem cells. Evidence suggests that oxidative damage to these populations of cells diminishes their restorative potential and contributes to the aging of stem cells (Lu and Finkel, 2008). In the setting of vascular disease, a reduction in circulating endothelial progenitor cells, and increased cellular senescence of those remaining cells, is observed in patients with vascular risk factors; this suggests that progenitor cells play a role in the aging process (Hill et al., 2003). Other recent studies suggest that stem cells populations may become exhausted with aging as a result of increased activity of signaling pathways. For example, increased activity of the TOR pathway led to increased proliferation of hematopoietic stem cells and contributed to senescence of these cells (Chen et al., 2009) Because stem cells play a role in longevity versus senescence, an interesting new idea is to use stem cell to preserve the function of aging organs. In an elegant study, researchers infused female mice with bone marrow derived cells from young female mice and observed a preservation of fertility in the older mice (Selesniemi et al., 2009). Collectively, these studies demonstrate that aging of stem cells can contribute to senescence of the entire organism, and that stem cells offer a potentially useful avenue for restoring tissue damaged by the aging process.

1.3 Cardiovascular aging and disease

Vascular and arterial aging

A major risk factor for vascular disease is the aging process itself. One obvious reason is that advanced age means greater lifetime exposure to risk factors, so the occurrence of disease may increase. Nevertheless, there is something inherent to the aging process such that aging alters the physiology in a way that increases susceptibility to cardiovascular diseases commonly associated with aging. "Disease" manifests as both overt disease for which patients seek treatment, as well as subclinical impairments which may only be detected upon examination or if the patient experiences some sort of challenge or stressor, such as exercise (Lakatta and Levy, 2003a).

As reviewed by Lakatta and Levy, changes in the vascular structure and function that characterize the aging process include dilation of the large elastic arteries, intimal media (IM) thickening, increased vascular stiffness, and endothelial dysfunction. Age-associated IM thickening can be a risk factor for atherosclerosis, and thickening can contribute to subclinical coronary artery disease that can worsen to overt disease over time (Stary et al., 1992). Increased arterial stiffness has been associated with increased deposition of collagen, reduced elastin, and increased vascular calcification. Impaired endothelial function may also contribute to vascular stiffening; furthermore, endothelial dysfunction is found in a variety of pathophysiological states such as hypertension and diabetes, so it may be a common mechanism that contributes to many age-associated vascular diseases (Gimbrone, 1999). Arterial stiffening causes systolic arterial pressure to increase, diastolic arterial pressure to decrease, and pulse pressure to increase (Vaitkevicius et al., 1993). Vascular stiffening and hypertension are related, and it is thought that stiffening precedes the increase in blood pressure. With increasing age, blood pressure becomes more dependent upon the stiffness of the large arteries and less dependent upon peripheral vascular resistance (Franklin et al., 1997).

In some cases, risk factors converge; for example, endothelium-dependent relaxation decreases at the same time in the life span when pulse pressure increases, and these changes feed on each other to promote disease. The overall vascular aging profile is subject to combinations of factors, such as endothelial dysfunction, IM thickening, arterial stiffness, and increased pulse pressure. Furthermore, lifestyle factors such as consumption of a high-fat diet and a sedentary lifestyle, as well as other co-morbid conditions such as diabetes, all contribute to how well or poorly an individual ages and that individual's chances of developing vascular disease (Lakatta and Levy, 2003a).

Cardiac aging

The heart undergoes its own set of characteristic changes specific to the aging process as well, and as in the vasculature, some of these changes can provide a background that favors cardiac disease. Heart failure, left ventricular (LV) hypertrophy, and atrial fibrillation are all cardiac diseases that increase with advancing age (Lakatta and Levy, 2003b). Even in the absence of cardiac pathology, LV wall thickness increases with age (Gerstenblith et al., 1977). Additionally, evidence of cardiomyocyte hypertrophy has been found in aged human hearts (Olivetti et al., 1995). LV diastolic and systolic function undergo characteristic age-related changes. Early diastolic filling (E) declines with age, and it is thought that the LV structural changes and/or calcium that continues to interact with myofilaments after systole could be contributing mechanisms. Late diastolic filling (A) concomitantly increases, in part because of increased atrial contractility, and the atria can enlarge as a result of this increased work (Swinne et al., 1992). Consequently, the ratio of early to late diastolic filling velocity (E/A) declines with age, and this can be a characteristic of the age-associated development of diastolic dysfunction reflecting impairment in the ability of the LV to relax and fill. When cardiac

volume was examined in aged humans, it was found that LV end-diastolic volume (LVEDV) normalized for body surface does not change with increasing age, and the LVEDV reserve increases, which is likely an adaptive compensatory mechanism (Fleg et al., 1995; Rodeheffer et al., 1986). In the absence of disease, ejection fraction (EF) and stroke volume (SV) do not change with aging, though the EF reserve and LV end-systolic volume (LVESV) reserve may diminish (Fleg et al., 1995).

Regulation of cardiac contractility and heart rhythm are often impaired with advancing age, and there are several mechanisms that may underlie deficient regulation in otherwise healthy older humans. Contractility, measured by the ratio of LV end-systolic pressure (LVESP) to LVESV during exercise, decreases; this is similar to the decline in LVESV reserve, which refers to the capacity of the heart to increase its output and volume based on increased workload. This decline in reserve is thought to reflect a deficit in the sympathetic modulation of heart rate and LV contractility (Yin et al., 1978). Norepinephrine dysregulation also occurs in the heart with increasing age, and this could be caused by impaired norepinephrine reuptake and norepinephrine spillover into the circulation (Esler et al., 1995; Lakatta, 1993). With increasing age, post-synaptic β-adrenergic receptor signaling declines (Lakatta, 1993). There are changes in LV afterload and vascular-ventricular load matching. At rest, vascular-ventricular matching is maintained because both the vasculature and the ventricle are stiffer; however, during exercise, a mismatch becomes evident because the LV elastance does not change proportionally to the vascular elastance (Chen et al., 1998). Since matching of ventricular and vascular loads is necessary for optimally efficient ejection of blood, this age-associated mismatch is thought to contribute to diminished cardiac reserve, particularly during exercise. Finally, there are changes associated with heart rhythm that come with aging. The rates of supraventricular and ventricular arrhythmias are increased (Fleg and Kennedy, 1982). An example is atrial fibrillation, which is itself

associated with a variety of poor outcomes, such as increased stroke risk (Maurer et al., 1995).

In conclusion, a variety of cardiac changes occur normally in the aging heart, and these may interact with the changes that concomitantly occur in the vasculature. While these changes are not diseases, they can increase the likelihood of developing cardiac disease and/or contribute to a poorer prognosis if cardiac disease is present. For example, aging causes increased arterial stiffness, which leads to hypertension, which over time results in LV hypertrophy. This remodeling that occurs in the LV leads to increased LV stiffness, which promotes diastolic dysfunction. Diastolic dysfunction can increase atrial contraction and atrial hypertrophy which can eventually result in atrial fibrillation, and the additional changes that occur in heart rhythm regulation can contribute to pathology as well (Lakatta and Levy, 2003b). Clearly, the ways in which age-associated changes impact development of overt disease is a complex and multifactorial process, and much effort is currently being focused on understanding the specific mechanisms that underlie these changes.

Figure 1.1. Age-associated changes in the heart.

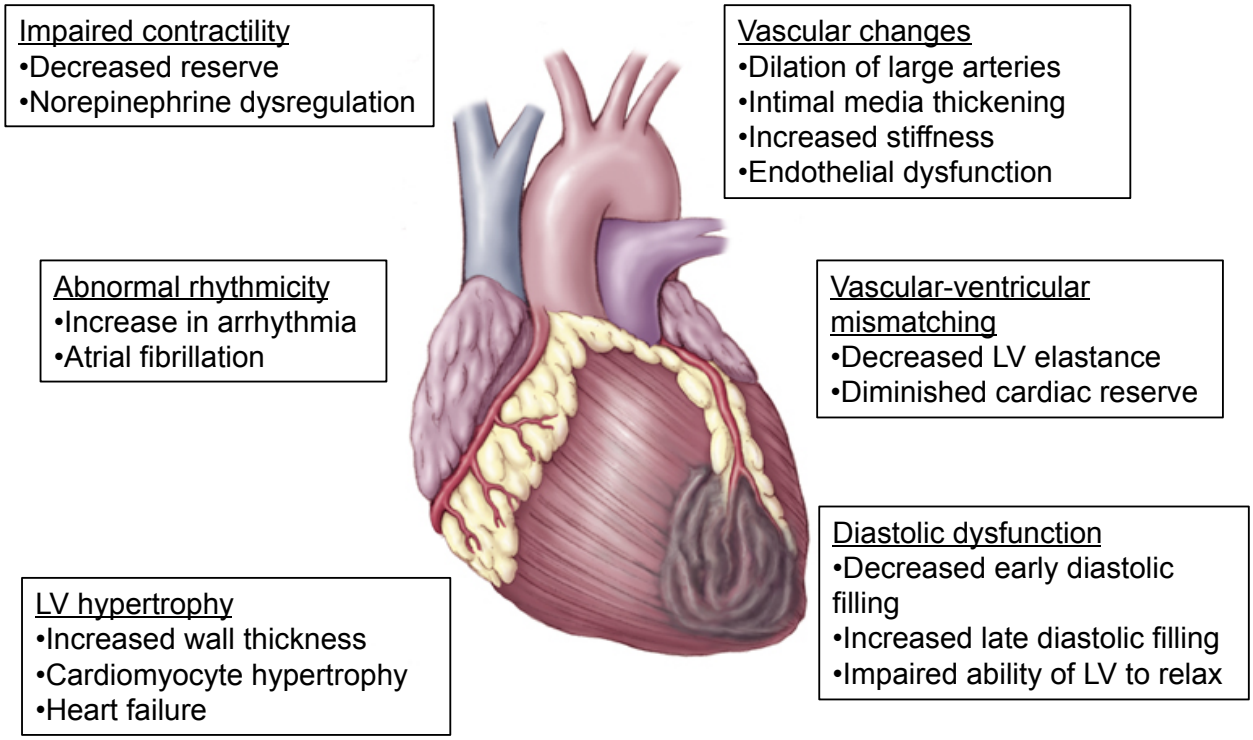

Cellular and molecular mechanisms driving the cardiovascular aging process

In the vasculature, aging is associated with luminal dilation, IM thickening, vascular stiffening, and endothelial dysfunction, and a number of cellular and molecular mechanisms drive these processes (Lakatta, 2003). In studies of aged rats, the thickened aortic intima showed increases in extracellular matrix (ECM) protein such as collagen and fibronectin as well as increased transforming growth factor-beta (TGF-β), inter-cellular adhesion molecule 1, and matrix metalloproteinase -2 (MMP-2). The presence of these molecules localized to the intima, and the fact that their presence was a function of senescence any not any experimental intervention or injury, suggests that the type of vascular remodeling that typically occurs in aging is milder but similar to the type of damage sustained from hypertension (Li et al., 1999). IM thickening resembles changes characteristic of vascular injury such as migration and proliferation of vascular smooth muscle cells and ECM remodeling accompanied by altered MMP activity (Galis et al., 1995; Jenkins et al., 1998; Motwani and Topol, 1998). Secretion of MMP-2 is enhanced by increased cytokine stimulation and production of growth factors, both of which are increased with aging (Li et al., 1999). TGF-β promotes ECM deposition and is stimulated by angiotensin II, which increases with age as a result of increased angiotensin-converting enzyme activity (Challah et al., 1997).

Endothelial structure and function changes at the cellular and molecular levels as well. Expression of adhesion molecules and adherence of monocytes is increased with advancing age. Aging impairs nitric oxide ($NO^{\bullet}$)-dependent and agonist-mediated vasodilation, which results in endothelial dysfunction (Asai et al., 2000; Hongo et al., 1988). Oxidative stress contributes to endothelial dysfunction as well; reduced $NO^{\bullet}$ reacts with increased $O_2^{\bullet-}$ to form peroxynitrite. Both the absence of the vasodilator $NO^{\bullet}$ as well as the production of peroxynitrite, which is capable of damaging lipids and

proteins, have a detrimental effect on endothelial function (Cai and Harrison, 2000). Diminished telomere length and function is correlated with increased endothelial dysfunction, which further supports the idea that aging is a major contributing factor (Minamino et al., 2002). Finally, increasing age is associated with decreased expression of vascular endothelial growth factor and hypoxia inducible factor 1 (Rivard et al., 2000) and may be related to increased accumulation of advanced glycation end products (Treins et al., 2001). While arterial aging and atherosclerosis are separate processes, many of the molecular changes that occur with aging promote an altered and more metabolically-active environment that also contributes to atherosclerosis (Lakatta, 2003).

A different set of molecular and cellular changes underlie the cardiac changes characteristic of aging. In animal studies, older rats have demonstrated LV and myocyte hypertrophy as well as altered cardiac fibroblast numbers and function (Fraticelli et al., 1989), and these changes correlated with ECM changes. It is thought that arterial stiffening causes increased load, which leads to myocyte hypertrophy. Increased LV stretch can also stimulate the release of angiotensin II and TGF-β, which can contribute to fibrosis as well as apoptosis (Cigola et al., 1997). Additionally, the cardiac action potential is prolonged in the aged rat. This prolongation is likely attributable to an increase in the calcium currents that develop with age (Wei et al., 1984). Prolonged calcium transients and the reduced removal of calcium, which leads to increased interaction of calcium with the myofilaments, likely prolong contraction. The prolonged contraction results in impaired relaxation, promoting diastolic dysfunction. On a molecular level, a number of proteins involved with calcium handling are impacted with aging. Expression of the sarcoplasmic reticulum calcium ATPase (SERCA2a) is reduced (Lakatta, 1993), and expression of the sodium/calcium exchanger NCX1 is increased (Koban et al., 1998). In addition, the myofilament proteins themselves change with increasing age. The expression of myosin heavy chain protein shifts from the alpha

isoform to the beta isoform with aging (Lakatta, 1993), and this may be caused by changes in thyroid hormones, which are themselves changed with aging (Long et al., 1999). In healthy aging, these changes may be adaptive; prolonged relaxation may be caused by changes in calcium handling, which itself may enable continued ejection of blood during late systole, which is advantageous if central arterial stiffness has increased.

Aging is an important risk factor for the development of a number of cardiovascular diseases, and the physiologic changes inherent to the aging process itself contribute to these diseases. With advancing age, arteries dilate and stiffen, IM thickening occurs, and endothelial dysfunction commonly occurs. These changes can alter blood pressure and indirectly affect the heart, and the heart itself undergoes changes characteristic of aging. In the aged heart, LV hypertrophy, atrial fibrillation, and diminished cardiac reserve are commonly observed. The incidence of heart failure increases; specifically, diastolic heart failure and diastolic dysfunction are commonly associated with advancing age. A number of different pathways are thought to contribute to diastolic dysfunction; however, these pathways are incompletely understood. An improved understanding of the molecular and cellular changes that underlie age-associated cardiovascular disease, and specifically diastolic dysfunction, is needed if we are to develop effective therapies to prevent or reverse it (Lakatta, 2003).

Diastolic heart failure and diastolic dysfunction

1.4 Characteristics and clinical perspective

Heart failure patient characteristics

Heart failure is a major and growing public health concern in the United States. The prevalence of heart failure was estimated at 700,000 in 2008, and 670,000 new cases were diagnosed that year. In 2007, heart failure was responsible for 990,000

hospitalizations and contributed to 277,193 deaths; it was listed as the underlying cause of death in 56,565 cases (Roger et al., 2011). Heart failure refers to impairment in LV filling or ejection such that the heart is unable to meet the circulatory demands of the body. Originally, heart failure was thought to be the result of inefficient pumping of blood during systole, associated with a reduced EF (Chen, 2009). Nevertheless, cross-sectional and population-based studies have revealed that approximately half of all heart failure patients display its signs and symptoms, such as pulmonary edema, reduced exercise capacity, and ventricular hypertrophy, but maintain a preserved EF. This condition has been referred to as heart failure with a normal EF, heart failure with a preserved EF, or diastolic heart failure, and it describes a group of patients whose clinical manifestation of congestive heart failure is characterized by normal LVEDV, slow or delayed active relaxation, and increased passive stiffness of the LV. The patient demographics associated with congestive heart failure with a reduced ejection fraction versus heart failure with a preserved ejection fraction are different as well. The typical congestive heart failure patient is a middle-aged man with a reduced EF, and the heart failure has occurred secondary to coronary artery disease or ischemic damage. Conversely, the typical diastolic heart failure patient is more likely to be an elderly female with hypertension (Chen, 2009). In older individuals, increased vascular stiffness results in a predisposition toward hypertension; this is a major risk factor for diastolic heart failure, and 90% of these patients are hypertensive (Chen, 2009). Based on clinical studies of patient demographics and other concurrent diseases, it appears that the most important determinants for development of diastolic dysfunction and diastolic heart failure are age and hypertension (Zile and Brutsaert, 2002a). After the age of 65, the incidence of heart failure is estimated at 10 per 1000 population, and 75% of heart failure patients also have hypertension (Roger et al., 2011). Complicating matters further, heart failure with systolic and diastolic impairment can occur. If the primary

manifestation of heart failure is systolic dysfunction with a reduced EF, it can progress such that the activation of compensatory mechanisms eventually compromise diastolic function as well.

Diagnosis and treatment

Clinically, the distinction between the two types of heart failure is generally made by measuring the EF using echocardiography. Doppler echocardiography, used to measure the velocity of blood flow into the LV through the mitral valve, and tissue Doppler imaging, used to measure the velocity of change in myocardial length, are two of the most useful diagnostic methods for the detection of diastolic heart failure (Aurigemma and Gaasch, 2004). Heart failure is progressive in nature, and acute exacerbations occur; these most often result from ischemia, transient increases in blood pressure, or arrhythmias. The prognosis for all forms of heart failure is poor, and only 50% of patients are still alive 5 years after the initial diagnosis is made. The goal of heart failure management is to increase lifespan, reduce hospitalizations, and improve the quality of life. Treatment strategies, particularly for diastolic heart failure, are fairly nonspecific and only modestly effective. Treatment has generally aimed to target the renin-angiotensin-aldosterone system (RAAS) (Chen, 2009). In this pathway, angiotensinogen is produced in the liver then it is converted to angiotensin I by renin secreted by the kidney in response to decreased renal perfusion. Angiotensin I is converted to angiotensin II by angiotensin-converting enzyme (ACE), and angiotensin II binds angiotensin receptors to mediate the downstream effects. Angiotensin II also increases the production of the hormone aldosterone, both of which culminate in increased water and salt retention, increased blood volume, and increased blood pressure. The first-line of treatment has generally administration of an ACE inhibitor, which functions by blocking the action of ACE and therefore the conversion of

angiotensin I to active angiotensin II. Previously, administration of ACE inhibitors had been thought to delay progression from diastolic abnormality to overt heart failure and to improve the elasticity of the aorta and LV, improve ventricular filling, and reduce the occurrence of atrial fibrillation. However, more recent clinical trials have demonstrated that while ACE inhibitors may be helpful in controlling comorbid conditions, they have no significant effect on improving diastolic dysfunction or patient outcomes (Shah et al., 2010). Angiotensin II receptor blockers work by preventing activation of angiotensin receptors by angiotensin II and may be used in combination with ACE inhibitors. Aldosterone antagonists also target the same pathway and serve to block only the action of aldosterone and may be used in combination as well; they have been shown to improve hypertrophy and fibrosis (Nishiyama and Kim-Mitsuyama, 2010). Beta-adrenergic receptor antagonists may be effective by decreasing adrenergic stimulation, thus increasing diastolic filling time. Furthermore, by reducing blood pressure they may help prevent hypertrophy. Diuretics can be used to relieve pulmonary congestion and reduce blood volume. Nonspecific vasodilators, such as a combination of isosorbide dinitrate and hydralazine, may be used when other medications are not well tolerated, and non-dihydropyridine calcium channel antagonists are sometimes used to improve calcium handling in the myocytes and increase diastolic filling time. Finally, hydroxy-methylglutaryl coenzyme A reductase inhibitors, commonly known as statins, are sometimes used, and they are also an effective treatment for co-morbid conditions, such as hypercholesterolemia, which many patients have as well. There are differing opinions about the best way to manage diastolic dysfunction pharmacologically, and the presence of co-morbid conditions is prevalent in the elderly population, so multiple approaches to treatment are often necessary but are unfortunately also somewhat complicated (Chen, 2009). Despite this list of drugs used in the treatment of diastolic heart failure, none of them are capable of reversing or curing the disease, and none are specific for diastolic

heart failure. Treatment strategies remain limited since the pathophysiological mechanisms underlying diastolic dysfunction and diastolic heart failure are poorly understood.

Diastolic dysfunction

Diastolic dysfunction refers to an abnormality in ventricular distensibility, relaxation, and filling (Aurigemma and Gaasch, 2004). Diastolic dysfunction can precede diastolic heart failure, and it is often clinically silent (Zile et al., 2005). Both diastolic heart failure and diastolic dysfunction result from impaired LV filling, and filling pressures are increased as a mechanism of compensating for impaired filling. The increased pressure results in increased pulmonary venous pressure, which manifests as shortness of breath. If the disease progresses long enough, eventually SV and cardiac output can be reduced as well. Particularly in elderly individuals, the impaired filling results from impaired relaxation, the consequence of a stiffened LV (Chen, 2009). LV hypertrophy occurs as a normal part of the aging process (Lakatta and Levy, 2003b), and this characteristic, in combination with collagen deposition, results in stiffening of the LV and the development of diastolic dysfunction (Chen, 2009).

After ejection of blood from the LV during systole, the LV relaxes and fills at a relatively low pressure. Diastolic dysfunction occurs when the ability of the LV to fill is impaired because of either abnormalities in relaxation or compliance. Diastole consists of four phases, the first of which is isovolumic relaxation. It is influenced by active processes because ATP is needed to release the interaction between actin and myosin as well as passive processes because the mechanical properties of the LV, such as elastic recoil, influence relaxation. If there is impairment in this phase, it can raise diastolic filling pressure in the subsequent phases. Hemodynamically, assessment of isovolumic relaxation is typically measured by τ, the time constant of isovolumic

relaxation; an increase in τ indicates prolongation of isovolumic relaxation. The second phase of diastole is early rapid filling, which occurs when the mitral valve opens and LV fills because of the decreased chamber pressure. In healthy individuals, approximately 80% of filling occurs during this phase. Impairment in this phase can decrease the rate of filling and the volume of blood that fills the LV. The third phase of diastole is diastasis, which occurs when pressure is equal in the atria and ventricle, and there is a momentary cessation of blood flow. Passive stiffness can be assessed at this phase hemodynamically by generating a family of pressure-volume loops at a number of different volumes and calculating the LV end-diastolic pressure-volume relationship (LVEDPVR). The final phase of diastole is atrial contraction, which is responsible for late diastolic filling and typically makes up the final 20% of the final diastolic volume. Aging and diastolic dysfunction often increase the role played by this phase of diastole (Borlaug and Kass, 2006). Like diastolic heart failure, diastolic dysfunction is most common in the elderly population.

1.5 Mechanisms of development

Most forms of heart failure have some component of diastolic abnormality, but the contribution to the overall clinical picture and the underlying pathophysiological mechanisms are unclear. There are many factors that contribute to diastolic dysfunction, and it is unlikely that there is one single cause of diastolic dysfunction. Changes at the level of myofilaments and their associated proteins, the myocytes, the ECM, the entire heart, and systemic circulation can all contribute to diastolic dysfunction (Kass et al., 2004).

Myofilaments and myofilament proteins

The properties of muscle proteins themselves contribute a great deal to cardiac muscle stiffness. The giant muscle protein titin acts as molecular spring and is largely responsible for passive stiffness and recoil of muscle. It contains an extensible region made up of immunoglobulin and PEVK elements located at the sarcomere I-band (Kass et al., 2004). Titin is expressed in two different isoforms, a stiffer N2B isoform and a more compliant N2BA isoform (Borlaug and Kass, 2006). A shift in the expression of these two isoforms that favors increased expression of N2B can result in a stiffer heart and contribute to diastolic dysfunction. Post-translational modification of titin can play a role in stiffness as well; for example, when titin is phosphorylated by protein kinase A, it becomes more compliant (Yamasaki et al., 2002). Titin also interacts with actin, and this interaction is inhibited by the calcium-binding protein S100A1. Therefore, changes in the expression of actin and S100A1 may play a role as well (Yamasaki et al., 2001).

Changes in the expression levels of contractile proteins or mutations in these proteins can contribute to the development of diastolic dysfunction. Patients who have familial hypertrophic cardiomyopathy (FHC) have also been found to have diastolic dysfunction, and evidence suggests that a mutation in MHC on chromosome 14 is responsible for this pathological condition (Seidman and Seidman, 1991). In another study of individuals with FHC, a mutation in myosin binding protein C resulted in LV hypertrophy that developed in mid-life and worsened with increasing age, predisposing these patients to diastolic dysfunction (Maron et al., 2001). In a mouse model of FHC, a mutation was introduced into troponin T that resulted in cardiac fibrosis and impaired relaxation. A similar mutation has been found in patients with FHC, and these patients have less LV hypertrophy than FHC patients with other mutations, yet they show higher than normal rates of sudden cardiac death (Tardiff et al., 1999). Finally, a mouse model with a mutation in the sarcomeric protein tropomyosin was developed, and these mice

exhibit LV hypertrophy, cardiac fibrosis, increase sensitivity to calcium, and diastolic dysfunction (Prabhakar et al., 2001). Taken together, these studies show that mutations in sarcomeric proteins are capable of causing impaired relaxation and have been implicated in delayed LV relaxation and cardiomyopathy.

Cardiac myocytes

Structural and biochemical changes within cardiac myocytes also contribute to LV relaxation and therefore can contribute to the development of diastolic dysfunction. Anything that interferes with detachment of myosin from actin or removal of calcium from the cytosol has the potential to delay relaxation. In order for myosin to dissociate from actin and relaxation to occur, ATP is needed to remove calcium from the cytoplasm and sequester it in the sarcoplasmic reticulum (SR). SERCA2a, as well as its negative regulator phospholamban (PLB), are responsible for the re-uptake of calcium into the sarcoplasmic reticulum. The Na^{+}/Ca^{2+} exchanger (NCX) removes calcium from the cytoplasm by pumping calcium out of the cell in exchange for moving sodium into the cell. Therefore, both SERCA2a and NCX are responsible for the maintaining an appropriate calcium balance in the cytosol. Decreased expression and activity of SERCA2a was found in the hearts of aged humans and animals; this was accompanied by decreased cardiac function and prolonged relaxation of the LV (Periasamy and Janssen, 2008). PLB interacts with SERCA2a; specifically, it increases SERCA2a activity when it is phosphorylated in response to beta-adrenergic stimulation. Conversely, unphosphorylated PLB inhibits SERCA2a activity. So, expression and phosphorylation of PLB have the potential to influence cardiac relaxation. Indeed, in a mouse model lacking PLB, calcium re-uptake into the SR was enhanced, and both relaxation and contraction of the LV were improved (Luo et al., 1994). Also, NCX is often upregulated in heart failure, which may be in part a compensatory change related

to decreased SERCA2a expression, but it may also contribute to abnormal myocyte relaxation as well. Metabolic abnormalities in the myocytes can contribute to impaired relaxation as well; an increase in free ADP makes dissociation of ADP from myosin more difficult (Borlaug and Kass, 2006). Finally, decreased myofilament calcium sensitivity and altered calcium handling are thought to play a role in impaired relaxation. Though the mechanism is not fully understood, poor calcium sequestration by the SR has been shown to be related to diastolic leak of calcium from the SR through the ryanodine receptors, and this has been demonstrated in impaired relaxation and heart failure (Marks, 2001) (Marx et al., 2000).

Fibrosis

Characteristics of fibrosis

In addition to changes in myofilaments and cardiac myocytes, changes in the cytoskeleton and ECM proteins can occur. Whether these changes cause diastolic dysfunction or function as compensatory mechanisms is not fully understood, but fibrosis has been implicated as an underlying cause of ventricular stiffness (Periasamy and Janssen, 2008). When tissue injury occurs, fibroblasts migrate into the wound where they secrete new ECM and produce a scar. Scars can be macroscopic or microscopic. Macroscopic scars occur when there is a necrotic injury, such as an infarct zone, where the tissue that has died is replaced by scar tissue (Skalli et al., 1989). Microscopic scars occur when individual myocytes are lost in response to some systemic derangement, such as chronic stimulation of the RAAS (Sun et al., 1995). Myofibroblasts, characterized by the presence of α-SMA, are primarily responsible for scar formation and thus wound healing. Myofibroblasts can be thought of as an amalgam of the fibroblast and the smooth muscle cell. They have an extensive rough endoplasmic reticulum and Golgi apparatus like fibroblasts, and they have large bundles of

myofilaments like smooth muscle cells (Lijnen et al., 2000). In cardiac scars, myofibroblasts express α-SMA, vimentin, and collagen IV (Willems et al., 1994). TGF-β plays a pivotal role in the transformation of fibroblasts into myofibroblasts (Desmouliere et al., 1993). Reparative fibrosis is necessary to maintain tissue integrity and function, but this process must be tightly regulated. If the presence of myofibroblasts persists after wound healing, excessive scar tissue may build up, resulting in tissue fibrosis and disease (Leask, 2007).

Mechanisms of fibrosis

The role of TGF-β

Cytokines stimulate the deposition of ECM, and TGF-β plays a pivotal role in this process. TGF-β is a protein that has a variety of functions, including promotion of inflammation and fibrosis. There are three isoforms of TGF-β: TGF-β_1, TGF-β_2, and TGF-β_3 (Border and Noble, 1998). All are produced in an inactive form, bound with a latency-associated peptide. They are activated when the latent TGF-β binding protein is proteolytically cleaved and active TGF-β is released. TGF-β binds to the constitutively-phosphorylated TGF-β type II receptor, which phosphorylates the type I receptor to begin the signaling cascade (Ebner et al., 1993). The activated type I receptor phosphorylates Smad2/3, which binds to Smad4 and translocates to the nucleus where it activates gene transcription. TGF-β can also signal independently of Smads through the MAP kinase pathway (Frey and Mulder, 1997; Hartsough and Mulder, 1995; Yan et al., 1994).

In the myocardium, TGF-β receptors are found on the myocytes and fibroblasts (Engelmann and Grutkoski, 1994; Li et al., 1998). TGF-β has been found intracellularly, associated with both mitochondria and myofilaments in cardiac myocytes (Heine et al.,

1991). Also, TGF-β can be released from both myocytes and fibroblasts (Lijnen et al., 2000). TGF-β acts as a pro-fibrotic cytokine in the heart. In cardiac infarct scar tissue, the expression of TGF-β is increased, as well as expression of collagen and Smads 2, 3, and 4 (Sun et al., 1998). Overexpression of TGF-β in the heart results in atrial fibrosis and atrial fibrillation (Everett et al., 2004; Verheule et al., 2004). When TGF-β is administered to cultured cells or to mice, it triggers a transient fibrotic response as long as TGF-β continues to be present. Furthermore, it upregulates other cytokines such as connective tissue growth factor (CTGF), which promotes a more permanent fibrotic state (Chen et al., 2002a; Leask et al., 2003; Stratton et al., 2002).

In the heart, it is well appreciated that angiotensin II is responsible for promoting fibrosis (Thannickal et al., 2003), and TGF-β is an important downstream mediator of angiotensin II in this fibrotic process. Angiotensin II has been found to increase TGF-β in cardiac fibroblasts (Campbell and Katwa, 1997; Lee et al., 1995). In angiotensin II-induced heart failure, Smad signaling is increased, implicating TGF-β in the disease process (de Boer et al., 2004). Infusion of rats with angiotensin II induces cardiac fibrosis, even at doses that do not produce hypertension (Crawford et al., 1994; Kim et al., 1995; Yoo et al., 1998). In vitro, stimulation of fibroblasts with angiotensin II induces TGF-β and increases synthesis of ECM proteins (Campbell and Katwa, 1997; Lee et al., 1995).

Since TGF-β is pleiotropic, it is unlikely that blocking TGF-β systemically would be useful in the treatment of fibrotic disease, and side effects would likely be intolerable. More selective anti-fibrotic therapies may be able to be developed by targeting the other cytokines and pathways with which TGF-β interacts (Leask, 2007).

The role of CTGF

CTGF is a member of the CCN family of proteins as well as the insulin-like growth factor superfamily of proteins. CTGF promotes deposition of ECM and has been associated with both wound repair and fibrotic diseases (Chen et al., 2000). TGF-β induces expression of CTGF through the Smad signaling pathway. Angiotensin II also induces expression of CTGF, and it does so through a protein kinase C-dependent pathway (Ahmed et al., 2004). Alone, CTGF is only moderately fibrotic, but when it acts synergistically with TGF-β, the combination is highly fibrotic (Mori et al., 1999). For example, in cardiac infarct zones, TGF-β and CTGF are highly expressed (Chuva de Sousa Lopes et al., 2004). TGF-β induces CTGF expression in cardiac fibroblasts and myocytes, and CTGF upregulation correlated with elevated collagen I, fibronectin, and plasminogen activator inhibitor-1. Upregulation of CTGF has also been associated with cardiac ischemia (Chen et al., 2000).

The role of the ECM

The ECM is a defining feature of connective tissue, and its main function is to provide structural support and integrity to tissues and organs. Collagen is a major component of the ECM, and it exists in several isoforms. Collagen types I, III, IV, V, and VI are present in the heart. Collagen I comprises 80% of myocardial collagen and is produced by cardiac fibroblasts. Collagen III comprises about 10%, with collagens IV, V, and VI making up the remainder (Pelouch et al., 1993). Collagen I has the highest tensile strength whereas collagen III is more elastic (Burton, 1954). TGF-β stimulates increased collagen production. In isolated rat cardiac fibroblasts, TGF-β caused an increase in collagen I and collagen III production (Eghbali et al., 1991). TGF-β also

increases collagen I and decreased collagenase and MMP expression in cultured human cardiac fibroblasts (Chua et al., 1991).

Collagen deposition can contribute to stiffness, and has been shown to occur with advancing age and pressure overload. Furthermore, changes in collagen cross-linking can contribute as well, and this has been demonstrated in aging- and diabetes-associated stiffness (Borlaug and Kass, 2006). In the heart, there are three important kinds of collagen network fibers. Endomysial fibers surround and connect myocytes and capillaries, perimysial fibers connect muscle bundles and are interwoven with endomysial fibers, and epimysial fibers connect with the endothelium. Perimysial fibers in particular have been associated with diastolic dysfunction, as specific digestion of these fibers reduces LV stiffness. Changes in collagen cross-linking with AGEs and activation of MMPs may play a role in collagen-associated stiffness, and this may be even more important than total collagen content (Kass et al., 2004). Increased MMPs have been associated with LV remodeling, hypertrophy, and poorer LV relaxation, and alterations in MMP and TIMP profiles can occur with persistent neurohormonal stress (Borlaug and Kass, 2006).

The role of fibrosis in age-associated heart failure

The prevalence of heart failure increases with aging, and one possible explanation is that aging is associated with LV hypertrophy and fibrosis. In addition to the characteristic changes the cardiovascular system undergoes with aging discussed in previous sections, the function of cardiac endothelial cells and fibroblasts is altered such that a pro-fibrotic phenotype is favored. Fibrosis in the senescent heart is associated with increased cardiac collagen content and increased collagen cross-linking. Generally, fibrosis is associated with a stiffer LV and diastolic dysfunction. Nevertheless, fibrosis can contribute to systolic dysfunction as well through disrupted excitation-contraction

coupling and activation of MMPs, which can degrade ECM and contribute to dilated cardiomyopathy. Since scar tissue impairs electrical conduction, fibrosis can also contribute to arrhythmias (Chen, 2009).

The mechanism of age-related cardiac fibrosis is poorly understood, but activation of the RAAS and increased production of ROS are thought to play a role. Cardiac angiotensin II increases with advancing age, and administration of angiotensin receptor antagonists attenuates fibrosis and diastolic dysfunction in rats (Basso et al., 2007). In mice, knocking out the angiotensin receptor led to decreased fibrosis (Benigni et al., 2009), while overexpressing the receptor led to increased fibrosis (Billet et al., 2007). Implicating increased ROS in the development of cardiac fibrosis, aged rats showed increased cardiac mitochondrial $O_2^{\bullet-}$ (Sawada and Carlson, 1987). In aged mice, catalase targeted to the mitochondria reduced hypertrophy, fibrosis, and diastolic dysfunction (Dai et al., 2009). ROS are capable of altering expression of cytokines, which can activate cardiac fibroblasts and promote inflammatory and fibrotic responses. It is widely accepted that TGF-β promotes fibrosis, and TGF-β is upregulated by both ROS and angiotensin II. In turn, increased TGF-β stimulates CTGF, and the synergistic actions of these two cytokines promote cardiac fibrosis. In cardiac fibroblasts, the cell type widely associated with fibrosis, it was found that TGF-β increased NADPH oxidase 4-derived ROS, which promoted the conversion of fibroblasts into pro-fibrotic myofibroblasts (Cucoranu et al., 2005).

Cardiac remodeling is altered with increasing age because there are age-related defects in the inflammatory and repair pathways. For example, aged myocardium has a decreased inflammatory response to ischemic damage, which leads to a diminished repair process (Ding et al., 1994). Cardiac fibroblasts isolated from aged mice have a blunted response to stimulation with TGF-β and angiotensin II (Bujak et al., 2008). This

pattern may be responsible for impaired scar formation in infarct zones, which can contribute to dilated cardiomyopathy and systolic dysfunction. Counter intuitively, aging hearts are characterized by increased baseline inflammatory and fibrotic processes but diminished reserve and healing capabilities, leaving senescent hearts more susceptible to pathological remodeling. Therapeutically, it is unclear whether or not fibrosis can actually be reversed. If fibrosis could be prevented, there is a chance that the treatment that would prevent fibrosis would also interfere with the natural protective mechanisms against aging in the heart or other cellular processes that depend upon scar formation (Chen, 2009). Currently, there are no specific treatments capable of reversing diastolic dysfunction, and treatment is aimed at controlling comorbid conditions and minimizing volume overload and hence the workload of the heart. A potentially fruitful future approach might be to target the impaired healing response that accompanies advancing age.

Cardiac and extra-cardiac effects

Cardiac load also influences relaxation. In the setting of heart failure, preload and afterload are often both increased. Preload is increased when cardiac volume is increased, and afterload is increased when there is increased arterial stiffness or increased peripheral vascular resistance, both of which can contribute to impaired relaxation. These extrinsic factors may play an even greater role during neurohormonal activation. For example, increased central venous volume and pressure, which often results from compensatory neurohormonal activation that occurs in heart failure, can increase filling pressure, contributing to the appearance of diastolic dysfunction. Increasing age causes increased arterial stiffness, which increases afterload and can reflect pressure back to the LV, interfering with relaxation (Borlaug and Kass, 2006).

1.6 Animal models of diastolic dysfunction

Diastolic heart failure and diastolic dysfunction are quite prevalent in the human population, but there currently exists no effective therapy to treat, reverse, or prevent these pathological conditions. The lack of therapeutic strategies is in part a result of a poor understanding of the mechanisms responsible for the development of diastolic dysfunction. While a number of animal models display diastolic dysfunction, it seems that there are many different mechanistic paths that lead to the same pathology of diastolic dysfunction. Therefore, the increasing use of mouse models, including transgenic mouse models, in basic research is a promising avenue for gaining a better understanding of diastolic dysfunction. While there is not one single well-established murine model of pure diastolic dysfunction, investigators have developed a number of models that recapitulate diastolic dysfunction in the setting of other associated conditions, such as hypertension, diabetes, and various genetic forms of cardiomyopathy.

One of the most common risk factors for developing diastolic dysfunction is hypertension, but how hypertension might mechanistically contribute to diastolic dysfunction has not been well elucidated. In a recent study by Silberman et al., a mouse model of hypertension was found to exhibit diastolic dysfunction mediated by oxidative stress caused by uncoupled nitric oxide synthase (NOS) (Silberman et al., 2010). The model used was the deoxycorticosterone acetate (DOCA)-salt mouse. In this model, mice undergo unilateral nephrectomy, are subcutaneously implanted with a controlled release DOCA pellet, and drink 1% saline; this treatment regimen produces mild hypertension. After 11 days of treatment, DOCA-salt mice exhibited hypertension accompanied by diastolic dysfunction with no changes in systolic function. Moreover, diastolic dysfunction was accompanied by increased $O_2^{\bullet-}$ in the LV that could be suppressed by administration of NOS inhibitors. The increase in oxidative stress was

accompanied by decreased cardiac tetrahydrobiopterin (BH_4) and decreased $NO^{\bullet}$. Furthermore, administration of BH_4 was successful in preventing diastolic dysfunction in DOCA-salt mice. Taken together, these data suggest that cardiac oxidative stress associated with hypertension can promote NOS uncoupling, further oxidative stress, and lead to diastolic dysfunction (Silberman et al., 2010).

Intimately tied to hypertension is the RAAS and its associated receptors, which have been implicated in diastolic dysfunction in various ways. In a study by Billet et al. (Billet et al., 2007), a constitutively active angiotensin receptor 1 knockin mouse was generated; the receptor was constitutively active because of a gain-of-function N111S/Δ329 mutation. These transgenic mice were hypertensive and had lower plasma renin and angiotensin and had an increased and more sustained response to angiotensin II infusion. Although these mice did not display evidence of cardiac hypertrophy, they did develop diastolic dysfunction and elevated filling pressures independent of changes in systolic function. Furthermore, cardiac fibrosis was found in both pericoronary and interstitial areas without changes in myocyte hypertrophy or inflammation (Billet et al., 2007). In another study by Di Zhang et al. (Di Zhang et al., 2008), a mouse model with conditional cardiac-specific overexpression of the human mineralocorticoid receptor in combination with chronic angiotensin II infusion displayed diastolic dysfunction. While systolic function was unchanged, angiotensin II-treated transgenic mice displayed increased isovolumic relaxation time (IVRT) and decreased tissue Doppler diastolic wave velocity. These changes were accompanied by augmented cardiac hypertrophy and enlargement of the left atrium. It was also found that infusion of angiotensin II worsened fibrosis; collagen 1A, collagen 3A and fibronectin were increased, as were MMP-2 and MMP-9. While inflammatory markers were not increased, NADPH oxidase-2 (Nox2) expression was increased, and this was associated with increased $O_2^{\bullet-}$ production and increased protein oxidation (Di Zhang et al., 2008).

Another study used a different approach to examine the role of hypertension in the development of diastolic dysfunction; a mouse model of pressure overload was created by transverse aortic constriction (TAC), triggering cardiac remodeling initially associated with diastolic dysfunction that appeared to progress to both systolic and diastolic heart failure. In this model, a transient increase in pro-inflammatory cytokines and chemokines was associated with increased cardiac macrophage infiltration, and this inflammatory response was associated with increased levels of TGF-β, increased Smad phosphorylation, and ECM protein expression leading to interstitial and perivascular fibrosis, including an increase in alpha smooth-muscle actin (α-SMA)-positive myofibroblasts. After 7 days of TAC, hearts showed normal systolic function and normal chamber dimensions but displayed concentric hypertrophy and increased LV mass, characteristic of diastolic dysfunction. By 28 days, the LV mass had further increased, the LV had begun to dilate, and systolic dysfunction was evident. This study demonstrates that a heart need not undergo tissue necrosis to develop activation of inflammatory and immune processes that contribute to remodeling and fibrosis (Xia et al., 2009). Taken together, these studies suggest that increased blood pressure could be associated with increased activation of the renin-angiotensin-aldosterone system, and that oxidative stress could be a mediating factor that contributes to inflammation and fibrotic changes that promote diastolic dysfunction.

Another disease that has been associated with diastolic dysfunction in the clinical population is diabetes, and several groups of investigators have studied diastolic dysfunction in various diabetes models. The *Ins*$^{2WT/C96Y}$, or Akita, mouse is a model of type I diabetes; the mutation causes early and sustained loss of insulin-producing β-cells and is not subject to obesity or confounding systemic effects. Akita mice show normal systolic function at both 3 and 6 months of age, but display persistent diastolic

dysfunction beginning at 3 months of age. These mice have a reduced E-wave deceleration rate, prolonged IVRT, reduced early diastolic tissue velocity, increased LV end-diastolic pressure (LVEDP), increased time constant of pressure decay (τ_{Weiss}), and reduced negative minimum change in pressure over time ($-dP/dt_{min}$). These changes are accompanied by downregulation of SERCA2a, increased levels of long-chain fatty acids, triacylglycerol, ceramide, and diacylglycerol, and increased expression of β-MHC protein without evidence of fibrosis or changes in ECM proteins. In this model, it is thought that lipotoxicity is the dominant mechanism of diastolic dysfunction (Basu et al., 2009). In another murine diabetes model, diabetes is induced by injection of streptozotocin, which is a cytotoxic agent for pancreatic β cells. Diastolic dysfunction was observed in this model, but it was also accompanied by systolic dysfunction, as these mice had a reduced ejection EF and CO as well as increased systolic diameter and thinning of the LV wall. Induction of diabetes was also accompanied by increased oxidative stress in the form of decreased NADH oxidase activity, compromised mitochondrial electron transport activity, and decreased mitochondrial complex I activity. It appears that in this model of diabetes, early mitochondrial dysfunction contributes to both diastolic and systolic dysfunction (Yu et al., 2007). In yet another model of diabetes-associated cardiac disease, the fatty acid transport protein was overexpressed specifically in the heart; in these mice, fatty acid storage and usage in the heart was increased, but systemic metabolism was unaltered. These transgenic mice demonstrated a restrictive pattern of diastolic impairment (E/A >1.5) and an increased heart-to-body weight ratio. In isolated cardiomyocyte studies, there were no differences in contraction, but relaxation of myocytes was impaired, and myocytes from transgenic mice had a shorter sarcomere length, indicating greater contraction in the resting state. It is believed that diastolic dysfunction originates at the cellular level in this model, and that it is

independent of changes in calcium cycling but that increased expression of β-MHC could contribute to slower cross-bridge cycling, impaired relaxation, and ultimately diastolic dysfunction (Flagg et al., 2009).

In addition to its association with cardiovascular disease, diabetes is also associated with kidney disease, which in and of itself can contribute to cardiovascular disease. Patients with chronic kidney disease often show evidence of cardiovascular disease, and this may be related to risk factors such as LV hypertrophy and aortic stiffness, which often occurs secondary to vascular calcification which is characteristic of renal disease. In a mouse model of chronic renal failure, echocardiography was used to demonstrate increased LV mass, prolonged IVRT, and an increased Tei index, which is an index of global myocardial performance. The Tei index is calculated by adding the isovolumic contraction time and the isovolumic relaxation time and dividing the sum by the ejection time. This index is used to assess systolic and diastolic function combined (Pellett et al., 2004). Diastolic dysfunction was also accompanied by increased aortic stiffness in the form of a higher pulse-wave velocity, LV hypertrophy, and impaired endothelium-dependent relaxation (Maizel et al., 2009). While it is interesting that these chronic renal failure mice develop diastolic dysfunction, the study of diastolic dysfunction is made more complex by their likely systolic abnormalities and other co-morbid pathologies.

A very different mouse model of cardiac hypertrophy was developed by overexpressing the protein Hop in the heart; Hop is a non-DNA-binding nuclear protein that can modulate gene transcription and has been shown to bind to serum response factor and inhibit transcription of certain cardiac genes. In neonatal development, Hop helps regulate the balance between replication of cardiac cells and differentiation of these cells. Overexpression of Hop was associated with cardiac hypertrophy, increased LVEDP, impaired diastolic relaxation, and increased fibrosis. Concentric remodeling

was observed, which progressed to dilation, systolic dysfunction, and sudden death from arrhythmias (Kook et al., 2003). Further studies using this model revealed that these mice had increased left atrial dimensions, a decreased E/A ratio, increased ventricular wall thickness, and a greater EF. Because of the relationship between Hop and histone deacetylation, treatment with the histone deacetylase inhibitor trichostatin A was capable of reversing the cardiac pathologies associated with overexpression of Hop (Liu et al., 2008). While the objective of these studies was not originally to create a mouse model of diastolic dysfunction and understand the mechanistic development of the disease, diastolic dysfunction was nevertheless observed in this model of hypertrophy. This provides further evidence that diastolic dysfunction is unlikely to develop because of one single pathway and is related to other cardiac disorders.

Another cardiovascular disease that has been associated with diastolic dysfunction is FHC, which is a family of genetic diseases that result from mutations in cardiac muscle proteins and can lead to sudden cardiac death in relatively young people. Several mouse models of FHC exist, and these models were generated by different single amino acid mutations. In humans, one mutation that results in FHC is an arginine to glutamine missense mutation at position 403 of the β-MHC gene. A group of investigators generated a mouse model to study this mutation causing FHC by mutating this amino acid in the α-MHC protein, since α-MHC is the predominant form of myosin in mice and because it is almost exactly homologous to β-MHC, the predominant form in humans, in the region of the mutated amino acid (Maass and Leinwand, 2000). The resulting mouse displayed diastolic dysfunction; LVEDP was increased and –dP/dt was reduced at high calcium concentrations. At high rates of inotropic stimulation, the heart failed to increase the rate of ventricular relaxation. Diastolic dysfunction appeared to be caused by aberrations in myocardial metabolism and energetics. These mice exhibited

decreased free energy release from ATP hydrolysis that was worsened during cardiac work. Unlike some of the previously mentioned models, there was no evidence of fibrosis in the hearts of these transgenic mice, and the investigators concluded that diastolic dysfunction could result from slowed calcium removal and/or slowed kinetics of actin-myosin dissociation related to altered myocardial energetics (Spindler et al., 1998).

Another cause of FHC is mutations in cardiac troponin T (cTnT), which is associated with mild or no hypertrophy and an increased risk of sudden death. A mouse model was created harboring a missense (R92Q) mutation in cTnT, expressed as 30%, 67%, or 92% of total cTnT. It was found that atrial hypertrophy increased dose-dependently in these mice whereas ventricular mass decreased equally in all three lines. Decreased ventricle size was accompanied by a decrease in cardiomyocyte size, and basal levels of myocyte contraction were found to be abnormally high. Other aberrations observed included cardiac fibrosis, inflammation, and myocellular disarray consistent with FHC. The R92Q-Myc-67% hearts showed increased systolic function but decreased diastolic function, including impairments in –dP/dt, time to 50% relaxation, and τ. So in this model, diastolic dysfunction appears to result from abnormal cardiomyocyte function and likely fibrosis (Tardiff et al., 1999). Aside from mutations in cTnT, FHC can be associated with mutations in cardiac troponin I (cTnI), so a mouse model harboring a R193H mutation was created. These mice displayed enlarged atria, decreased LV end-diastolic diameter (LVEDD), decreased LV volume, increased IVRT, and an increased ratio of mitral peak velocity of early filling (E) to early diastolic mitral annular velocity (E'), (E/E' ratio), all indicative of diastolic dysfunction. Isolated cardiomyocytes from these transgenic mice showed impaired sarcomere shortening, prolonged relaxation time, and an increased sensitivity to calcium, and it was concluded that diastolic dysfunction was likely resulted from hypersensitivity to calcium, which causes the myofilaments of the myocytes to show impaired relaxation (Li et al., 2010).

Mouse models that recapitulate FHC via mutations in another cardiac muscle protein, tropomyosin have diastolic dysfunction. When a glutamine to glycine mutation was introduced at position 180 in α-tropomyosin (Glu180Gly), hearts showed concentric hypertrophy, atrial enlargement, increased fibrosis within 1 month of life, and life span was 4 to 5 months of age. Echocardiographic findings in these transgenic mice included increased E/A ratio, reduced ventricular compliance, decreased propagation velocity of transmitral flow, but unchanged systolic function compared to littermate controls. Hemodynamic findings included a decreased –dP/dt and increased LVESP and LVEDP. Skinned fiber bundle studies revealed increased calcium sensitivity (Prabhakar et al., 2001). Further studies on these mice revealed increased atrial natriuretic factor, and increased β-MHC in transgenic hearts. Isolated papillary muscles from transgenic mice showed prolonged time to 90% relaxation, suggestive of diastolic dysfunction, as well as increased sensitivity to calcium. Further implicating problems with calcium handling, neonatal adenoviral gene transfer of SERCA2a improved cardiac function (Pena et al., 2010). Taken together, these FHC studies show that a variety of different mutations can cause FHC in mouse models, and while each different mutation may be associated with a slightly different phenotypic expression of abnormalities, they all result in diastolic dysfunction.

Many murine models of diastolic dysfunction exhibit diastolic dysfunction in the context of other pathological cardiovascular conditions. Some demonstrate diastolic dysfunction secondary to some other condition, such as hypertension or diabetes. Some display diastolic dysfunction as merely one part of some other complicated disease, such as the cardiac muscle protein mutations that contribute to FHC, arrhythmias, and sudden cardiac death. Finally, many of these models are complicated models of diastolic dysfunction because there is a component of systolic dysfunction

present. Based on these studies, it is likely that diastolic dysfunction is a complicated pathological condition, and that there are multiple pathways that lead to the same clinical manifestation of impaired LV relaxation characteristic of diastolic dysfunction. As of yet, there has not been a model that demonstrates pure diastolic dysfunction that arises spontaneously and is not a downstream effect of another condition. Such a model could provide great mechanistic insight into the process of how diastolic dysfunction is initiated and develops, and perhaps illuminate potential interventional strategies.

The senescence-accelerated mouse (SAM) model

1.7 Development and characterization of the SAM model

The senescence-accelerated mouse, or SAM as it is commonly known, is comprised of a group of related inbred strains of mice, and it is a unique model for senescence acceleration and age-associated disorders. Senescence is defined by four characteristics; changes in the organism that occur with advancing age must be universal, irreversible, intrinsic, and deleterious. The accelerated senescence-prone (SAMP) strains undergo accelerated senescence, which is characterized by an increased rate of aging, as opposed to premature senescence, which is characterized by an early onset of aging but normal rate of aging. The accelerated senescence-resistant (SAMR) strains age normally. In the study of age-associated disorders, some are age-related, meaning they tend to occur in older organisms, while others are age-dependent, meaning they are inherent to the process of aging. The SAM model is useful in the study of age-related disorders such as deficits in learning and memory, cataracts, immunosenescence, osteoporosis, degenerative joint disease, and senile amyloidosis (Chiba et al., 2009).

The SAM strains were derived from the AKR/J strain of mice by continuous sister-brother mating selective for either a tendency toward accelerated senescence or resistance to senescence (Takeda et al., 1981). Mice were retrospectively selected for breeding based on three criteria: degree of senescence at eight months as determined by a specific grading scale, life span, and degree of age-associated disorders (Takeda et al., 1991). Therefore, the SAM model is actually comprised of two series: SAMP for senescence-prone, and SAMR, for senescence-resistant. SAMP mice were created by breeding together mice selected for displaying the most pronounced senescent phenotype, and SAMP mice undergo accelerated senescence. SAMR mice were created by breeding together mice that displayed normal aging, so SAMR mice are normally aging controls. Accelerated senescence refers to the tendency for the SAMP series of mice to experience a more rapid progression of senescence after reaching maturity and a subsequently shorter life span by about 40% (9.7 months) when compared to the SAMR series (Takeda, 1999). The fact that SAMP strains undergo accelerated senescence was concluded based on survivorship curves, Gompertzian function, growth patterns, and a specifically developed grading score; furthermore, these parameters were also used to confirm that these mice underwent accelerated senescence after the developmental period was complete as opposed to premature aging (Takeda et al., 1991). Takeda et al. used a grading score system that assesses mice with respect to such criteria as passive and reactive behavior, skin and hair quality, eye and skin lesions, and lordokyphosis of the spine (Takeda et al., 1981). Further characterization of the mice selected for breeding using this scoring system revealed that SAMP mice are particularly prone to amyloid deposition, cataracts, osteoporosis, memory loss and impaired learning, degenerative joint disease, decreased immune responses, increased lordokyphosis, and various other hallmarks of aging (Hosokawa et al., 1997). Currently, there are 9 SAMP strains and 3 SAMR strains (Takeda et al.,

1997a), and it is noteworthy that each strain seems to have its own unique profile of pathologic changes and phenotypes (Takeda et al., 1997b). For example, the SAMP8 strain is a model of impaired learning and memory, emotional disturbances, abnormal circadian rhythm, immune impairment, and compromised blood-brain barrier function (Chiba et al., 2009). The SAM model is important experimentally because it is the only mouse model of spontaneous accelerated aging, without any experimental manipulation, and it displays most of the common age-associated geriatric disorders seen in the aging human population (Takeda et al., 1997b).

1.8 Oxidative stress in the SAM model

Aging is thought to be influenced, at least in part, by oxidative stress and damage, and accumulating evidence suggests that oxidative stress is an important factor in the aging process in SAM mice. SAMP1 mice have increased lipid peroxidation in their skin as young as 3 -4 months of age. Murine dermal fibroblasts from SAMP11 mice show increased mitochondrial ROS production accompanied by impaired mitochondrial function (Chiba et al., 2009). Edamatsu et al. found that systemic administration of the free radical spin trapping agent N-*tert*-*a*-phenyl-butylnitrone significantly increased the lifespan of SAMP8 mice, suggesting that an overall oxidized state contributes to the early death of these mice (Edamatsu et al., 1995). A potential source of excess $O_2^{\bullet-}$ is mitochondria. Oxidative damage to mitochondria occurring as a result of a lifetime of aerobic metabolism can promote further production of $O_2^{\bullet-}$ by damaged mitochondria. In liver mitochondria from SAMP8 mice, the respiratory control ratio decreased with increasing age. By 18 months of age, the ADP/OI, an index of ATP synthesis efficiency, was decreased as well. To calculate the ADP/OI, mitochondrial respiration was measured in the presence of succinate and inorganic phosphate, then respiration was increased by adding ADP, then respiration decreased, corresponding to

completion of ATP synthesis. In these liver mitochondria from 12-month-old and 18-month-old SAMP8 mice, mitochondrial respiration was more easily uncoupled by administration of dinitrophenol. Calcium transport decreased in liver mitochondria of SAMP8 mice with age, and the addition of exogenous calcium triggered mitochondrial uncoupling in mitochondria from 18-month-old mice. In cardiac mitochondria, state 3 respiration, state 4 respiration, and uncoupled respiration all decreased by 12 months of age (Nakahara et al., 1998). This study by Nakahara et al. did not correlate increased oxidative stress with tissue damage or remodeling, but the possibility exists that this is the case. In a separate study, SAMP8 mice were found to exhibit extensive liver pathology. At 12 months of age, livers from SAMP8 mice displayed signs of fibrosis compared to SAMR1 controls. Fibrosis was accompanied by fatty degeneration, hepatocyte death, inflammatory cell infiltration, and compromised liver function (Ye et al., 2004). Taken together, these two studies suggest the possibility of oxidative stress contributing to tissue damage, fibrosis, and organ dysfunction. Since oxidative stress is influenced by antioxidants as well as ROS, Rebrin et al. looked at the role of glutathione (GSH) in SAM mice. Dietary supplementation with vitamins C and E plus a wide variety of phytochemicals known to induce phase II antioxidant enzymes resulted in decreased serum GSSG and increased plasma cysteine. The GSH/GSSG ratio was increased in homogenates from metabolically active tissues such as the liver and heart. In the skeletal muscle, the mitochondrial GSH/GSSG ratio was increased (Rebrin et al., 2005). While this particular study did not correlate GSH/GSSG ratio with any changes in oxidative status or physiology, it does suggest that perhaps age-related changes in GSH occur, and these could be modified through dietary supplementation. Based on the results of these studies, it appears that the SAM model displays evidence of systemic oxidative stress as well as oxidative stress in specific organs and that antioxidant systems may be altered with aging.

The SAM strains exhibit increased oxidative stress in the brain, which may be related to their tendency to develop neurodegenerative diseases. Specifically, the SAMP8 and SAMP10 strains are common models of neurodegenerative disorders such as Alzheimer's disease. Elevated brain lipid peroxidation was found in SAMP8 mice at 10-12 months of age. Increased oxidative stress and mitochondrial dysfunction has been found in the brains of SAMP8 mice at relatively young ages (1 month to 5 months of age). It is thought that damaged mitochondria produce ROS, and the accumulation of oxidative damage over the life span results in neurological problems. In these mice, treatment with antioxidants has been able to prevent age-associated neurodegeneration, which implies that oxidative stress plays a causative role. In astrocytes cultured from SAMP8 mice, treatment with H_2O_2 significantly reduced cell viability; this suggests that the cells have a decreased ability to detoxify ROS and are thus more susceptible to oxidative damage. SAMP10 mice also showed evidence of increased oxidative stress in the brain; the level of 8-oxo-dG was increased, $O_2^{\bullet-}$ was increased, and the activity of GPX was decreased (Chiba et al., 2009). Using electron spin resonance (ESR) labeling, Butterfield et al. found increased protein oxidation in synaptosomal membrane preparations from SAMP8 mice compared to SAMR1 controls, and it was found that administration of PBN prevented protein oxidation (Butterfield et al., 1997). In the cerebral cortex of SAMP8 mice, increased NOS activity was observed in aged versus young adult mice. Interestingly, there were no differences in $NO^{\bullet}$ levels between the two groups, suggesting that NOS activity is upregulated in an attempt to compensate for $NO^{\bullet}$ being scavenged by $O_2^{\bullet-}$ (Inada et al., 1996). An increase in electron leakage was found in brain mitochondria of SAMP8 mice when compared to SAMR1, and investigators postulate that it is likely that mitochondrial complex III is responsible for excess $O_2^{\bullet-}$ generation (Nishikawa et al., 1998). A rise in lipid peroxidation levels was found in the brains of 5-month-old SAMP8 mice compared to SAMR1, suggesting a more oxidized

state. Furthermore, the increased lipid damage was accompanied by a decrease in SOD activity, indicating that a decrease in an important antioxidant enzyme may be contributing to oxidative stress overall (Alvarez-Garcia et al., 2006).

Taken together, the aforementioned studies strongly suggest that increased production of ROS together with changes in antioxidants and ROS scavengers cause SAMP8 mice to be more oxidized than their SAMR1 counterparts, and that oxidative stress worsens with advancing age. Since oxidative stress contributes to cardiovascular disease in humans, and because the incidence of cardiovascular disease increases with advancing age, the SAM model may be useful for the study of age-related cardiovascular disease and the role played by oxidative stress.

1.9 Cardiovascular diseases in the SAM model

Since cardiovascular disease is strongly associated with aging, a number of investigators have sought to characterize the cardiovascular pathologies of SAM mice such as atherosclerosis and hypertension. Yagi et al. found that the serum lipid peroxide level in SAMP1 mice was significantly higher than in SAMR1 mice at 3 and 5 months of age. Histological analysis revealed an accumulation of macrophage-like cells beneath the endothelium of the aorta, which is an early change indicative of atherosclerosis. These observations seem to suggest that lipid peroxidation causes atherosclerosis (Yagi et al., 1995). Expanding upon this work, Fenton et al. (Fenton et al., 2004) also found evidence of early atherosclerosis in SAMP8 mice. Mice were fed a Western-style diet (21% fat as compared to 4.3% fat for standard diet), and exhibited increased total cholesterol, high-density lipoprotein, and triglycerides. SAMP8 mice, when compared to SAMR1 mice, developed a greater number of fatty lesions in the aortic root, and these lesions were larger in size and more likely to be infiltrated by macrophages, indicating a greater predisposition to early atherosclerosis. In a different

study that focused on the effect of aging on blood pressure, Zhu et al. (Zhu et al., 2001) found a greater increase in aortic wall thickness in SAMP11 mice as compared to SAMR1 mice. Additionally, other changes such as disorganization of elastic lamellae, an increase in collagen, and smooth muscle cell hypertrophy with a decrease in the total number of smooth muscle cells, were both more pronounced and occurred earlier in the lifespan of SAMP11 mice. At 12 months of age, SAMP11 mice exhibited a significantly higher systolic blood pressure. Changes in vascular function have also been observed. Llorens et al. (Llorens et al., 2007) found that vascular smooth muscle contractility in response to both potassium chloride and phenylephrine stimulation was increased in aortas from 6-month-old SAMP8 mice compared to SAMR1 mice. Vascular smooth muscle relaxation in response to acetylcholine was slightly but significantly decreased in SAMP8 vessels, and $NO^{\bullet}$-dependent relaxation was impaired as well, suggestive of endothelial dysfunction. Malondialdehyde, a marker of ROS-mediated lipid peroxidation, was increased in aortas from SAMP8 mice. Taken together, these data suggest that SAMP8 mice show increased vascular reactivity and diminished relaxation, and these changes may result from oxidative damage and endothelial dysfunction. Collectively, these studies demonstrate that the SAM model exhibits vascular changes characteristic of aging.

The SAM model also shows cardiac changes associated with aging. In a study by Forman et al. (Forman et al., 2010), tumor necrosis factor-alpha and interleukin-1, both markers of inflammation, were increased in the hearts of SAM8 mice at 10 months of age compared to SAMP8 mice at 2 months of age. Inducible NOS (iNOS) was increased in the hearts of both SAMR1 and SAMP8 mice at 10 months of age versus 2 months of age, and the increase was markedly greater in SAMP8 mice. In the hearts of SAMR1 mice, endothelial NOS (eNOS) increased from 2 to 10 months of age, but it decreased in SAMP8 mice. Interleukin-10 was lower in the hearts of SAMP8 mice

compared to SAMR1 mice at both 2 and 10 months of age. Nuclear factor-kappa B, which can function as a mediator of cellular response to oxidative stress, was increased in the hearts of SAMP8 mice at 10 months of age compared to 2 months of age and SAMR1 mice at either time point. Taken together, these data suggest a pro-inflammatory state of the myocardium in aged SAMP8 mice that may be associated with alterations in NO production and oxidative stress. Increased cardiac oxidative stress has also been found in the SAM model. Rodriguez et al. found increased lipid peroxidation in cardiac mitochondria from 10-month-old female SAMP8 mice compared to 5 month old SAMP8 mice and SAMR1 controls. GPX was increased in SAMP8 mice at 5 months of age; by 10 months of age, it decreased to a level comparable to that observed in SAMR1 mice. Glutathione reductase decreased in both SAMR1 and SAMP8 mice from 5 to 10 months of age. In cardiac mitochondria from SAMR1 mice, the GSH/GSSG ratio decreased from 5 to 10 months of age, and in SAMP8 mice, the ratio was lower at 5 months of age and continued to decline by 10 months of age. The changes in mitochondrial GSH balance were accompanied by changes in the activity of mitochondrial complexes II, III, and IV. Mitochondrial complex II activity decreased with age in both SAMR1 and SAMP8 mice. Complex III and IV activity decreased with age in SAMP8 mice while activity remained unchanged in SAMR1 mice. Finally, ATP production was diminished in the cardiac mitochondria of aged SAMP8 mice compared to young SAMP8 mice and SAMR1 controls. These data suggest that SAMP8 mice have increased cardiac oxidative stress, it worsens with increasing age, and the mitochondria contribute significantly to the production of ROS (Rodriguez et al., 2007a) (Rodriguez et al., 2007b).

Objectives of this dissertation

The overall objective of this research has been to investigate potential mechanisms that lead to the development of age-associated diastolic dysfunction in a mouse model of spontaneous accelerated senescence. The first objective was to establish the presence of diastolic dysfunction in the SAM model. Next, the role of cardiac fibrosis was examined as a pathophysiological characteristic and potential mechanism of diastolic dysfunction. Because of the role of fibroblasts in tissue fibrosis, the next objective was to examine the role of the cardiac fibroblasts in cardiac fibrosis observed in SAM mice. Finally, a related objective was to examine the potential role played by oxidative stress in age-associated diastolic dysfunction and tissue fibrosis in the SAM model.

Chapter 2:

The SAM model is a model of age-related diastolic dysfunction

2.1 Introduction

Heart failure is a major and growing public health concern in the United States; there are an estimated 5 million people living with this disease, and another 550,000 patients will be diagnosed yearly (Brutsaert, 2003). Approximately half of all heart failure patients in the United States suffer from diastolic heart failure, and it is a major cause of mortality in the elderly population (Zile and Brutsaert, 2002a). Diastolic heart failure describes a group of patients whose clinical manifestation of congestive heart failure is characterized by normal left ventricular diastolic volume, a normal ejection fraction, delayed active relaxation, and increased passive stiffness of the left ventricle (Zile et al., 2005). Diastolic dysfunction precedes diastolic heart failure and is often clinically silent; it is characterized by abnormal ventricular distensibility, relaxation, and filling (Aurigemma and Gaasch, 2004). Both diastolic dysfunction and diastolic heart failure are most common in the elderly population. In a study that examined the prevalence of this form of heart failure, 50% of patients over the age of 70 showed evidence of diastolic heart failure. Studies indicate that the most important determinants for development of diastolic dysfunction and diastolic heart failure are age and hypertension (Zile and Brutsaert, 2002a).

While well-established murine models exist to study such common cardiovascular diseases as hypertension, atherosclerosis, and congestive heart failure, a model of isolated age-related diastolic dysfunction has yet to be established and characterized (Taffet et al., 1997). Previous studies have established that the ratio of early to late mitral filling velocity is decreased in aged wild-type mice and that caloric restriction improves diastolic function in aged mice (Taffet et al., 1997), but there has not been a model of pure spontaneous diastolic dysfunction or a model that has established the connection between age-related diastolic dysfunction and fibrosis. Since advancing age is such an important risk factor for the development of this pathophysiological

condition, the SAM model, a murine model of spontaneous senescence that displays many common geriatric disorders in the human population, was used for these studies (Hosokawa et al., 1997; Takeda, 1999; Takeda et al., 1981; Takeda et al., 1997b). This model was derived from the AKR/J strain of mice by continuous sister-brother mating selecting for a tendency toward either accelerated or normal senescence; breeders were retrospectively chosen based on the degree of senescence at eight months as determined by life span and clinical signs of aging (Takeda et al., 1981). The SAM model is comprised of the senescence-prone and control senescence-resistant strains. Accelerated senescence refers to the tendency of SAMP mice to experience a rapid progression of senescence after reaching maturity and a shorter life span by about 40% when compared to the SAMR series (Takeda, 1999). Though some variability exists with respect to life span of these mice, the median life span of SAMR1 mice has been reported to be between 12 and 21 months of age, and the median life span of SAMP8 mice has been reported as 10 to 17 months of age (Flood and Morley, 1998). While these mice display a number of pathological changes at autopsy after their natural death, including pneumonia, abscess, colitis, amyloidosis, contracted kidney, neoplasms, and a number of other abnormalities, the most likely causes of death in SAMP8 mice are lymphoid neoplasms and contracted kidney (Takeda et al., 1997b). Of all the SAM strains, SAMR1 and SAMP8 strains are the most studied strains with respect to cardiovascular disease and oxidative stress. Based on the knowledge that diastolic dysfunction is associated with aging, the hypothesis is that SAMP8 mice will develop diastolic dysfunction.

2.2 Methods

Animal maintenance

SAMR1 and SAMP8 mice were purchased from Harlan (Indianapolis, IN). All experiments were carried out using 3-month-old, 6-month-old, and 12-month-old male mice. All experiments were approved by the Atlanta VA Institutional Animal Care and Use Committee (protocol approval number V018-03). The investigation conforms to the *Guide for the Care and Use of Laboratory Animals* published by the US National Institutes of Health.

RNA isolation and quantitative real-time PCR (qRT-PCR)

Total RNA was isolated from LV heart tissue homogenates using a chloroform-phenol-based extraction procedure. It was reverse transcribed using the SuperScript II kit (Invitrogen, Carlsbad, CA) and random nanomer primers. Expression of p19 and 18S RNA was measured by amplification of cDNA using a LightCycler real-time thermocycler (Roche Diagnostics Corp, Indianapolis, IN). Primer sequences 5' to 3' were p19 (+1) TGAGGCTAGAGAGGATCTTGAGA and p19 (-2) TTGAGCAGAAGAGCTGCTACGT. Transcripts were detected using SYBR Green I (Invitrogen, Carlsbad, CA) and were normalized to 18S RNA.

Assessment of cardiac dimensions and diastolic function using echocardiography

Echocardiography studies were completed as described previously (Silberman et al., 2010). Mice were anesthetized with 4% isoflurane, hair was removed from the thorax, and they were maintained under light anesthesia (1-1.5% isoflurane) at approximately 37°C and demonstrated a physiological heart rate >500 bpm during the procedure. Two-dimensional and M-mode transthoracic echocardiography modalities were used to

assess wall motion, chamber dimensions, and wall thickness and to calculate percent fractional shortening (FS), SV, and EF. Pulsed-wave Doppler echocardiography was used to measure early (E) and late (A) blood flow velocities through the mitral valve. Tissue Doppler imaging was used to measure the early (E') and late (A') velocity of the mitral annulus. For each measurement, at least 3 beats were averaged per measurement, at least 3 measurements were taken per animal, and beats were taken at end expiration. Studies were reviewed by two different investigators, one of which was blinded. Inter-observer variability was based on 6 studies and was 9.7% ± 0.8%. Intra-observer variability was also based on 4 studies and was 7.8% ± 0.9%. Measurements were made using a VisualSonics® Vevo 770TM in-vivo micro-imaging system equipped with a RMV-707B cardiovascular scanhead (Toronto, ON). Different groups of mice were used for studies carried out at 3, 6, and 12 months of age.

Assessment of cardiac function using invasive hemodynamics

Invasive hemodynamic studies were performed as described previously using a closed-chest procedure (Simpson et al., 2007). Mice were anesthetized with 1-2% isoflurane. An initial intraperitoneal bolus injection of 0.3 mL normal saline was given, and the body temperature was maintained at 37-38°C during the procedure. After a single dose of pancuronium (0.12 mg/kg IV) through left jugular vein, the mechanical ventilation (MA1 55-7059, Harvard Apparatus, Holliston, Massachusetts, USA) was started via tracheoectomy with a rate of 118-133 breaths per minute and a tidal volume of 0.19-0.28 mL. A pressure-volume catheter (SPR-839, Millar Instruments, Houston, TX, USA) was inserted into the right common carotid artery and advanced into the LV. Inferior vena cava occlusion was performed via a midline abdominal incision. Volume and parallel conductance calibration were performed as previously described (Yang et al., 2001). The end-diastolic pressure volume points were fitted using the following linear function:

LVEDP = LVEDPVR x LVEDV + intercept (for both groups combined: median r^2= 0.97 ± 0.04; range 0.84 to 0.99). The group of mice used for invasive hemodynamic studies was separate from the group used for echocardiography; however, all mice were 6 months old at the time of study.

Measurement of sarcomere length shortening and relengthening

The mechanical properties of the cardiomyocytes were assessed using an IonOptix Myocam System (Ionoptix Inc., Milton, MA). Unloaded cardiomyocytes were placed on a glass slide and allowed to adhere for 10 minutes. Cardiomyocytes were then imaged with an inverted microscope and perfused with a normal Tyrode's solution containing 1.2 mmol/L $CaCl_2$ at 37°C by temperature controller and heater (mTC-II, Ionoptix Inc., Milton, MA). Cardiomyocytes were paced at 1.0 Hz for 4 ms duration, and sarcomere shortening and relengthening were assessed using the following indices: peak fractional shortening (FS), time to 90% peak shortening, and τ, the relaxation time constant ($a_0+a_1e^{t/\tau}$, t = time). Cardiomyocytes (47-59) from 5-6 different mice were used to measure sarcomere shortening. A separate group of 6-month-old male mice was used for sarcomere length shortening measurements.

Acquisition of blood pressure data using telemetry

Blood pressure was measured as described previously (Kleinhenz et al., 2009). Anesthesia was induced using 4% isoflurane and maintained at 1-1.5% isoflurane. A 2-cm ventral incision was made from the chin to the sternum, and the carotid artery was isolated by blunt dissection. A 25-guage bent needle was used to cannulate the artery with a sterile TA11PA-C10 transmitter (Data Sciences International, St. Paul, MN). The catheter connected to the transducer was advanced into the thoracic aorta and held in place with sutures, and the transmitter was positioned along the right flank, close to the

hindlimb. Mice were allowed to recover for 1 week prior to initiation of monitoring. Blood pressure measurements were telemetrically collected for 10 seconds each minute during a 24-hour period at the baseline time point of 3 months of age, and then weekly up to 6 months of age. The group of mice used for telemetry was separate from the groups used for echocardiography and invasive hemodynamics.

Measurement of lung weight and right/left ventricle weight ratio

Lungs (n=6) were explanted, rinsed in phosphate-buffered saline (PBS), blotted semi-dry, and weighed to obtain the wet weight of the lungs. Whole hearts were explanted (n=6) and dissected in PBS. The right ventricle (RV) was dissected apart from the LV plus the septum, and each part was weighed and the ratio calculated from wet weights of tissue (RV/LV+S ratio).

Measurement of right ventricular systolic pressure (RVSP) using a pressure-transducing catheter

RVSP was measured in isoflurane-anesthetized mice (n=6) using an SPR-671 Mikro-Tip® pressure catheter (Millar Instruments, Houston, TX). The catheter was inserted into the jugular vein and advanced into the right ventricle for pressure recordings. Data acquisition and analysis were accomplished using Chart 5^{TM} software in conjunction with a PowerLab® data acquisition unit (ADInstruments, Colorado Springs, CO).

Statistical Analysis

Data are represented as the mean ± standard error and are compared using the Student's *t*-test when SAMR1 and SAMP8 mice are being compared for 6-month time point studies. A two-way ANOVA is used when SAMR1 and SAMP8 mice are being compared for 3-month and 6-month studies. Bonferroni post-hoc tests were used to

determine significance of specific pair-wise comparisons. A p value <0.05 is considered statistically significant.

2.3 Experimental results

SAMP8 mice show accelerated senescence at 6 months of age.

To determine if the SAMP8 mice have accelerated senescence, levels of $p19^{ARF}$ also known as ARF, a tumor suppressor protein encoded by the *INK4a/ARF* locus regulating the p53 pathway by stabilizing p53, were measured. Since senescence requires activation of the p53 pathway, elevated $p19^{ARF}$ is consistent with aging and accelerated senescence (Sharpless, 2004). $p19^{ARF}$ is increased in 6-month-old SAMP8 mice compared to SAMR1 controls as measured by qRT-PCR (Figure 2.1).

Figure 2.1. Gene expression of p19. p19 expression was measured by qRT-PCR normalized to 18S copy number in cardiac samples from 6-month-old SAMR1 and SAMP8 mice. SAMP8 mice showed accelerated senescence at 6 months of age as confirmed by p19, a marker of senescence (n=7, **p*<0.05). Figure generated with the assistance of Atsuko Tanaka.

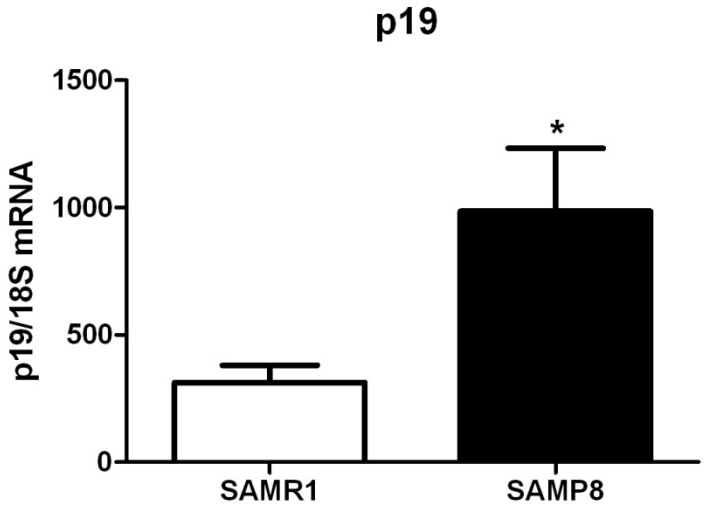

SAMP8 mice show diastolic dysfunction by 6 months of age.

Echocardiography

At 6 months of age, SAMP8 mice display echocardiographic evidence of diastolic dysfunction compared to SAMR1 controls. Using conventional pulsed-wave Doppler echocardiography, the ratio of early to late mitral inflow velocity (E/A) is reduced in SAMP8 mice compared to SAMR1 controls (1.2 ± 0.03 *vs.* 1.3 ± 0.03. $p<0.05$). Tissue Doppler imaging was used to measure the mitral valve annulus velocity. In SAMP8 mice, the tissue mitral annulus early longitudinal velocity (E') is reduced compared to SAMR1 controls (21.1 ± 0.8 *vs.* 25.7 ± 0.9 mm/s, $p<0.05$). Likewise, the ratio of early to late tissue mitral annulus velocities (E'/A') is reduced in SAMP8 mice (0.8 ± 0.03 *vs.* 1.1 ± 0.02, $p<0.05$) (Table 2.1). The dependency of the phenotype upon age was confirmed with echocardiographic studies performed at 3 months of age that showed no differences in diastolic function (Table 2.1). Furthermore,12-month-old SAMR1 and SAMP8 mice were studied to more solidly establish that diastolic dysfunction in the model is age-related. Similar to the findings at 6 months of age, the E'/A' ratio is reduced in SAMP8 mice compared to SAMR1 controls (0.8 ± 0.03 *vs.* 1.0 ± 0.04, $p<0.05$) (Table 2.2). In addition, when diastolic function was compared between both types of mice at 6 and 12 months of age, it seemed that diastolic function remains impaired in SAMP8 mice at 12 months of age, and in SAMR1 mice at 12 months of age, E'/A' decreases to a level comparable to SAMP8 mice at 6 months of age. So, it appears that with advancing age, SAMR1 mice begin to display evidence of diastolic dysfunction, further supporting the observation that diastolic dysfunction is related to aging.

Conventional M-mode echocardiography was used to measure cardiac dimensions. There are no differences in LV dimensions between SAMR1 and SAMP8 mice during either systole or diastole. Furthermore, the SV (44.5 ± 1.0 *vs.* 45.7 ± 2.2 μL,

p=NS), the EF (64.3 ± 1.5 *vs.* 65.0 ± 1.2. %, p=NS), and the FS (34.7 ± 1.1 *vs.* 35.3 ± 0.8 %, p=NS) are unchanged between SAMP8 and SAMR1 mice, respectively, suggesting that changes in diastolic function could not be explained by changes in systolic function (Table 2.1).

Table 2.1. Echocardiographic comparison of SAMR1 and SAMP8 mice at 3 and 6 months of age. LV, left ventricle; LVID;s, systolic LV internal diameter; LVID;d, diastolic LV internal diameter; LVESV, LV end-systolic volume; LVEDV, LV end-diastolic volume; LVWT, LV wall thickness; SV, stroke volume; EF, percent ejection fraction; FS, percent fractional shortening; E/A, ratio of early to late diastolic filling measured by pulsed-wave Doppler; E', mitral annulus velocity during early diastole measured by tissue Doppler imaging (TDI) ; A', mitral annulus velocity during late diastole measured by TDI; E'/A', ratio of mitral annulus velocities during early and late diastolic filling. Values were compared between SAMR1 and SAMP8 groups at 3 and 6 months of age. *$p < 0.05$ when comparison made between SAMR1 and SAMP8 mice of the same age, and §$p < 0.05$ when comparison made between the same type of mice at 3 and 6 months of age.

	SAMR1 at 3 months	**SAMP8 at 3 months**	**SAMR1 at 6 months**	**SAMP8 at 6 months**
	(n=7)	(n=7)	(n=8)	(n=8)
Body weight (g)	29.0 ± 0.3	30.7 ± 0.5	§ 39.1 ± 1.1	*§ 42.3 ± 1.0
LV weight (mg)	82.0 ± 2.2	* 90.5 ± 2.3	§ 110.4 ± 1.9	*§ 120.0 ± 2.2
LV/body weight	2.8 ± 0.05	2.9 ± 0.4	2.8 ± 0.07	2.9 ± 0.08
Heart rate (bpm)	550 ± 25	550 ± 25	550 ± 25	550 ± 25
LV dimensions				
LVID;s (mm)	2.9 ± 0.07	2.7 ± 0.1	2.6 ± 0.07	2.6 ± 0.07
LVID;d (mm)	4.0 ± 0.05	4.0 ± 0.1	4.0 ± 0.06	4.0 ± 0.08
LVESV (μL)	32.3 ± 1.8	28.1 ± 2.8	25.1 ± 1.7	24.8 ± 1.7
LVEDV (μL)	71.6 ± 2.2	70.9 ± 4.7	69.7 ± 2.3	70.5 ± 3.6
LVWT (mm)	0.8 ± 0.01	*1.0 ± 0.03	0.7 ± 0.04	0.9 ± 0.03
Systolic				
SV (μL)	39.3 ± 1.2	42.7 ± 2.7	44.5 ± 1.0	45.7 ± 2.2
EF (%)	55.0 ± 1.6	60.5 ± 2.0	64.3 ± 1.5	65.0 ± 1.2
FS (%)	28.3 ± 1.1	32.0 ± 1.4	34.7 ± 1.1	35.3 ± 0.8
Diastolic				
E/A	1.4 ± 0.03	1.4 ± 0.04	1.3 ± 0.03	*§ 1.2 ± 0.03
E' (mm/s)	28.1 ± 1.03	30.8 ± 2.0	25.7 ± 0.9	§ 21.1 ± 0.8
A' (mm/s)	20.7 ± 0.9	20.8 ± 1.7	23.3 ± 0.8	§ 25.8 ± 1.1
E'/A'	1.4 ± 0.03	1.4 ± 0.04	§ 1.1 ± 0.02	*§ 0.8 ± 0.03

Table 2.2. Echocardiographic comparison of SAMR1 and SAMP8 mice at 12 months of age. LV, left ventricle; LVID;s, LV internal diameter during systole; LVID;d, LV internal diameter during diastole; LVESV, LV end-systolic volume; LVEDV, LV end-diastolic volume; LVWT, LV wall thickness; SV, stroke volume; EF, percent ejection fraction; FS, percent fractional shortening; E/A, ratio of early to late diastolic filling measured by pulsed-wave Doppler; E', mitral annulus velocity during early diastole measured by tissue Doppler imaging (TDI); A', mitral annulus velocity during late diastole measured by tissue Doppler imaging; E'/A', ratio of mitral annulus velocities during early and late diastolic filling measured by TDI. Values were compared between SAMR1 and SAMP8 groups at 6 months of age. * $p < 0.05$.

	SAMR1 at 12 months	**SAMP8 at 12 months**
	(n=6)	(n=6)
Body weight (g)	50.5 ± 1.4	* 44.7 ± 1.8
LV weight (mg)	146.5 ± 2.6	144.9 ± 2.8
LV/body weight	2.9 ± 0.06	* 3.3 ± 0.17
Heart rate (bpm)	550 ± 25	550 ± 25
LV dimensions		
LVID;s (mm)	2.8 ± 0.14	2.9 ± 0.12
LVID;d (mm)	4.2 ± 0.09	4.3 ± 0.09
LVESV (μL)	32.6 ± 3.6	34.0 ± 3.5
LVEDV (μL)	80.7 ± 3.8	83.8 ± 4.1
LVWT (mm)	1.03 ± 0.05	1.00 ± 0.05
Systolic		
SV (μL)	48.0 ± 1.42	49.8 ± 1.8
EF (%)	60.2 ± 2.9	59.8 ± 2.5
FS (%)	32.0 ± 2.0	31.7 ± 1.7
Diastolic		
E/A	1.1 ± 0.04	1.1 ± 0.04
E' (mm/s)	22.9 ± 0.7	22.8 ± 0.9
A' (mm/s)	22.9 ± 0.9	25.3 ± 1.1
E'/A'	1.0 ± 0.04	* 0.8 ± 0.03

Invasive hemodynamics

To confirm the echocardiographic observations, invasive hemodynamics studies were conducted, and as expected, SAMP8 mice display hemodynamic evidence of diastolic dysfunction compared to SAMR1 controls. Compared to SAMR1 mice at 6 months of age, SAMP8 mice have an increased LVEDP (5.6 ± 0.9 *vs.* 3.4 ± 0.3 mmHg, $p<0.05$). Additionally, transient occlusion of the inferior vena cava was used to generate a family of pressure-volume loops at varying volumes. The LVEDPVR is represented as the slope of the best-fitting line connecting the end-diastolic pressure-volume points, and it represents the passive physical properties of the LV (Burkhoff et al., 2005). Consistent with the data demonstrating diastolic dysfunction, the slope of the LVEDPVR is increased in SAMP8 mice compared to SAMR1 controls (0.8 ± 0.1 *vs.* 0.5 ± 0.05 mmHg/μL, $p<0.05$) (Table 2.3). No differences were observed in dP/dt_{min}, the maximal slope of ventricular pressure decline during diastole or in τ_{Glantz}, τ_{Weiss}, or $t_{1/2}$, three different ways of assessing LV pressure decay, however, suggesting that the pressure-volume relation, and hence passive diastole, but not active relaxation, is affected in the model. Arterial elastance (Ea) and the ventricular-vascular coupling ratio (Ea/Es) were measured to determine whether abnormal ventricular-vascular coupling could account for the changes in cardiac function that were observed. There were no differences between SAMP8 and SAMR1 mice in Ea (8.8 ± 1.1 *vs.* 7.0 ± 0.5) or Ea/Es (1.2 ± 0.2 *vs.* 1.3 ± 0.2), respectively, suggesting changes are not the result of altered ventricular-vascular coupling.

Table 2.3. Invasive hemodynamic comparison of SAMR1 and SAMP8 mice at 6 months of age. HR, heart rate; LVESV, LV end-systolic volume; LVEDV, LV end-diastolic volume; LVESP, LV end-systolic pressure; LVEDP, LV end-diastolic pressure, dP/dt_{max}, maximal slope of left ventricular pressure rise during systole; dP/dt_{min}, maximal slope of left ventricular pressure decline during diastole; dP/dt_{EDV}, dP/dt divided by end-diastolic volume; Ea, arterial elastance; Ea/Es, ventricular-vascular coupling ratio; τ_{Glantz}, time constant of pressure decay by the Glantz method; τ_{Weiss}, time constant of pressure decay by the Weiss method; $t_{1/2}$, time interval of the pressure decay to 50% of peak pressure; LVEDPVR, LV end-diastolic pressure-volume relationship; LVESPVR, LV end-systolic pressure-volume relationship; PRSW, preload recruitable stroke work. * $p < 0.05$. Table generated with the assistance of Hong Liu.

	SAMR1	**SAMP8**
	(n=11)	(n=8)
Baseline HR (bpm)	603.1 ± 12.05	583.4 ± 11.41
LVESV (μL)	10.23 ± 0.93	* 4.27 ± 1.18
LVEDV (μL)	19.91 ± 1.46	10.93 ± 2.27
LVESP (mmHg)	85.82 ± 3.37	79.50 ± 4.00
LVEDP (mmHg)	3.41 ± 0.28	* 5.59 ± 0.93
dP/dt_{max} (mmHg/sec)	8093 ± 721.2	7534 ± 787.7
dP/dt_{min} (mmHg/sec)	-9138 ± 831.8	-9089 ± 1055
dP/dt_{EDV} (mmHg/sec)	461.7 ± 68.00	624.5 ± 102.5
Ea (mmHg/μL)	6.95 ± 0.45	8.79 ± 1.10
Ea/Es	1.30 ± 0.16	1.23 ± 0.18
τ_{Glantz} (ms)	8.50 ± 0.59	8.66 ± 0.66
τ_{Weiss} (ms)	5.09 ± 0.26	5.73 ± 0.43
$t_{1/2}$	4.10 ± 0.21	4.20 ± 0.30
LVEDPVR (mmHg/μL)	0.49 ± 0.05	* 0.79 ± 0.14
LVESPVR (mmHg/μL)	5.90 ± 0.59	7.87 ± 1.00
PRSW	72.11 ± 8.39	65.40 ± 11.47

SAMP8 mice do not show differences in myocyte contraction or relaxation at 6 months of age.

Since diastolic dysfunction could be caused by impairment in the relaxation of cardiac myocytes, sarcomere length shortening and relengthening were assessed. Relaxation was measured in freshly isolated ventricular cardiomyocytes at 1.0 Hz stimulation and 37°C. The baseline sarcomere length of cardiac myocytes is modestly shorter in SAMP8 mice compared to SAMR1 mice (1.72 ± 0.01 μM *vs.* 1.78 ± 0.01 μm, $p<0.05$) (Figure 2.2A). Nevertheless, there are no significant differences in FS (12.42 ± 0.67% *vs.* 12.43 ± 0.48%), time to 90% peak shortening (0.33 ± 0.01 seconds *vs.* 0.33 ± 0.01 seconds), and τ, the relaxation time constant (0.13 ± 0.01 *vs.* 0.12 ± 0.01) between SAMR1 and SAMP8 mice, respectively (Figure 2.2B-D). This suggests that diastolic dysfunction observed in this model is not the result of changes in cardiomyocyte function.

Figure 2.2. Functional analysis of isolated cardiomyocytes. (A) The mean of diastolic sarcomere length was significantly shorter in cardiomyocytes from SAMP8 compared to SAMR1 at 6 month of age (n=53, 59, $*p < 0.05$) (B) Fractional shortening (FS) of isolated cardiomyocytes paced at 1.0 Hz at 37°C represented as the peak shortening divided by the baseline sarcomere length (n=53, 59, *p*=NS). (C) Time to 90% peak contraction in isolated cardiomyocytes (n=47, 51, *p*=NS). (D) Isolated cardiomyocytes from SAMP8 mice have a prolonged τ compared to SAMP1 mice (n=53, 59, *p*=NS). Figure generated with the assistance of Euy-Myoung Jeong and Megan Sturdy.

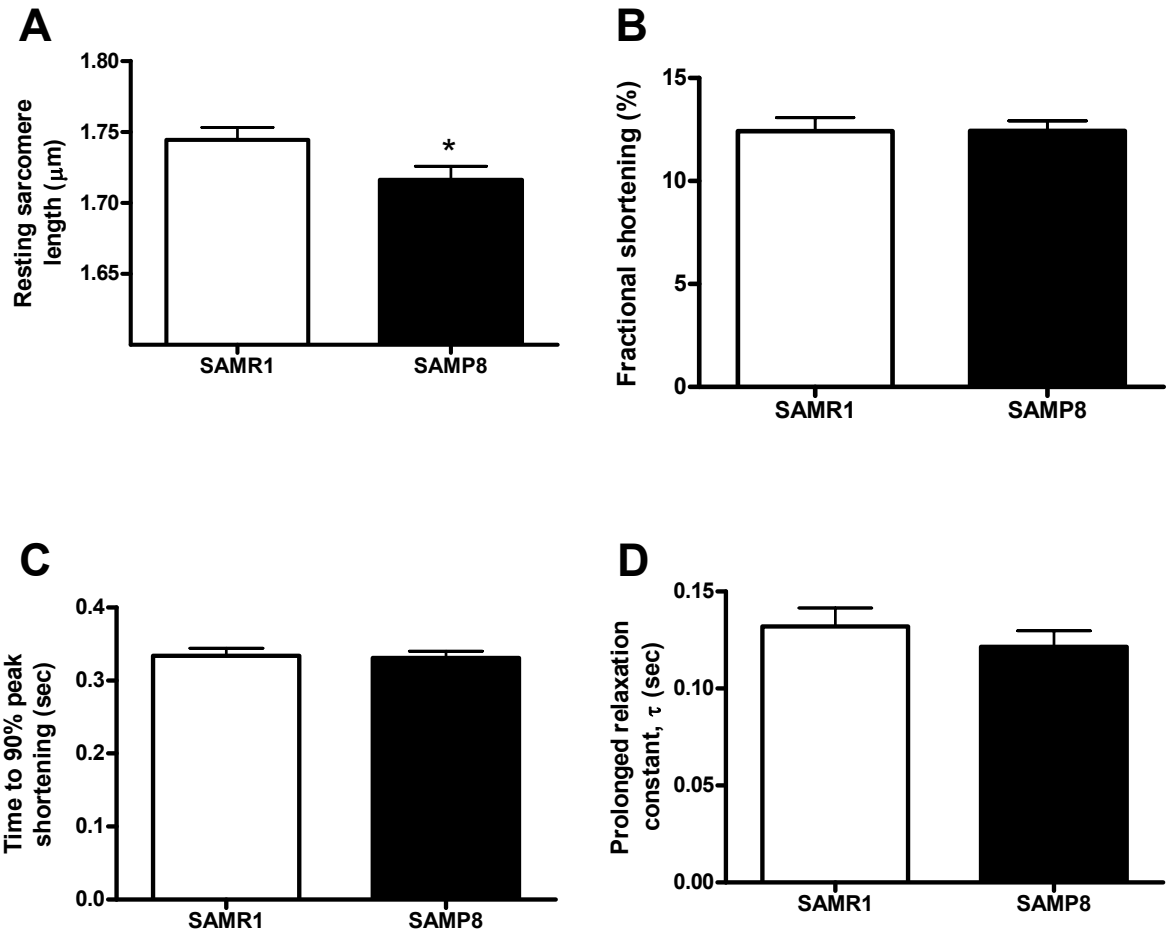

SAMP8 mice do not show differences in blood pressure from 3 to 6 months of age.

Since hypertension is an established risk factor for the development of diastolic dysfunction (Zile and Brutsaert, 2002a; Zile and Brutsaert, 2002b), mean arterial pressure was measured by telemetry in SAMR1 and SAMP8 mice from 3 through 6 months of age. There are no differences in mean arterial pressure between the two groups of mice at any time point, and there is no change in pressure over the 3-month course of measurement (Figure 2.3). Therefore, changes in diastolic function observed were independent of blood pressure changes.

Figure 2.3. Blood pressure in SAM mice. Mean arterial pressure was measured from 3 to 6 months of age using telemetry. Pressure was not different between SAMR1 and SAMP8 mice at any time point (n=5,. *p*=ns). Figure generated with the assistance of Erik Walp.

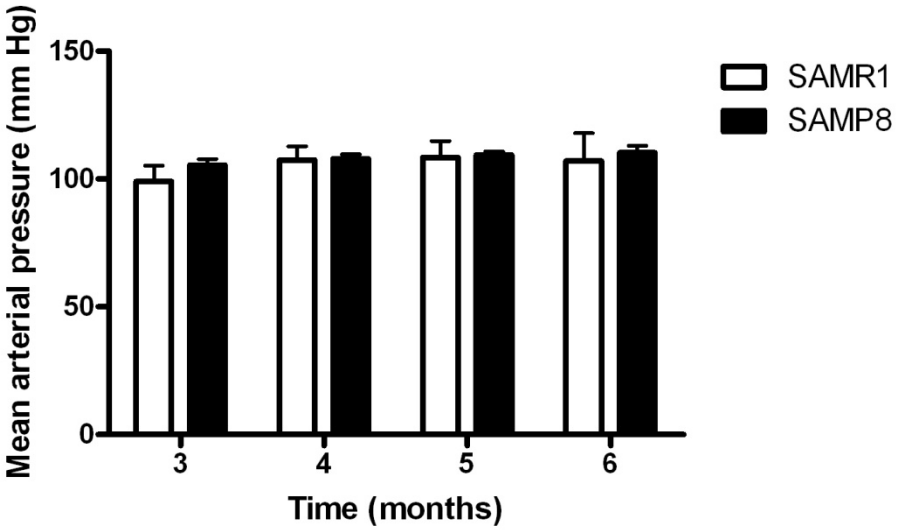

Body and metabolic characteristics of SAM mice

Since the SAM model develops other pathologies in addition to those related to cardiac function and because cardiac and renal function are often interrelated, the metabolic profiles of SAM mice at 6 months of age were examined. Plasma blood urea nitrate (BUN) was 15.9 ± 0.5 in 6-month-old SAMR1 mice and was only mildly elevated to 17.8 ± 0.4 in SAMP8 mice. Plasma creatinine was unchanged in SAMR1 versus SAMP8 mice (0.21 ± 0.01 *vs.* 0.20 ± 0.0) (Table 2.4). Finally, the diastolic dysfunction observed did not progress fully to diastolic heart failure; no difference between lung weights between SAMR1 and SAMP8 mice at 6 months of age was observed (Figure 2.4).

Table 2.4. Metabolic profile of SAM mice at 6 months of age.

	SAMR1 (n=8)	**SAMP8** (n=8)
Na^+ (mM)	155.0 ± 0.5	154.4 ± 0.7
K^+ (mM)	7.6 ± 0.2	7.5 ± 0.2
Ca^{2+} (mg/dL)	10.4 ± 0.2	* 11.0 ± 0.1
Cl^- (mM)	100.3 ± 0.5	* 106.5 ± 0.5
Bicarbonate (mM)	18.6 ± 1.6	20.4 ± 1.4
Glucose (mg/dL)	251.1 ± 11.3	270.0 ± 8.4
BUN (mg/dL)	15.9 ± 0.5	* 17.8 ± 0.4
Creatinine (mg/dL)	0.21 ± 0.01	0.20 ± 0.0
ALP (U/L)	73.3 ± 2.6	65.0 ± 2.9
ALT (U/L)	33.0 ± 2.4	36.4 ± 5.9
AST (U/L)	65.6 ± 7.6	69.3 ± 17.5
Total bilirubin (mg/dL)	0.3 ± 0.02	0.3 ± 0.0
Albumin (g/dL)	1.8 ± 0.04	* 1.7 ± 0.02
Total protein (g/dL)	6.2 ± 0.07	6.3 ± 0.3

Figure 2.4. Pulmonary measurements in SAM mice. The wet weight of the lungs and the weight ratio of the RV/LV+S were measured. The RV systolic pressure was measured using a pressure-transducing catheter. There were no differences in (A) lung wet weight, (B) RV/LV+S ratio, or (C) RVSP between SAMR1 and SAMP8 mice at 6 months of age (n=6, *p*=ns). Figure generated with the assistance of Alex El-Ali.

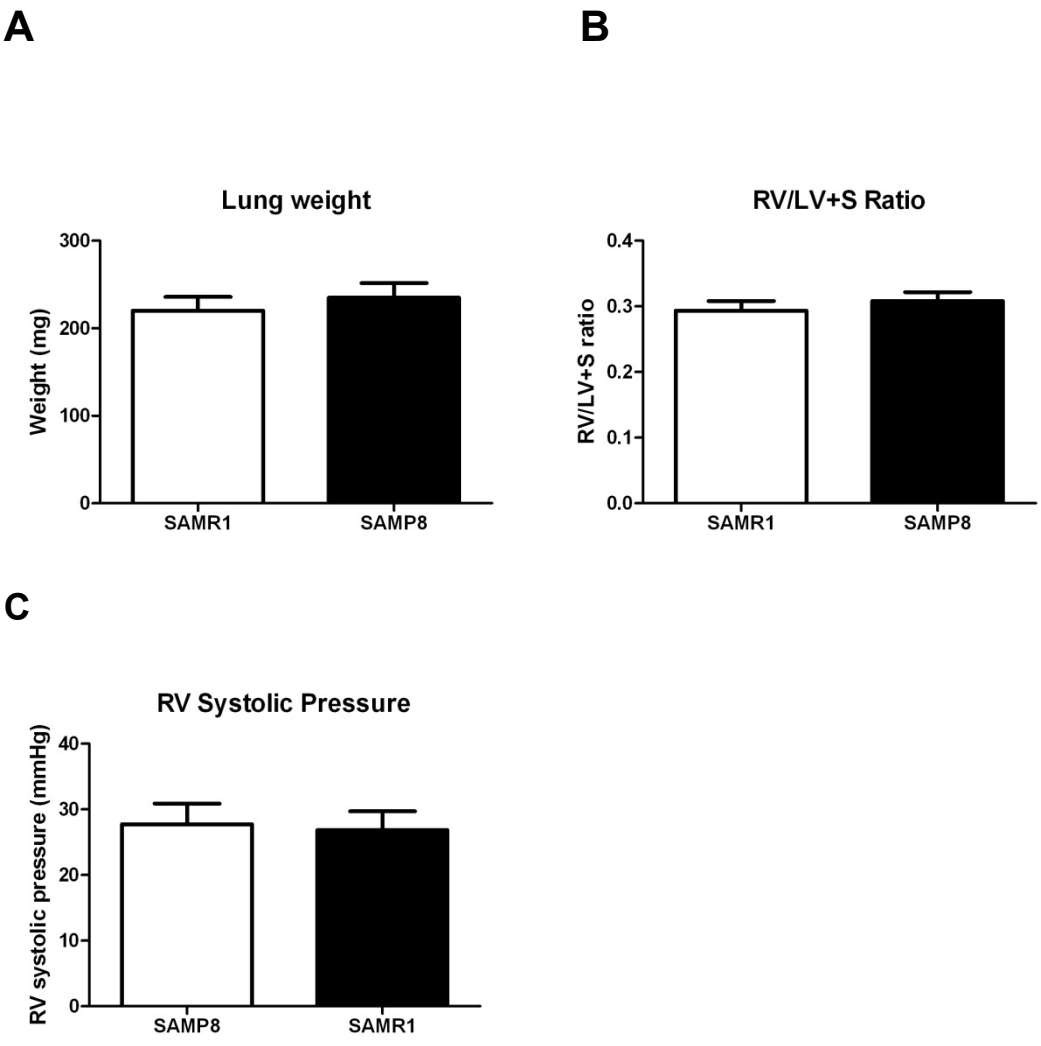

2.4 Discussion

Diastolic heart failure is increasing in prevalence (Schocken et al., 2008). It carries significant morbidity and mortality, and treatment strategies are nonspecific because of a poor mechanistic understanding of the disease (Owan et al., 2006). Diastolic heart failure is characterized by abnormal relaxation of the LV (Aurigemma and Gaasch, 2004). Since diastolic dysfunction is more common in the elderly population, the hypothesis was that the SAM model would show diastolic dysfunction. The present study shows that SAMP8 mice have diastolic dysfunction in the absence of alterations in systolic function using two different modalities, echocardiography and invasive hemodynamics, which were previously found to be well-correlated (Silberman et al., 2010). Additionally, the data demonstrate that diastolic dysfunction can occur in the absence of an increase in blood pressure, perhaps explaining the lack of efficacy of antihypertensive medications in human clinical trials (Cleland et al., 2006; Massie et al., 2008; Yusuf et al., 2003). Since renal function often impacts both blood pressure and cardiac function, plasma metabolic profiles of SAM mice were examined as well and only minor differences in BUN were found between SAMR1 and SAMP8 mice. Taken in combination with the lack of change in blood pressure, it does not appear that renal abnormalities contribute to diastolic dysfunction in this aging model.

Another potential pathophysiologic variable that could contribute to abnormal diastolic function is altered ventricular-vascular coupling. Nevertheless, when Ea and Ea/Es were measured using invasive hemodynamics, no difference was found between the two groups of mice. These data suggest that the diastolic dysfunction observed in this model cannot be explained by increased vascular stiffness or abnormalities in the interaction between the heart and the systemic vasculature.

Another variable that could contribute to abnormal diastolic function is impaired cardiac myocyte relaxation. The baseline sarcomere length of cardiac myocytes,

fractional shortening, time to 90% peak shortening, and the relaxation time constant τ were measured to assess myocyte function. There were no differences in time to 90% peak shortening or τ between SAMR1 and SAMP8 mice, which suggests myocyte relaxation is not impaired and is not responsible for diastolic dysfunction. Taken together, the evidence suggests that the SAM model develops isolated age-related diastolic dysfunction by 6 months of age and could thus be a useful model for continued studies.

While it is recognized that diastolic dysfunction, which is often clinically silent, can progress to diastolic heart failure in humans, in this study diastolic dysfunction did not progress to overt heart failure in the mice by 6 months of age. At 6 months of age, there was no difference in lung weight between SAMR1 and SAMP8 mice, indicating the absence of pulmonary edema secondary to heart failure (Figure 2.4). Nevertheless, the development of diastolic dysfunction by 6 months of age in this model is significant in that it represents a point in the development of the disease where underlying mechanisms of pathology could be studied to investigate possible interventions before heart failure has occurred.

Since an aim of this study was to demonstrate that diastolic dysfunction is an age-dependent pathophysiological development in this model, the cardiac function of SAMR1 and SAMP8 mice at 12 months of age was evaluated. While there were no differences in cardiac structure or systolic function between SAMR1 and SAMP8 mice, there was evidence of diastolic dysfunction in SAMP8 mice, suggesting diastolic impairment continued with aging. Furthermore, a modest decrease in the diastolic function of SAMR1 mice at 12 months of age was observed compared to 3 or 6 months of age, suggesting that as the control mice age further, they begin to show decreases in diastolic function as well. Taken with the absence of diastolic dysfunction at 3 months of

age, this piece of evidence suggests that the diastolic dysfunction we have observed in the SAM model is age-related. In summary, diastolic dysfunction independent of hypertension has been demonstrated in an aging model and, this establishes the SAM model as a viable model for the mechanistic study of age-associated diastolic dysfunction.

Chapter 3:

Diastolic dysfunction is associated with fibrosis in the SAM model

3.1 Introduction

Although the exact molecular mechanisms behind diastolic dysfunction are poorly understood, fibrosis is thought to contribute to its progression. When tissue injury occurs, ECM is deposited by fibroblasts, forming a scar. Specifically, myofibroblasts, which are characterized by their extensive expression of α-SMA, play a pivotal role in wound healing and scar formation. Under normal conditions, the deposition of ECM and scar tissue is tightly regulated and is terminated when the scar has adequately formed. Many pathological conditions characterized by fibrosis are associated with a dysregulation in this process, and consequently excess scar tissue is deposited and tissue fibrosis results.

Increased activity of cytokines, which stimulate the accumulation of ECM proteins, are key features of most fibrotic diseases (Leask, 2007). The pro-fibrotic cytokine TGF-β plays a pivotal role in the fibrotic process. It is bound to a latency-associated protein in its inactive form, and it becomes activated once released. TGF-β binds to its receptors, where it elicits a downstream signaling cascade that culminates in either activation of Smads, which translocate to the nucleus and activate gene transcription, or activation of the MAP kinase pathway. TGF-β receptors are found on cardiac myocytes and fibroblasts, and TGF-β is produced in and released by both of these cells as well. Overexpression of this pro-fibrotic cytokine results in a fibrotic response, and if sustained, cardiac fibrosis. Furthermore, TGF-β is capable of upregulating other pro-fibrotic cytokines with which it acts synergistically. CTGF is an example of a pro-fibrotic cytokine that is upregulated in response to TGF-β, as well as angiotensin II. It is a member of the CCN family of proteins, and it promotes ECM deposition and has been associated with wound repair. While CTGF is only moderately fibrotic on its own, it works synergistically with TGF-β to promote fibroblast proliferation

and deposition of collagen and fibronectin (Lim and Zhu, 2006). Collagen and fibronectin are the major components of the ECM, which comprises connective tissue that functions to give organs structure and integrity. There are 5 isoforms of collagen present in the heart, and collagens I and III make up 90% of the collagen content. Collagen I has a tensile strength comparable to that of steel whereas collagen III is more elastic. A proper balance of collagen deposition and degradation is necessary for proper cardiac function, and when collagen deposition is excessive, such as in the case of increased TGF-β and CTGF, fibrosis can result.

Cardiac fibrosis and LV hypertrophy are two important characteristics associated with age-associated heart failure. On a cellular level, cardiac endothelial cells and fibroblasts undergo changes that favor a pro-fibrotic environment. In the aged heart, there is increased collagen deposition and cross-linking, and it is thought that this contributes to stiffening of the LV and diastolic dysfunction. Since age-associated diastolic dysfunction was observed in the SAM model, and it was not associated with hypertension, metabolic abnormalities, or cardiomyocyte dysfunction, fibrosis as a pathological feature of diastolic dysfunction was investigated. The hypothesis is that increased cardiac fibrosis will be present in the hearts of 6-month-old SAMP8 mice. Since fibroblasts play a pivotal role in the fibrotic process, cardiac fibroblasts were characterized and their response to TGF-β was assessed. The hypothesis is that cardiac fibroblasts from SAMP8 mice will exhibit differences in either phenotype or response to TGF-β that could contribute to cardiac fibrosis.

3.2 Methods

Histology

Hearts were fixed in 10% buffered formalin for 24 hours, embedded in paraffin, and 5 μm transverse sections were cut using a microtome. Tissue sections were de-waxed, rehydrated, and then stained. For picrosirius red staining, sections were stained in a 0.1% solution of sirius red in a saturated aqueous solution of picric acid for 1 hour then washed in acidified water, dehydrated with graded alcohols, and mounted on slides. Both bright-field and polarized light microscopy were used to image and photograph the slides. Slides were imaged using a using a Zeiss microscope and AxioVision 4.5 software. For slides stained with Masson's trichrome, ImagePro 6.2 software was used to calculate the percent area of collagen content.

RNA isolation and qRT-PCR

Total RNA was isolated from LV heart tissue homogenates using a chloroform-phenol-based extraction procedure. It was reverse transcribed using the SuperScript II kit (Invitrogen, Carlsbad, CA) and random nanomer primers. Expression of collagen 1A1, collagen 3A, fibronectin 1, TGF- β, CTGF, and 18S RNA was measured by amplification of cDNA using a LightCycler real-time thermocycler (Roche Diagnostics Corp, Indianapolis, IN). Primer sequences 5' to 3' were as follows:

Collagen 1A1 (+1) CTAAGGGTCCCCAATGGTGAGAC

Collagen 1A1 (-2) GGGGGTTGGGACAGTCCAGTTCTTC

Collagen 3A (+1) CCCAACCCAGAGATCCCATTTGGAG

Collagen 3A (-2) GGCCACCAGTTGGACATGATTCACA

Fibronectin 1 (+1) CTCAACCTCCCTGAAACGGCCAACT

Fibronectin 1 (-2) TCTTGGGGTGCCAGTGGTCTCTTGT

TGF-β (+1) CCGAGCCCTGGACACCAACTATTGCTTC

TGF-β (-2) TGGTTGTACAGGGCCAGGACCTTGCTG

CTGF (+1) AGCAGCTGGGAGAACTGTGT

CTGF (-2) GCTGCTTTGGAAGGACTCAC

Transcripts were detected using SYBR Green I (Invitrogen, Carlsbad, CA) and were normalized to 18S RNA.

Western blot analysis

LV heart tissue homogenates were prepared in a buffer containing 20 mM Tris (pH 7.4), 2.5 mM EDTA, 1% triton X-100, 1% deoxycholic acid, 0.1% SDS, 100 mM NaCl, 10 mM NaF, and 1 mM Na_3VO_4 and quantified using the BCA protein assay according to the manufacturer's instructions (Thermo Scientific, Rockford, IL). Heart samples (40 µg protein per lane) were run on a 10% SDS-PAGE gel (Invitrogen, Carlsbad, CA) for 90 minutes at 150V then transferred to a polyvinylidene fluoride (PVDF) membrane. Membranes were blocked for 30 minutes in 5% nonfat dry milk and probed with primary antibody (1:1,000) specific to TGF-β (Santa Cruz Biotechnology) or α-smooth muscle actin (Thermo Fisher Scientific, Fremont, CA) on a rocking platform overnight at 4ºC. Membranes were washed, then incubated with horseradish peroxidase-conjugated secondary antibody (Jackson ImmunoResearch), and detected using the SuperSignal West Pico peroxide and luminol enhancer solution (Thermo Scientific, Rockford, IL).

Membranes were imaged, photographed, and quantified using the BioRad ChemiDoc system (Hercules, CA). Proteins of interest were normalized to cdk4 content.

TGF-β enzyme-linked immunosorbent assay (ELISA)

TGF-β was measured in plasma, tissue, and tissue culture supernatant using the TGFβ_1 E_{max}® ImmunoAssay System (Promega, Madison, WI) which detects TGF-β in the antibody sandwich format in a 96-well plate. For plasma sample preparation, blood was collected using lithium heparin to prevent coagulation and centrifuged at 2000 x g for 5 minutes. For heart tissue samples, tissue was homogenized in TBS-based lysis buffer containing 1% NP40, 10% glycerol, and protease inhibitors, centrifuged at 2000 x g for 5 minutes, and supernatant was collected. Tissue culture supernatants were collected and centrifuged as well. For all types of samples, one aliquot was acidified to a pH of 3.0 using HCl then neutralized back to a pH of 7.6 using NaOH to free TGF-β from its latency-associated peptide and thus measure biologically-active TGF-β. A second aliquot was left untreated, which was used to measure naturally-processed TGF-β. Once samples were prepared, TGF-β was determined according to the manufacturer's instructions.

Cardiac fibroblast isolation and culture

For all isolated cardiac fibroblasts studies, 6-month-old male SAMR1 and SAMP8 mice were used. Mice were sacrificed by CO_2 inhalation and hearts were rapidly removed, cleaned of fat and vessels, the atria and right ventricle were removed, and the LV was rinsed 5 times in sterile phosphate-buffered saline (PBS) supplemented with 1% penicillin/streptomycin/amphotericin B (P/S/A; Cellgro, Manassas, VA). Under the cell culture hood, tissue was transferred to a fresh dish of PBS and minced into 20-25 pieces to facilitate digestion. Each minced heart was incubated with 3 mL Liberase TH (Roche,

Indianapolis, IN) in PBS (0.1 mg/mL) in a 37°C water bath with stirring for 5 minutes to dissociate the tissue. The supernatant was removed and discarded and another 3 mL of Liberase was added and the heart was incubated for 5 minutes then that supernatant was discarded as well. A third 3 mL of Liberase was added and the heart was incubated for 5 minutes, and this supernatant was added to a 50 mL tube containing 20 mL Dulbecco's Modified Eagle's Medium (DMEM; Sigma-Aldrich, St. Louis, MO) supplemented with 10% fetal bovine serum (FBS) and 1% P/S/A. The addition of Liberase, incubation, and saving of the supernatant was repeated 4-5 more times until the pieces of heart tissue were completely digested. The mixture containing digested cells and media was centrifuged at 1200 rpm for 10 minutes at room temperature to pellet cells, then cells were resuspended in 10 mL fresh DMEM and plated in a 60 mm cell culture dish. Dishes were incubated at 37°C and 21% O_2 and 5% CO_2 for 4-6 hours to allow cells to adhere, then the cells were washed with PBS and the media was changed and cells were grown to confluence, changing the media every 3 days. After 7 days, cells were split using TrypLE Express Stable Trypsin Replacement (Gibco, Carlsbad, CA).

MTT cell proliferation assay

Cellular proliferation was assessed using The MTT (3-(4, 5- dimethylthiazolyl-2)-2, 5-diphenyltetrazolium bromide) cell proliferation assay kit (ATCC, Manassas, VA) according to the manufacturer's instructions. Isolated cardiac fibroblasts at passage 1-2 were grown to approximately 70% confluence and split; suspended cells were harvested by centrifugation and resuspended at 1 x 10^6 per mL. Serial dilutions of cells in DMEM were prepared from 1 x 10^6 to 1 x 10^3 cells per mL and were plated in triplicate in a 96-well plate. Following overnight recovery, cells were incubated with MTT reagent (5

mg/mL) added in a 1:10 dilution to each well. Cells were incubated with the MTT reagent for 2 to 4 hours, or until the development of a purple precipitate was evident. Detergent reagent was added to each well in a 1:1 dilution and cells were incubated overnight and the absorbance was read at 562 nm.

Amplex® Red H_2O_2 assay

Isolated cardiac fibroblasts at passage 1-2 were seeded at a density of 1 x 10^6 cells per 100 mm dish and grown to approximately 70% confluence in DMEM supplemented with 10% FBS and 1% P/S/A. A working solution consisting of 10 μM Amplex® Red reagent (N-acetyl-3,7-dihydroxyphenoxyazine; Invitrogen Molecular Probes, Carlsbad, CA) and 0.2 units/mL horseradish peroxidase was prepared in Krebs Ringer's phosphate glucose buffer containing 145 mM NaCl, 5.7 mM NaH_2PO_4, 4.86 mM KCl, 0.54 mM $CaCl_2$, 1.22 mM $MgSO_4$, 5.5 mM glucose. Cells were washed with KRPG buffer then incubated with 10 mL working solution for 30 minutes at 37°C protected from light. Supernatant was collected and the fluorescence was detected at 590 nm using an excitation of 530 nm. Background fluorescence, determined using a reaction without cells, was subtracted from each value.

TGF-β stimulation, RNA isolation, and qRT-PCR

Isolated cardiac fibroblasts at passage 2 were seeded at a density of 1 x 10^6 cells per 100 mm dish and grown to approximately 80% confluence in DMEM supplemented with 10% FBS and 1% P/S/A. Cells were serum-starved for 24 hours then treated with 0.5, 1.0, or 2.0 ng/mL TGF-β (Sigma-Aldrich, St. Louis, MO) or vehicle (DMSO) for 24 hours. RNA from cultured cardiac fibroblasts was isolated using The RNeasy Mini Kit (Qiagen, Valencia, CA) according to the manufacturer's instructions. In summary, lysis buffer was

prepared by adding 10 μL β-mercaptoethanol to each mL RLT buffer from the RNeasy kit. Immediately prior to RNA harvest, cells were washed several times with PBS then 600 μL lysis buffer was added, plates were scraped to lyse cells and get all RNA into the lysate, and the samples were snap-frozen in liquid nitrogen and stored at -80°C until further analysis. Total RNA was isolated cardiac fibroblast homogenates using the RNeasy kit according to the manufacturer's instructions. It was reverse transcribed using the SuperScript II kit (Invitrogen, Carlsbad, CA) and random nanomer primers. Expression of α–SMA, fibronectin 1, collagen 1A1, collagen3A and 18S RNA was measured by amplification of cDNA using a LightCycler real-time thermocycler (Roche Diagnostics Corp, Indianapolis, IN). Primer sequences 5' to 3' were as follows:

Fibronectin 1 (+1) CTCAACCTCCCTGAAACGGCCAACT

Fibronectin 1 (-2) TCTTGGGGTGCCAGTGGTCTCTTGT

Collagen 1A1 (+1) CTAAGGGTCCCCAATGGTGAGAC

Collagen 1A1 (-2) GGGGGTTGGGACAGTCCAGTTCTTC

Collagen 3A (+1) CCCAACCCAGAGATCCCATTTGGAG

Collagen 3A (-2) GGCCACCAGTTGGACATGATTCACA

Transcripts were detected using SYBR Green I (Invitrogen, Carlsbad, CA) and were normalized to 18S RNA.

Statistical Analysis

Data are represented as the mean ± standard error and are compared using the Student's *t*-test when SAMR1 and SAMP8 mice are being compared for 6-month time point studies. A p value <0.05 is considered statistically significant.

3.3 Experimental results

SAMP8 mice show evidence of myocardial fibrosis by 6 months of age.

Since diastolic dysfunction in the SAM model is not secondary to hypertension, other causes and mechanisms of age-associated diastolic dysfunction were investigated. Since diastolic dysfunction has been found to be correlated with stiffening of the LV and diminished distensibility of the heart muscle in a population of patients with the disorder (Borlaug and Kass, 2006), fibrotic response was examined next in the SAM model. Collagens represent an important component of fibrotic tissue, so myocardial collagen content was examined using two different histological methods. When transverse myocardial tissue sections were stained with sirius red, greater collagen accumulation in whole hearts of SAMP8 mice was evident as a result of increased red staining of the tissue using brightfield microscopy (Figure 3.1A, upper panels). Tissue sections were also imaged using polarized light, where large collagen fibers appear yellow or orange, and thinner fibers appear green.(Junqueira et al., 1979) In both interstitial and perivascular regions of the myocardium, SAMP8 mice showed increased collagen deposition compared to SAMR1 controls. The accumulation of large collagen fibers was particularly markedly increased in the perivascular regions of hearts from SAMP8 mice (Figure 3.1A, lower panels). To confirm and quantify these findings, Masson's trichrome staining was used. Again, greater collagen accumulation was observed in the interstitial and perivascular regions of the myocardium in SAMP8 mice. In the interstitial and perivascular tissue, the percentage of tissue comprised of collagen was greater in SAMP8 mice compared to SAMR1 controls (0.8 ± 0.1 *vs.* 0.3 ± 0.04, $p<0.05$) and (1.6 ± 0.1 *vs.* 1.0 ± 0.1, $p<0.05$), respectively (Figure 3.1B).

To further examine which collagens and other associated ECM proteins might be increased in the myocardium of senescence-accelerated mice, qRT-PCR was used to

measure myocardial gene expression of collagen 1A1, collagen 3A, and fibronectin. In SAMP8 mice compared to SAMR1 controls, gene expression of collagen 1A1, which is the main component of scar tissue, and collagen 3A, commonly associated with collagen 1A1, were increased (Figures 3.2A and 3.2B). Fibronectin is an ECM protein that can bind to collagen, and gene expression of fibronectin 1 was increased in SAMP8 mice (Figure 3.2C).

Figure 3.1. Histological analysis of cardiac collagen deposition. Cardiac collagen deposition was assessed in 6-month-old SAMR1 and SAMP8 mice histologically using picrosirius red staining and Masson's trichrome staining. SAMP8 mice show greater collagen deposition and hence increased cardiac fibrosis in both the interstitial areas and perivascular areas compared to SAMR1 controls at 6 months of age (A) Picrosirius red staining to evaluate collagen deposition. Using bright-field microscopy, SAMP8 mice show a more intense red stain than SAMR1 mice, indicating greater collagen accumulation. When polarized light is used, larger collagen fibers appear as bright yellow or orange, and thinner fibers are green. Both modalities show increased collagen accumulation in SAMP8 mice at 6 months of age. (B) Masson's trichrome staining to evaluate collagen deposition (n=4, *p<0.01).

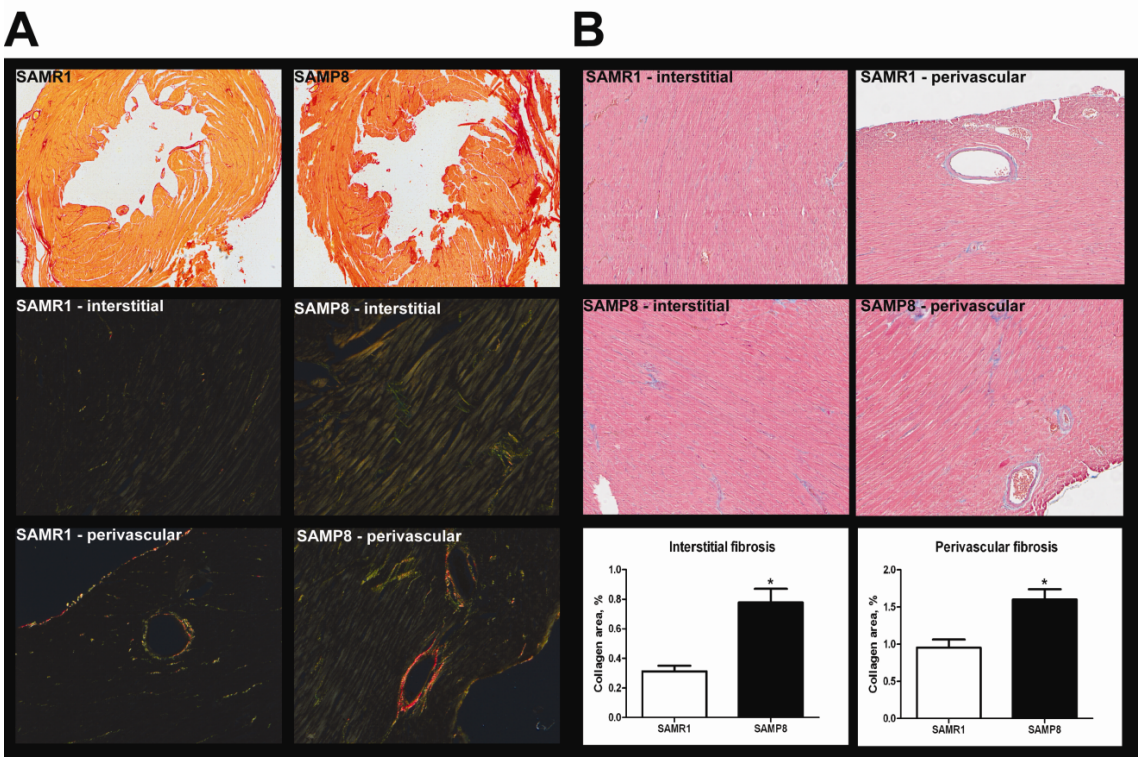

Figure 3.2. Gene expression of cardiac ECM components. Collagen 1A1, collagen 3A, and fibronectin 1 gene expression were measured by qRT-PCR normalized to 18S copy number in cardiac samples from 6-month-old SAMR1 and SAMP8 mice. SAMP8 mice show increased gene expression of (A) collagen 1A1, (B) collagen 3A, and (C) fibronectin 1 compared to SAMR1 controls at 6 months of age (n=7, **p*<0.05). Figure generated with the assistance of Atsuko Tanaka.

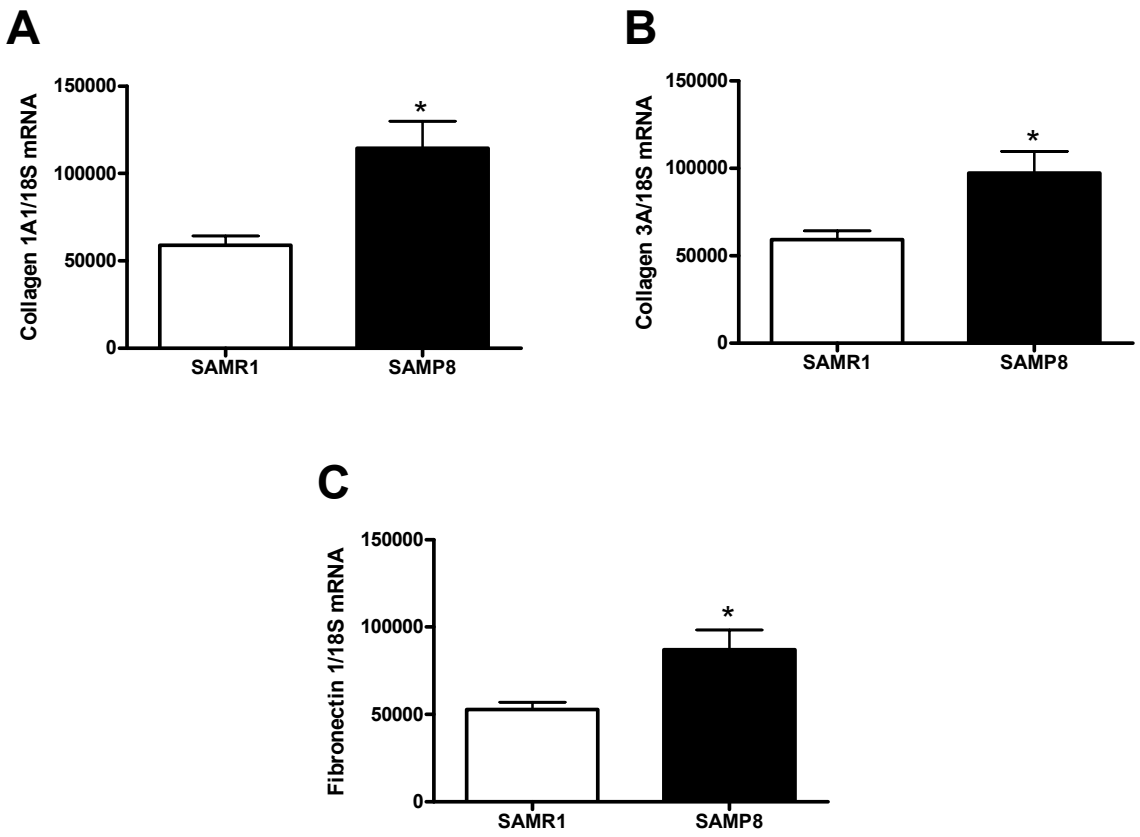

Cardiac fibrosis in SAMP8 mice is associated with increased expression of pro-fibrotic cytokines.

Since cardiac fibrosis is present in this model of age-related diastolic dysfunction, the signaling pathways that might contribute to the fibrotic response were investigated. TGF-β is a potent pro-fibrotic cytokine that influences the development of cardiac fibrosis by promoting cellular events such as increased collagen synthesis and decreased protease expression (Lijnen et al., 2000; Lim and Zhu, 2006). CTGF is induced by TGF-β and acts synergistically with TGF-β to promote deposition of ECM proteins (Chen et al., 2000; Leask, 2007; Lim and Zhu, 2006). These pro-fibrotic cytokines are capable of converting fibroblasts into myofibroblasts, which express α-SMA and synthesize collagen, promoting the fibrotic process (Lijnen et al., 2000). Cardiac gene expression of TGF-β and CTGF were increased in SAMP8 mice compared to SAMR1 controls (Figures 3.3A and 3.3B, respectively). When fibroblasts become activated and transition from normal fibroblasts to pro-fibrotic myofibroblasts, the expression of α-SMA increases in these cells. Consistent with increased collagen disposition, α-SMA protein expression was modestly but significantly increased in the hearts of SAMP8 mice compared to controls, suggesting a conversion of fibroblasts into myofibroblasts (Figure 3.3C). The fact that this change is very small could reflect the fact that while fibroblasts are numerous in the heart, they make up a smaller volume of cells compared to myocytes because of their smaller size. Consequently, an increase in fibroblast α-SMA is likely to manifest as a small change in a sample of homogenized heart tissue that contains many myocytes as well.

Figure 3.3. Gene expression of pro-fibrotic cytokines and protein expression of α-SMA. TGF-β and CTGF expression were measured by qRT-PCR normalized to 18S copy number in cardiac samples from 6-month-old SAMR1 and SAMP8 mice. α-SMA protein expression was measured by Western blot and normalized to ckd4. SAMP8 mice show increased gene expression of cardiac TGF-β and CTGF and increased protein expression of α-SMA compared to SAMR1 controls at 6 months of age (n=7, **p*<0.05). Figure generated with the assistance of Atsuko Tanaka.

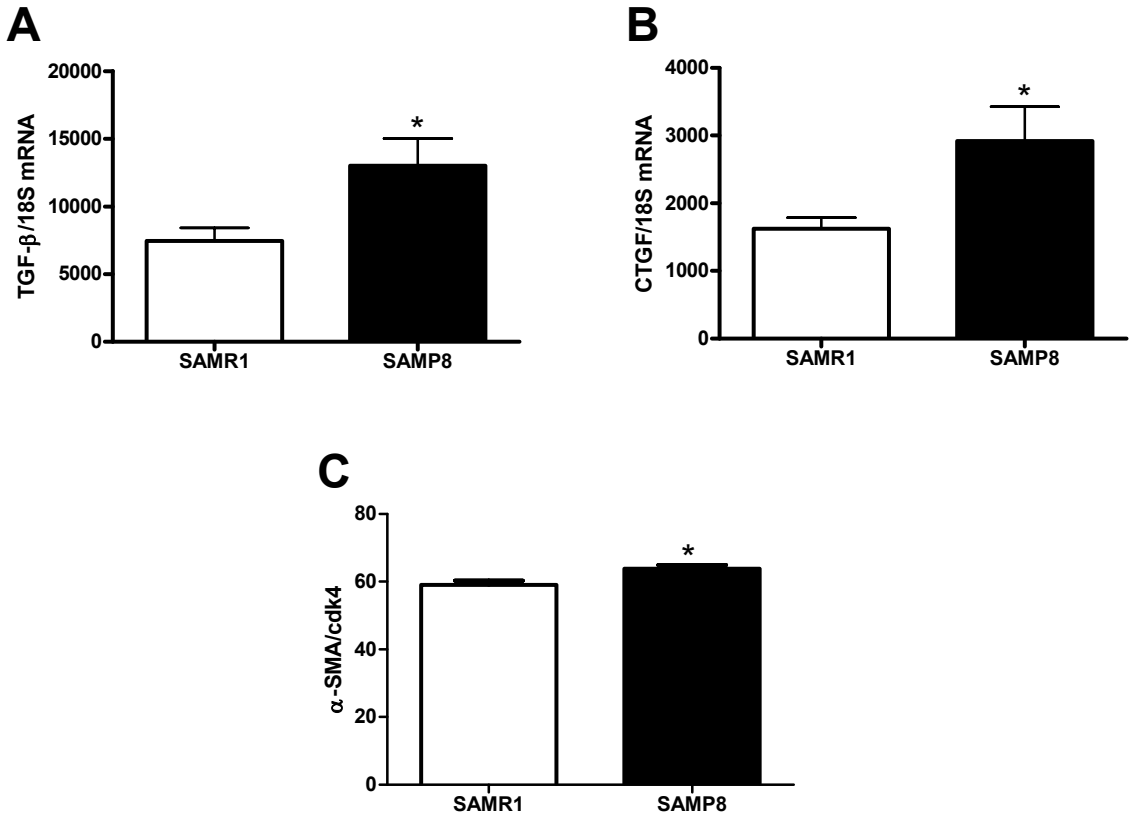

Assessment of TGF-β.

TGF-β was measured in plasma and heart tissue homogenates from 6-month-old SAMR1 and SAMP8 mice using the TGFβ_1 E_{max}® ImmunoAssay System. This assay allows for quantification of TGF-β in the range of 32-1,000 pg/mL, an improved alternative over Western blotting. TGF-β was measured in two forms: biologically active (total) TGF-β, which requires that samples be acid-treated to unbind TGF-β from its latency-associated peptide, as well as naturally-processed TGF-β, which omits the acid treatment and assays only free TGF-β. In plasma from 6-month-old SAM mice, no difference were found between SAMR1 and SAMP8 mice in either biologically active or naturally-processed TGF-β (Figure 3.4A and 3.4B). In heart tissue samples from the same mice, again no difference in biologically active TGF-β was found between SAMR1 and SAMP8 mice (Figure 3.4C). Naturally-processed TGF-β was undetectable in heart tissue samples (data not shown). TGF-β was also assayed in conditioned media from cardiac fibroblasts grown to 80-90% confluence then serum starved for 24 hours. Media was collected and assayed; however, no TGF-β was detected, either in the biologically active or naturally-processed form (data not shown).

Figure 3.4. Quantification of TGF-β_1 by ELISA. A TGF- β ELISA was used to quantify TGF-β_1 in plasma and cardiac tissue from 6-month-old SAMR1 and SAMP8 mice. (A) Naturally-processed TGF- β_1 measured in untreated plasma from 6-month-old mice showed no significant difference between SAMR1 and SAMP8 mice. (B) Total TGF-β_1 measured in acid-treated plasma from 6-month-old mice, again showed no significant difference between SAMR1 and SAMP8 mice. Samples were acid-treated to unbind TGF-β_1 from its latency-associated peptide and thus measure total bioactive TGF-β_1. (C) Total TGF-β_1 measured in acid-treated cardiac tissue homogenates from 6-month-old mice showed o significant difference between SAMR1 and SAMP8 mice (n=6, *p*=ns).

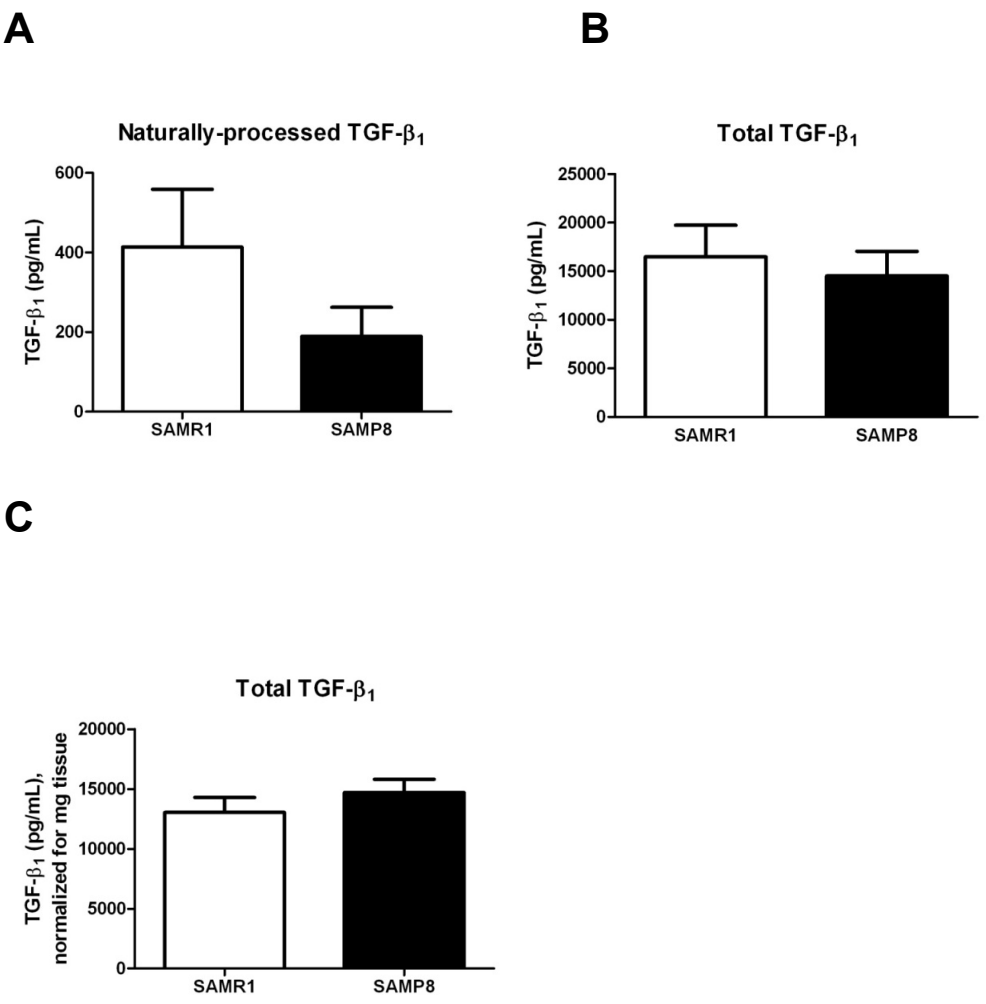

Cardiac fibroblasts from 6-month-old SAMP8 mice show no differences in cell proliferation or H_2O_2 production.

Cardiac fibroblast proliferation was assessed using the MTT cell proliferation assay. Cultured fibroblasts were exposed to the yellow tetrazolium salt MTT (3-(4, 5-dimethylthiazolyl-2)-2, 5-diphenyltetrazolium bromide, which is reduced by metabolically active cells to generate reducing equivalents such as NADH and NADPH which in turn produce an intracellular purple formazan which is then solubilized by detergent and quantified spectrophotometrically. Cardiac fibroblasts at passage 1-2 and approximately 70% confluence were compared using this assay, and no difference in cell proliferation was found between SAMR1 and SAMP8 mice (n=6) (Figure 3.5). This seems to indicate that differences between SAMR1 and SAMP8 fibroblasts cannot be attributed to differences in proliferation capability.

Since H_2O_2 can play roles in both oxidative stress and cellular signaling, production of H_2O_2 from cardiac fibroblasts was measured using the Amplex® Red assay in which H_2O_2 reacts with the Amplex® Red reagent in the presence of horseradish peroxidase to produce the fluorescent product, resorufin, that can be quantified fluorometrically. Cardiac fibroblasts at passage 1-2 and approximately 70% confluence were compared using this assay, and no difference in H_2O_2 production was found between SAMR1 and SAMP8 mice (n=6) (Figure 3.6). This suggests that cardiac fibroblast production of H_2O_2 is unlikely to play a role in differences observed in the SAM model.

Figure 3.5. MTT assay for cardiac fibroblast proliferation. Fibroblast proliferation in passage 2 cardiac fibroblasts from 6-month-old SAMR1 and SAMP8 mice was measured using the MTT cell proliferation assay. There was no difference in cell proliferation between cardiac fibroblasts isolated from SAMR1 and SAMP8 mice (n=6, *p*=ns).

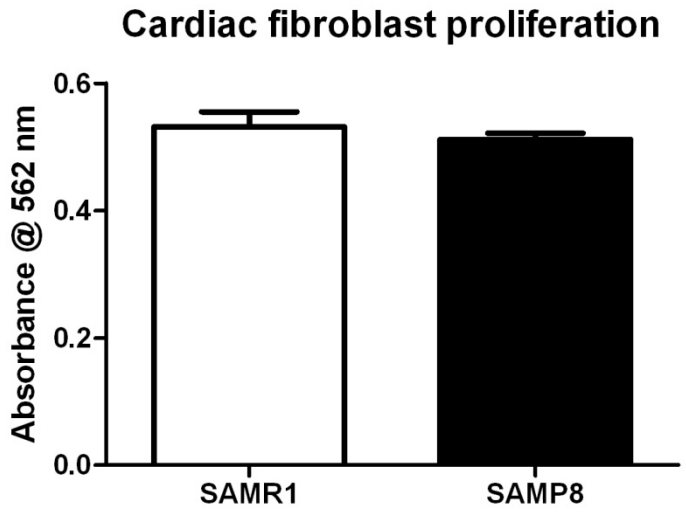

Figure 3.6. Amplex® Red assay of cardiac fibroblast H_2O_2 production. H_2O_2 production in passage 2 cardiac fibroblasts from 6-month-old SAMR1 and SAMP8 mice was measured using the Amplex® Red assay. There were no differences in fibroblast H_2O_2 production between SAMR1 and SAMP8 fibroblasts (n=6, *p*=ns).

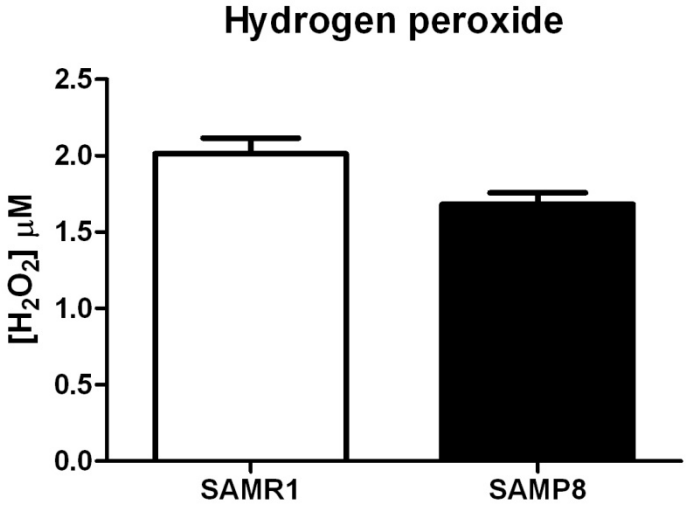

Gene expression of fibrosis markers in isolated cardiac fibroblasts.

To investigate whether SAMP8 cardiac fibroblasts have a more pro-fibrotic phenotype than SAMR1 fibroblasts, gene expression of α-SMA, fibronectin 1, collagen 1A1, and collagen 3A were measured in isolated cardiac fibroblasts from 6-month-old SAM mice. However, there were no differences between SAMR1 and SAMP8 fibroblasts in any of these markers (Figure 3.7 vehicle-treated condition), suggesting that the fibroblasts alone are not responsible for promoting the fibrotic changes that correlated with diastolic dysfunction or that phenotype not maintained in culture.

Response of cardiac fibroblasts to TGF-β stimulation.

To investigate the possibility that a difference in SAMR1 and SAMP8 cardiac fibroblasts only becomes apparent once the fibroblasts are challenged, cultured fibroblasts were serum starved for 24 hours then treated with 2 ng/mL TGF-β for 24 hours, then gene expression of the same markers was measured. As a preliminary experiment, the dose-dependence of these markers was assessed by treating fibroblasts with either vehicle (0), 0.5, 1.0, or 2.0 ng/mL TGF-β. As represented in Figure 3.8, the gene expression of α-SMA, fibronectin 1, and collagen 1A1 increased steadily in response to increasing concentrations of TGF-β. The concentration of 2.0 ng/mL was selected, as it was expected to produce the most pronounced response. As expected, treatment with TGF-β caused expression of α-SMA to markedly increase (Figure 3.7A); however, it increased to a similar degree in both SAMR1 and SAMP8 fibroblasts. Unexpectedly, treatment with TGF-β had no significant effect on fibronectin 1 (Figure 3.7B) or collagen 1A1 (Figure 3.7C). However, treatment with TGF-β was associated with a significant decrease in collagen 3A, but this change was observed only in SAMP8 fibroblasts (Figure 3.7D). This is particularly interesting in light of recent work by Davis et al. (Pendergrass et al., 2011) that demonstrates that collagen 3A is a more compliant

and beneficial isoform of collagen, so its loss is associated with an overall stiffer myocardium in the context of myocardial infarction. This observation fits with the observed phenotype of a stiffer LV in SAMP8 mice that is associated with diastolic dysfunction. It seems that when SAMP8 cardiac fibroblasts are challenged with a pro-inflammatory cytokine such as TGF-β, their expression of the more elastic collage 3A isoform decreases, which could in part explain ventricular stiffening.

Figure 3.7. Response of isolated cardiac fibroblasts to treatment with TGF-β. Passage 2 cardiac fibroblasts from 6-month-old SAMR1 and SAMP8 mice were serum-starved for 24 hours then treated with either vehicle or 2.0 ng/mL TGF-β for 24 hours. α-SMA, fibronectin 1, collagen 1A1, and collagen 3A expression were measured by qRT-PCR and copy number was normalized to 18S copy number in cardiac fibroblasts from 6-month-old SAMR1 and SAMP8 mice. (A) There was a significant increase in expression of α-SMA in both SAMR1 and SAMP8 fibroblasts in response to TGF-β stimulation. (B and C) There were no differences in expression of fibronectin 1 or collagen 1A1 between SAMR1 or SAMP8 fibroblasts, either in the vehicle-treated or TGF-β treated condition. (D) Treatment with TGF-β resulted in a significant decrease in expression of collagen 3A in SAMP8 fibroblasts (n=4, **p*<0.05).

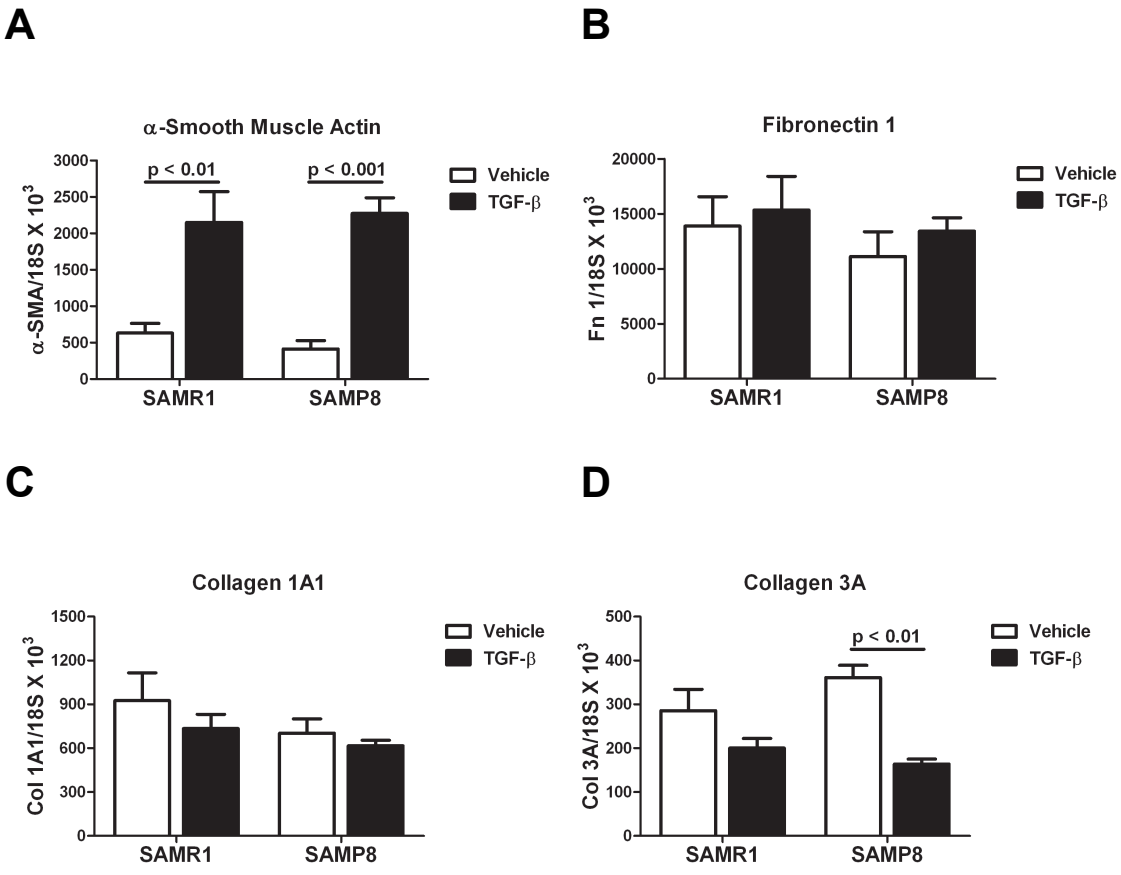

Figure 3.8. Dose-dependence of the treatment of isolated cardiac fibroblasts with TGF-β. Cardiac fibroblasts from 6-month-old SAMR1 mice at passage 2 were serum-starved for 24 hours then treated with 0, 0.5, 1.0, or 2.0 ng/mL TGF-β for 24 hours to establish the dose-dependence of TGF-β treatment of cardiac fibroblasts. (A) α-SMA and (B) collagen 1A1 expression were measured by qRT-PCR and copy number was normalized to 18S copy number in cardiac fibroblasts from 6-month-old SAMR1 and SAMP8 mice.

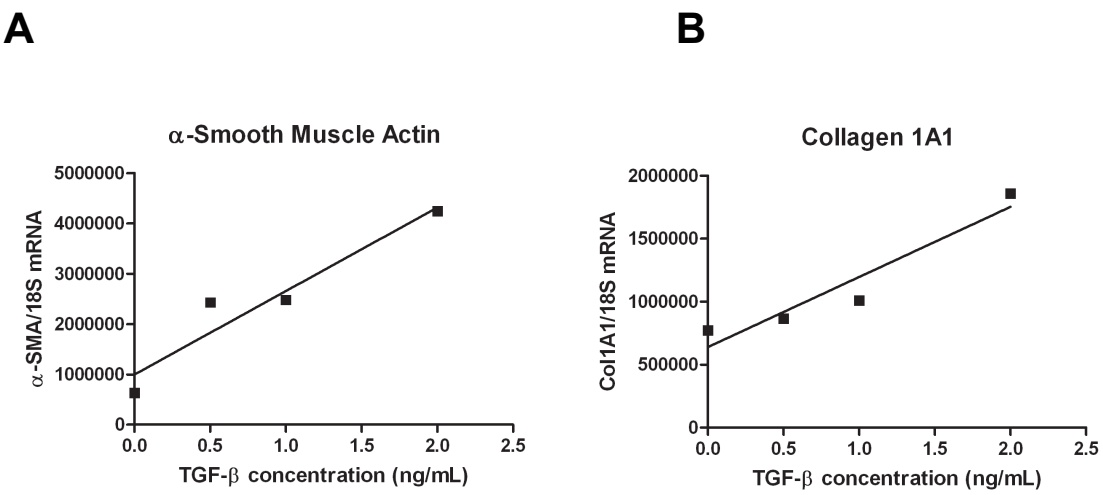

3.4 Discussion

One proposed cause of diastolic dysfunction is fibrosis. Consistent with this observation, increased collagen deposition was found in the hearts of senescence-prone mice. This fibrotic response and collagen deposition was accompanied by an increase in the gene expression of several pro-fibrotic cytokines, CTGF and TGF-β. As expected, the increases in CTGF and TGF-β paralleled the increase in the myofibroblast phenotype. Many forms of tissue fibrosis are associated with increased signaling through the TGF-β pathway. In this pathway, increased TGF-β upregulates CTGF, and these two cytokines act synergistically to increase Smad signaling in the nucleus, which ultimately leads to conversion of fibroblasts into myofibroblasts, which secrete additional ECM proteins. However, there was no difference in TGF-β in either plasma or LV tissue homogenates, which was an unexpected finding. The fact that gene expression of TGF-β is increased while protein expression is not increased could result from the mRNA transcript not being fully translated into protein. This observation could also result from experimental error or inadvertent mishandling of the samples. Because TGF-β is bound to a latency-associated peptide, it requires processing before active TGF-β can be measured in the ELISA, and TGF-β could have been destroyed or altered in this process. Perhaps TGF-β is not the most important cytokine in the fibrotic process; CTGF may play a more important role, or there could be other pro-inflammatory or pro-fibrotic mediators as well. Another possibility is that while overall TGF-β levels are not different between SAMR1 and SAMP8 mice, the hearts or a subset of cardiac cells respond differently to TGF-β in SAMP8 mice to result in cardiac fibrosis. For example, while TGF-β protein expression is not different between SAMR1 and SAMP8 mice, the density of TGF-β receptors could be different, which could result in a different response to the same concentration of TGF-β between SAMR1 and SAMP8 mice.

Since fibroblasts, and in particular, their transition into myofibroblasts, are the main cell type driving the fibrotic process, cardiac fibroblasts were isolated and evaluated for pro-fibrotic markers. To investigate the possibility that fibroblasts from SAMR1 versus SAMP8 mice respond differently to TGF-β, isolated cardiac fibroblasts were stimulated with TGF-β and again pro-fibrotic markers were measured. While it was expected that cardiac fibroblasts isolated from SAMP8 mice would show increased α-SMA, fibronectin1, and collagens at baseline, no difference was observed. Treatment with TGF-β induced a large increase in α-SMA expression in both cell types, and there were no differences in fibronectin or collagen 1A1 (Figure 3.7A-C). These results are in contrast to a similar study by Cucoranu et al. (Cucoranu et al., 2005) that demonstrated increased expression of CTGF and ECM proteins in cultured human cardiac fibroblasts treated with TGF-β. It is possible that murine fibroblasts respond differently than human fibroblasts to TGF-β stimulation. Additionally, a higher concentration of TGF-β was used in the human fibroblasts study than in the present study, and that could account for the difference. Furthermore, the human cardiac fibroblasts were purchased and used at passage 3-6 while the murine fibroblasts were isolated then used at passage 2, which might also explain the discrepancy in results. Despite these unexpected results, a significant decrease in collagen 3A was observed upon stimulation with TGF-β in SAMP8 fibroblasts but not SAMR1 fibroblasts (Figure 3.7D). Since collagen 3A is a more compliant, elastic isoform of collagen, it is possible that treatment with TGF-β decreases expression of collagen 3A, and the stiffer collagen 1A1 isoform persists, contributing to stiffening of the LV. It is possible that a different concentration of TGF-β or a different treatment time course may have yielded different results. Furthermore, it is also possible that maintaining isolated cardiac fibroblasts in cell culture altered their physiology such that they diverged from their typical behavior in the working heart.

In summary, diastolic dysfunction has been observed in the SAM model accompanied by increased cardiac fibrosis. By 6 months of age, SAMP8 animals demonstrate increased deposition of collagen in the LV, which is consistent with a stiffened chamber and the elevated LVEDPVR observed using invasive hemodynamics. Gene expression of TGF-β and CTGF are increased in myocardial samples, suggesting a role for pro-fibrotic cytokines in the fibrotic process. The exact role of TGF-β and other cytokines in the LV and in isolated cardiac fibroblasts needs further elucidation. Nevertheless, isolated cardiac fibroblast studies suggest that upon stimulation with TGF-β, fibroblasts from SAMP8 mice decrease expression of the more elastic form of collagen, collagen 3A, which may be an early step in the process of LV stiffening and ultimately diastolic dysfunction.

Chapter 4:

The role of oxidative stress in the SAM model

4.1 Introduction

The link between aging, aerobic metabolism, and ROS has been investigated for many years and is now widely accepted. In his "free radical theory of aging," Denham Harman suggested that aging results from exposure to ROS generated during aerobic metabolism over a lifetime (Harman, 1956). More specifically, it appears that ROS generated by mitochondria, especially mitochondria that have become sequentially more damaged by aging, contribute greatly to the production of ROS. While low levels of ROS are needed for cell signaling pathways, excessive levels of ROS are deleterious and can damage lipids, proteins, and DNA. Because ROS are commonly increased with aging and because the tight regulation of ROS concentration is important for avoiding oxidative damage, antioxidants play an important role in modulating intracellular levels of ROS. Antioxidant upregulation is triggered by increased levels of ROS as a compensatory mechanism to protect the cells and organism from oxidative damage. SOD converts $O_2^{\bullet-}$ to H_2O_2, which is then converted to H_2O by catalase and GPX. The relationship between aging and ROS production has been investigated using several rodent models. For example, a long-lived mouse strain was found to have a lower body temperature, indicative of altered metabolism, as well as increased antioxidant capacity (Quarrie and Riabowol, 2004). In a mouse model expressing a proofreading-deficient form of mitochondrial DNA polymerase, increased mitochondrial mutations, decreased mitochondrial function, a shorter lifespan, and early onset of age-related pathologies were observed (Trifunovic et al., 2004).

There is accumulating evidence that oxidative stress plays a role in the age-associated pathologies observed in the SAM model. The SAMP1 strain of mice have increased skin lipid peroxidation as early as 3-4 months of age, and increased mitochondrial $O_2^{\bullet-}$ as well as impaired mitochondrial function has been found in dermal fibroblasts from SAMP11 mice (Chiba et al., 2009). In SAMP8 mice, liver mitochondria

showed evidence of impaired respiration and ATP synthesis, and mitochondrial uncoupling was more easily induced in these mice (Nakahara et al., 1998). In the brain, increased oxidative stress and mitochondrial dysfunction have been found in the brains of relatively young SAMP8 mice (1 month to 5 months of age), and antioxidant treatment has been used to prevent the neurodegenerative disorders thought to be associated with oxidative damage, supporting the idea that ROS play a role in age-related pathologies in these mice (Chiba et al., 2009) Changes have also been observed in antioxidants in the SAM model. Dietary supplementation with vitamins C and E in addition to other phytochemicals known to induce phase II antioxidant enzymes resulted in an increased GSH/GSSG ratio in many tissues, particularly in the mitochondria. Taken together, these data suggest that the SAM model, in addition to displaying evidence of diastolic dysfunction and cardiac fibrosis, may exhibit increased oxidative stress and/or changes in compensatory antioxidants.

4.2 Methods

High-performance liquid chromatography (HPLC) detection of reduced and oxidized forms of plasma GSH and cysteine

Blood was drawn using a closed-chest cardiac puncture as part of a terminal bleed and sacrifice. Fifty μL of whole blood was mixed with 250 μL of a solution containing 80 mM boric acid, 20 mM sodium tetraborate, 105 mg L-serine, 5 mg heparin, 10 mg bathophenanthrolinedisulfonic acid (BPDS), and 20 mg iodoacetic acid. The sample was centrifuged at 3000 x g for 30 seconds, and 200 μL of supernatant was transferred to 200 μL of a solution containing 10% perchloric acid, 0.2 M boric acid, and 10 μM gamma-glutamyl glutamate, which functioned as an internal standard, and stored at -80°C until they were derivatized with iodoacetic acid and dansyl chloride then analyzed by HPLC with fluorescence detection by the General Clinical Research Center Core Lab at the Emory University School of Medicine.

ESR detection of $O_2^{\bullet-}$

The cell permeable spin probe 1-hydroxy-3-methoxycarbonyl-2,2,5,5-tetramethyl-pyrrolidine hydrochloride (CMH) (Alexis Corp., San Diego, CA) was used to examine intracellular $O_2^{\bullet-}$ production using ESR spectroscopy. For ESR, freshly isolated aortas or heart tissue were cut into 1-2 mm pieces then allowed to equilibrate in deferoxamine-chelated Krebs-HEPES solution containing 0.5 mM CMH, 25 μM deferoxamine and 5 μM DETC for 90 minutes at 37°C. After the incubation period, tissue samples were transferred into 1 mL syringes filled with Krebs-HEPES solution and frozen in liquid nitrogen. Then, the samples were placed in a liquid nitrogen ESR dewar and time scans are obtained at 77ºK with a Bruker EMX spectrometer (5 G; conversion time 655 ms;

time constant 5243 ms; modulation frequency 100 kHz; microwave power 10 mW; microwave frequency 9.78 GHz; scan time 335 s). Analyses of slope of the time scans are used to quantify the amount of $O_2^{\bullet-}$ produced by the tissue and compared to buffer-only control spectra or spectra in the presence of SOD.

HPLC detection of intracellular $O_2^{\bullet-}$ with dihydroethidium (DHE)

Freshly isolated heart tissue was incubated with 50 μM DHE in a Krebs-HEPES buffer at 37°C for 30 minutes then stored in 300 μL MeOH until analysis. Tissue was homogenized in the MeOH then 50 μL homogenate kept for protein determination. The remaining homogenate was passed through a 0.22 μm syringe filter and used for HPLC analysis. DHE, 2-hydroxyethidium, and ethidium were separated using a C-18 reverse phase column (Nucleosil 250-4.5 mm) and a mobile phase containing 0.1% trifluoroacetic acid and an acetonitrile gradient (from 37% to 47% over 23 minutes) at a flow rate of 0.5 mL/minute. Ethidium and 2-hydroxyethidium were detected with a fluorescence detector using an emission wavelength of 580 nm and an excitation of 480 nm. UV absorption at 355 nm was used for detection of DHE. The 2-hydroxyethidium peak reflects the amount of $O_2^{\bullet-}$ formed in the tissue during incubation and is expressed per mg protein. A Beckman Gold HPLC with a Jasco fluorescence detector was used.

HPLC detection of cardiac biopterin content

Cardiac biopterin content was measured using HPLC analysis and a differential oxidation method, as described by Antonozzi et al. (Antonozzi et al., 1988). A known amount of ventricular myocardial tissue was homogenized in a 0.1 N phosphate buffer at a pH of either 12.0 or 2.0. Pterins at the two pHs were differentially oxidized by exposure to 1% iodine/2% potassium iodide. After the differential oxidation, the

particulate material was removed by centrifugation at 3,000 g for 30 minutes. Supernatants were then passed over a Dowex 50 column to concentrate the pterins and to eliminate other fluorescent molecules. HPLC was performed using a C_{18} column (5 × 250 mm, 5 μm) and a mobile phase of 5% methanol and 95% water at a flow rate of 1 mL/minute. Peaks were detected using a fluorescence detector with authentic biopterin as the standard. The fluorescence detector was set at 350 nm for excitation and 450 nm for emission. The amount of BH_4 was determined from the difference between total (BH_4 plus BH_2 plus biopterin) and alkaline-stable oxidized (BH_2 plus biopterin) biopterin. Protein concentration was measured by the method of Lowry et al (1951) with bovine serum albumin as the standard. Biopterin levels are expressed as picomoles per mg protein.

RNA isolation and qRT-PCR

Total RNA was isolated from LV heart tissue homogenates using a chloroform-phenol-based extraction procedure. It was reverse transcribed using the SuperScript II kit (Invitrogen, Carlsbad, CA) and random nanomer primers. Expressions of Nox2, Nox4, catalase, GPX1, GPX3, GPX4, and 18S RNA were measured by amplification of cDNA using a LightCycler real-time thermocycler (Roche Diagnostics Corp, Indianapolis, IN). Primer sequences 5' to 3' were as follows:

Nox2 (+1) GTTGGGGCTGAATGTCTTCCTCTTT

Nox2 (-2) CCACATACAGGCCCCCTTCAG

Nox4 (+1) CTGGTCTGACGGGTGTCTGCATGGTG

Nox4 (-2) CTCCGCACAATAAAGGCACAAAGGTCCAG

Catalase (+1) TTGACAGAGAGCGGATTCCT

Catalase (-2) GGCATCCCTGATGAAGAAAA

GPX1 (+1) TATGTGTGCTGCTCGGCTCT

GPX1 (-2) GTGTAGTCCCGGATCGTGGT

GPX3 (+1) AGGAGATGTGAACGGGGAGA

GPX3 (-2) CTGACTGTGGTCCGGTGGTA

GPX4 (+1) GGATGAAAGTCCAGCCCAAG

GPX4 (-2) AGGCTGGTTTTCAGGCAGAC

Transcripts were detected using SYBR Green I (Invitrogen, Carlsbad, CA) and were normalized to 18S RNA.

4.3 Experimental Results

SAMP8 mice show evidence of altered systemic redox state independent of changes in cardiac redox state at 6 months of age.

As an index of systemic oxidative stress, the redox states of plasma and heart tissue were measured. In the plasma, the following were measured: cysteine, cystine, cysteine/cystine ratio, cysteine redox potential, total plasma cysteine, GSH, GSSG, GSH/GSSG ratio, GSH redox potential, and total plasma GSH. Compared to SAMR1 mice, SAMP8 mice demonstrated decreased total plasma cysteine, and decreased total plasma GSH at 6 months of age ($p<0.05$, $n=7$) (Figure 4.1). In the heart tissue from the same mice, the following were measured: GSH, GSSG, GSH/GSSG ratio, GSH redox potential, and total heart tissue GSH. There were no significant differences in any of these measurements between SAMR1 and SAMP8 mice ($n=7$) at 6 months of age. These data suggest that SAMP8 mice at 6 months of age have increased plasma oxidative stress without an increase in oxidative stress in heart tissue.

Figure 4.1. Measurement of plasma redox states. Total plasma cysteine and glutathione were measured using HPLC analysis in plasma from 6-month-old SAMP8 and SAMR1 mice. SAMP8 mice show evidence of antioxidant depletion in the blood at 6 months of age (n=8, *p<0.05).

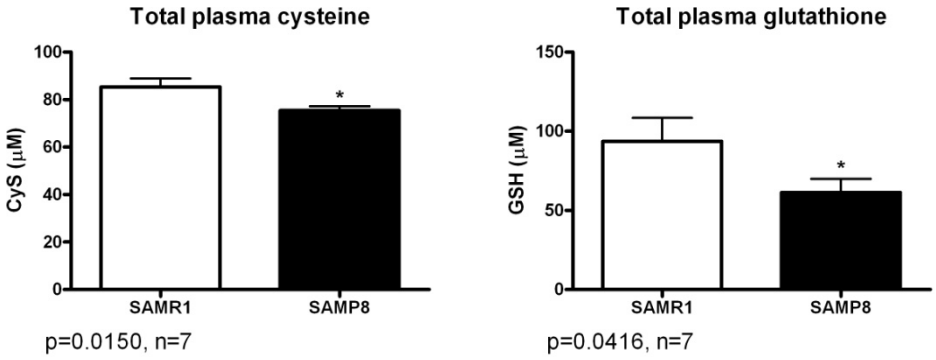

SAMP8 mice demonstrate vascular, but not myocardial, oxidative stress at 6 months of age.

Vascular oxidative stress was assessed by measuring $O_2^{\bullet-}$ in aortas from 6-month-old SAM mice using ESR. SAMP8 mice showed a significant increase in aortic $O_2^{\bullet-}$ production ($p<0.05$, $n=3$) compared to SAMR1 controls, suggesting increased vascular oxidative stress in SAMP8 mice (Figure 4.2).

Oxidative stress has been implicated in the development of diastolic dysfunction in other diastolic dysfunction models, so the contribution of oxidative stress was evaluated by measuring intracellular $O_2^{\bullet-}$ using DHE-HPLC. There were no differences in myocardial intracellular $O_2^{\bullet-}$ levels between SAMR1 and SAMP8 mice at 6 months of age ($n=7$) (Figure 4.3). It is unclear whether the lack of difference in $O_2^{\bullet-}$ observed reflects a true lack of difference in $O_2^{\bullet-}$ production, production of $O_2^{\bullet-}$ by a subset of cells which is not adequately captured by the current methodology, or if there exists the possibility that $O_2^{\bullet-}$ is being eliminated by compensatory antioxidants.

SAMP8 mice do not show differences in myocardial biopterin content at 6 months of age.

Since other models of diastolic dysfunction have implicated NOS uncoupling and BH_4 depletion, biopterin content in heart tissue was measured. Total biopterins, oxidized biopterins, BH_4, and the BH_4/oxidized biopterins ratio were measured. There were no significant differences in any of these measurements between SAMR1 and SAMP8 mice ($n=5$) at 6 months of age (Figure 4.4A-D). This suggests that BH_4 depletion, and hence NOS uncoupling, is unlikely to be a mechanism that contributes to diastolic dysfunction in the SAM model.

Figure 4.2. Measurement of vascular oxidative stress. The spin-probe CMH was used to trap $O_2^{\bullet-}$, which was then detected and quantified by ESR in aortic samples from 6-month-old SAMR1 and SAMP8 mice. SAMP8 mice show increased aortic $O_2^{\bullet-}$ production compared to SAMR1 controls at 6 months of age (n=4, $p<0.05$).

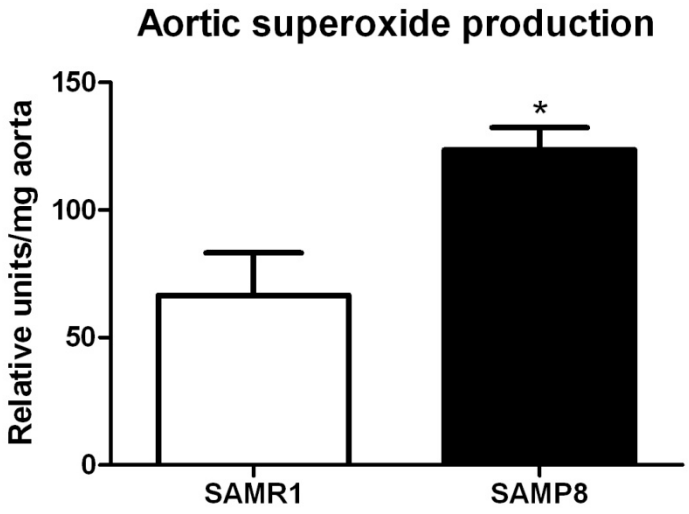

Figure 4.3. Measurement of myocardial oxidative stress. $O_2^{\bullet-}$ was measured using HPLC analysis with DHE detection in cardiac samples from 6-month-old SAMR1 and SAMP8 mice. There was no difference in cardiac intracellular $O_2^{\bullet-}$ between SAMR1 and SAMP8 mice at 6 months of age (n=8, *p*=ns).

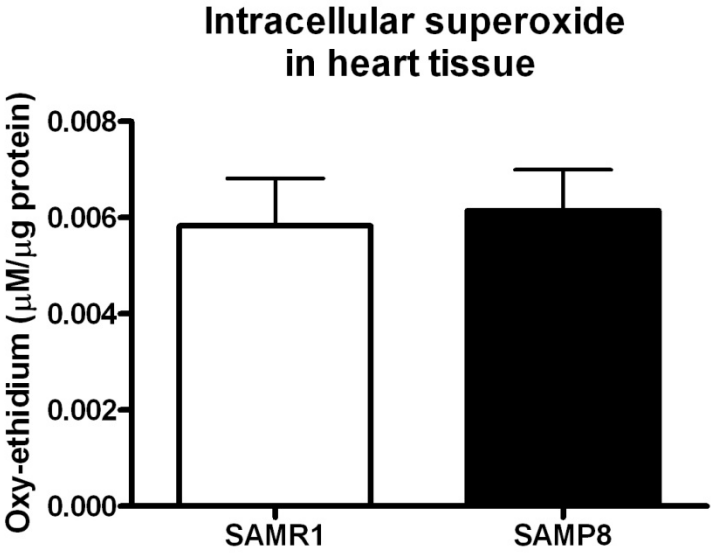

Figure 4.4. Measurement of myocardial biopterin isoforms. Biopterin content was measured with HPLC analysis and a differential oxidation method in cardiac samples from 6-month-old SAMR1 and SAMP8 mice. No differences in (A) total biopterins, (B) oxidized biopterins, (C) BH_4, or (D) BH_4/oxidized biopterins were observed between 6-month-old SAMR1 and SAMP8 mice (n=6, *p*=ns).

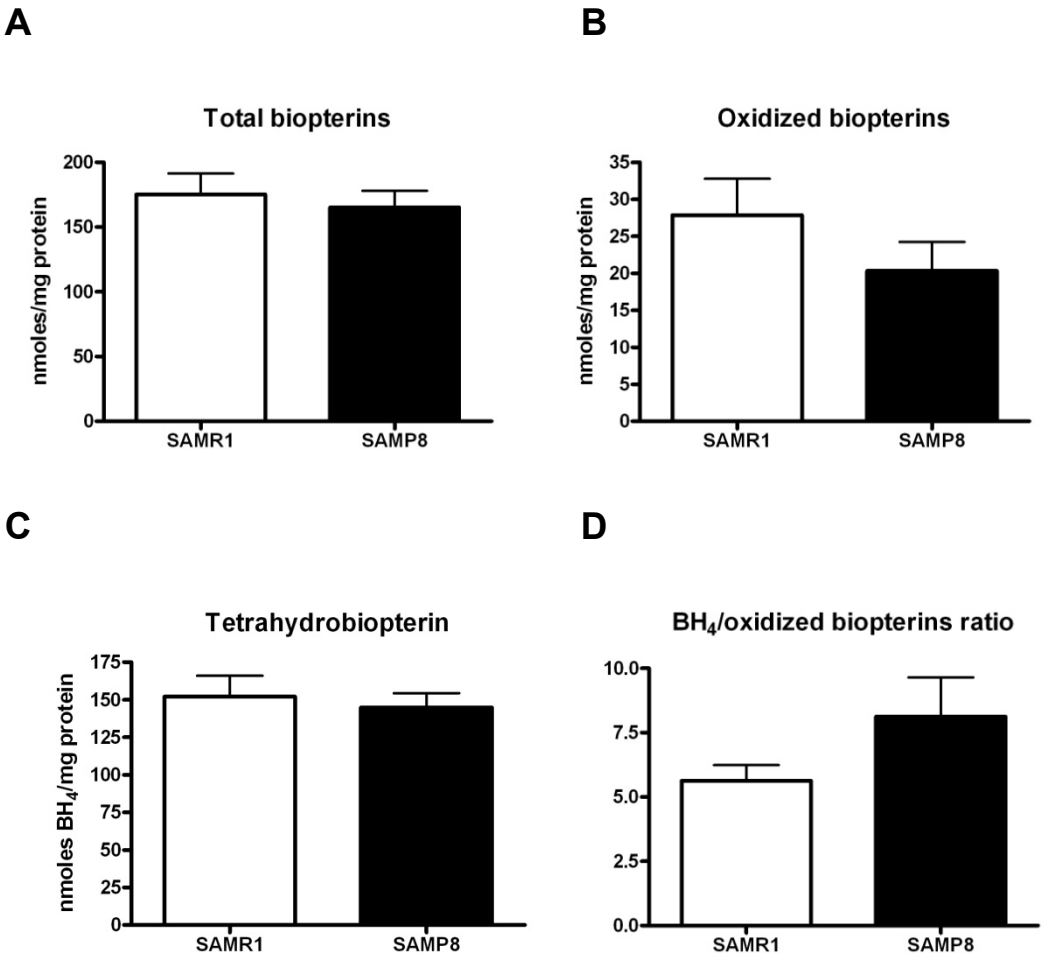

SAMP8 mice exhibit increased myocardial gene expression of oxidative stress-associated genes at 6 months of age.

To gain a more comprehensive picture of oxidative stress, gene expression of Nox2 and Nox4 were measured along with gene expression of catalase, GPX1, GPX3, and GPX4, all antioxidant enzymes responsible for detoxification of ROS. In heart tissue from 6-month-old SAM mice, expression of Nox2 and Nox4 is increased in SAMP8 mice compared to SAMR1 controls ($p<0.05$, $n=6$) (Figure 4.5). Nox2 has been shown to primarily produce $O_2^{\bullet -}$, while Nox4 is known for producing H_2O_2. When antioxidants were measured, it was found that catalase as well as the GSH peroxidases were increased in the hearts of SAMP8 mice compared to SAMR1 controls ($p<0.05$, $n=6$), suggesting upregulation of compensatory antioxidants in response to ROS produced by increased Nox2 and Nox4 (Figure 4.6).

Figure 4.5. Gene expression of NADPH oxidases. Nox2 and Nox4 expression were measured by qRT-PCR and copy number was normalized to 18S copy number in cardiac samples from 6-month-old SAMR1 and SAMP8 mice. SAMP8 mice showed increased cardiac gene expression of Nox2 and Nox4 at 6 months of age compared to SAMR1 controls (n=7, **p*<0.05). Figure generated with the assistance of Atsuko Tanaka.

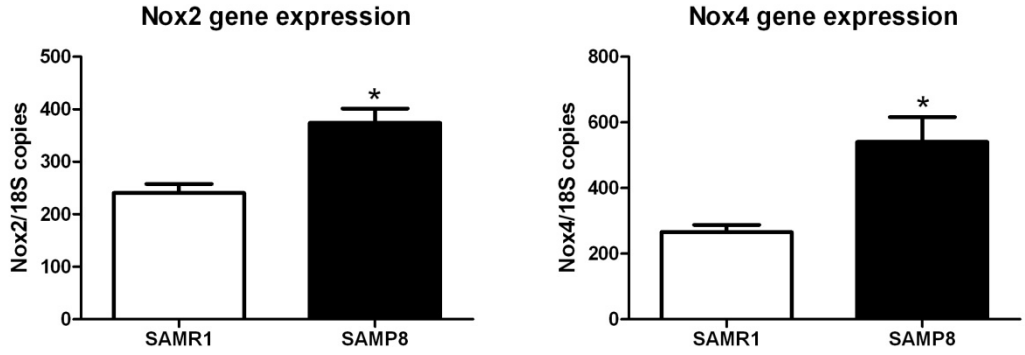

Figure 4.6. Gene expression of antioxidant enzymes. Catalase, GPX1, GPX3, and GPX4 expression were measured by qRT-PCR and copy number was normalized to 18S copy number in cardiac samples from 6-month-old SAMR1 and SAMP8 mice. SAMP8 mice showed increased cardiac gene expression of catalase, GPX1, GPX3, and GPX4 at 6 months of age compared to SAMR1 controls (n=7, *p<0.05). Figure generated with the assistance of Atsuko Tanaka.

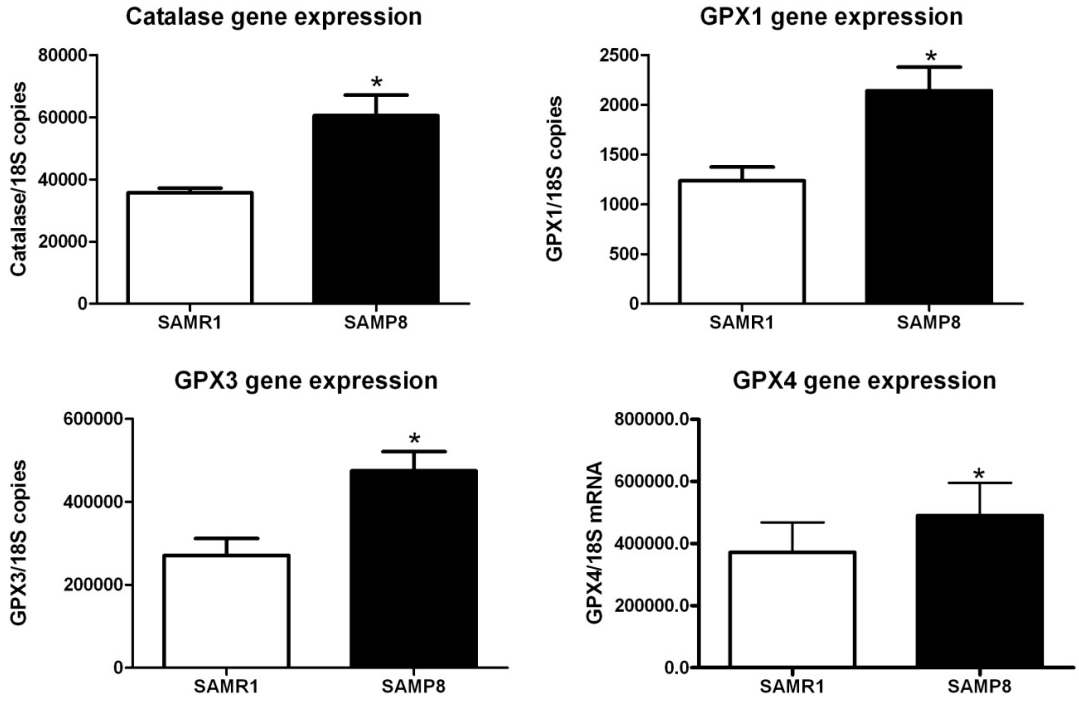

4.4 Discussion

Since it is known that advancing age is associated with increased oxidative stress and that oxidative stress plays a role in a variety of pathological cardiac conditions, the possibility that oxidative stress contributes to diastolic dysfunction has been investigated in the SAM model. Originally, hypothesis was that oxidative stress would be the driving force behind the development of diastolic dysfunction in the SAM model. It was expected that increased $O_2^{\bullet-}$ would be seen in the plasma, vasculature, and hearts of SAM8 mice at 6 months of age. Furthermore, it was also hypothesized that, based on findings in the DOCA-salt mouse model of hypertension that demonstrated diastolic dysfunction (Silberman et al., 2010), BH_4 depletion and NOS uncoupling would be the primary source of increased ROS. First, plasma redox states were assessed, and it was found that in plasma from 6-month-old SAMP8 mice, total cysteine and total GSH were reduced compared to SAMR1 controls. While this is not a direct measurement of ROS, depletion of these antioxidant reserves suggests increased oxidative stress in the plasma, indicative of systemic oxidative stress. Next, $O_2^{\bullet-}$ was measured in the aorta and in the heart. While increased $O_2^{\bullet-}$ was found in the vasculature of 6-month-old SAMP8 mice as expected, no difference in cardiac $O_2^{\bullet-}$ was found. There are several possible explanations for this. First, it is possible that the antioxidant systems are different and more active in the heart than in the blood or vasculature, so there is no net difference in $O_2^{\bullet-}$. Another possibility is that another ROS, such as H_2O_2, and not $O_2^{\bullet-}$, is the predominant source of oxidative stress in the heart. To examine these two possibilities, gene expression of NADPH oxidases and antioxidant enzymes was measured. Nox2 and Nox4 were both increased in the hearts of SAMP8 mice at 6 months of age, suggesting the production of increased ROS. It is noteworthy that Nox4 was increased as well because it primarily produces H_2O_2, not $O_2^{\bullet-}$, which lends support to the idea that the most important ROS in this model is not $O_2^{\bullet-}$, but may

in fact be H_2O_2. However, isolated cardiac fibroblast studies revealed no difference in H_2O_2 production between fibroblasts from SAMR1 and SAMP8 mice (Figure 3.6), so this discrepancy merits further investigation. It is possible that fibroblasts are not the cell type responsible for release of H_2O_2 in the heart. For example, in a study of human cardiac fibroblasts by Cucoranu et al. (Cucoranu et al., 2005), it was found that fibroblast released $O_2^{\bullet-}$ in response to pro-fibrotic signaling. Another possibility is that while fibroblasts do not release H_2O_2, they are phenotypically changed by exposure to H_2O_2 produced by other cell types, such as myocytes or immune cells. Increased Nox4 gene expression was observed in whole heart homogenate, not isolated fibroblasts. The most direct way to assess the role of H_2O_2 in future studies would be to measure H_2O_2 directly in heart tissue. While the measurement of H_2O_2 in cardiac tissue samples was attempted using the Amplex® Red assay, tissue permeability of the reagent prevented accurate measurement. Further studies are needed to elucidate which cell types produce and are targeted by which specific ROS.

When the gene expression of antioxidant enzymes was measured, it was found that in the hearts of 6-month-old SAMP8 mice, catalase, GPX1, GPX3, and GPX4 were all increased. The upregulation of antioxidants suggests an increase in the levels of ROS triggered a compensatory upregulation of antioxidants. Since these antioxidants reduce H_2O_2 to H_2O, their upregulation suggests an increased concentration of H_2O_2. The increased expression of H_2O_2-detoxifying enzymes, in combination with increased expression of Nox4, suggests that H_2O_2 may be the predominant ROS in this model. Furthermore, since H_2O_2 is a more stable ROS than $O_2^{\bullet-}$, the possibility that it influences signaling pathways is greater. While $O_2^{\bullet-}$ likely causes more acute damage to macromolecules, H_2O_2 has been found to exert its effects as a signaling molecule. For example, it has been found that Nox4-derived H_2O_2 plays a pivotal role in the transition of cardiac fibroblasts into myofibroblasts in response to TGF-β treatment (Cucoranu et

al., 2005). Because of the increase in Nox4 and the compensatory antioxidants, as well as the importance of fibrosis in this mouse model, the investigation of H_2O_2 in signaling pathways represents a potentially interesting area of future research.

In summary, it appears that by 6 months of age, SAMP8 mice display evidence of systemic oxidative stress and vascular oxidative stress compared to SAMR1 controls. Nevertheless, increased myocardial oxidative stress could not be directly demonstrated. Gene expression of several NADPH oxidases, as well as antioxidants, were increased in the hearts of SAMP8 mice. It is likely that the antioxidants are upregulated in response to increased oxidative stress, that the most important ROS in this system may be H_2O_2, not $O_2^{\bullet-}$, and that H_2O_2 may have an impact on pro-fibrotic signaling pathways that lead to cardiac fibrosis and diastolic dysfunction.

Chapter 5:

Discussion

Advancing age is well correlated with an increase in the incidence of cardiovascular disease, and with the increasing numbers of older Americans, this presents a challenge in modern medicine (Lakatta, 2003; Lakatta and Levy, 2003a; Lakatta and Levy, 2003b). One example of a specific pathological condition directly related to aging is diastolic dysfunction. In the patient population, about half of all patients that present with the clinical manifestations of heart failure, such as pulmonary edema, shortness of breath, and reduced exercise capacity, maintain a normal or near-normal EF. This subset of heart failure is referred to as heart failure with a preserved EF, or diastolic heart failure, and it is intimately related to diastolic dysfunction (Zile et al., 2005). Diastolic dysfunction refers to an impaired ability for the LV to relax and is often characterized by increased stiffening of the LV. Diastolic dysfunction can progress to overt heart failure over time (Aurigemma and Gaasch, 2004; Borlaug and Kass, 2006). While there are a number of treatment strategies used to control diastolic heart failure, such as the administration of ACE inhibitors and angiotensin II receptor blockers, no treatment is specific for this condition, and no treatment is capable of stopping or reversing this progressive pathological condition (Cheng et al., 2009). Therapeutic strategies have remained limited largely because of an incomplete mechanistic understanding of this disease and a paucity of models. Therefore, research is currently focused on elucidating the molecular pathways that result in diastolic dysfunction, and establishing models of this disease so that new strategies for treating the mechanisms underlying diastolic dysfunction can be developed.

There are a number of mouse models that display diastolic dysfunction and, many of them appear to develop diastolic dysfunction secondary to some other primary pathological condition (Basu et al., 2009; Billet et al., 2007; Di Zhang et al., 2008; Flagg et al., 2009; Maass and Leinwand, 2000; Maizel et al., 2009; Pellett et al., 2004; Prabhakar et al., 2001; Silberman et al., 2010; Tardiff et al., 1999; Xia et al., 1998; Yu et

al., 2007). Furthermore, as with other diseases, such as cancer, it appears that there is not simply one single pathway that results in diastolic dysfunction. Perhaps diastolic dysfunction could be viewed as an end-result pathophysiological condition that can be reached by the development of abnormalities in a number of distinct pathways. For example, Silberman et al. (Silberman et al., 2010). have demonstrated diastolic dysfunction in a mouse model of hypertension, the DOCA-salt model, and determined that oxidative stress and NOS uncoupling contribute to diastolic dysfunction. This model appears to effectively recapitulate diastolic dysfunction that occurs secondary to hypertension, and this is highly physiologically relevant because hypertension is one of the most significant risk factors for the development of diastolic dysfunction (Silberman et al., 2010). Also supporting the role of hypertension in diastolic dysfunction is a study where transverse aortic constriction was used to create pressure overload, and it resulted in fibrosis, diastolic dysfunction, and LV hypertrophy (Xia et al., 2009). The SAM model appears to be best suited to study diastolic dysfunction in the absence of hypertension as it is the first to demonstrate the development of diastolic dysfunction independent of hypertension. This is significant because despite the relationship between hypertension and diastolic dysfunction, not every case of diastolic dysfunction occurs in the presence of hypertension. Diastolic dysfunction has been shown to occur in patients with few if any identifiable risk factors, particularly those who are elderly. This patient demographic likely reflects a different mechanism of development of diastolic dysfunction. Because of the large aging population and the fact that diastolic dysfunction is often initially clinically silent, this abnormality likely affects a sizeable number of patients, putting them at risk for development of diastolic heart failure and poor cardiovascular outcomes.

Other models have helped establish the role of RAAS, which is involved in the regulation of blood volume and blood pressure, in diastolic dysfunction. Diastolic

dysfunction accompanied by cardiac fibrosis was found in a transgenic mouse expressing a constitutively active form of the angiotensin receptor 1 (Billet et al., 2007). In another study that examined the same pathway, a combination of cardiac-specific overexpression of the mineralocorticoid receptor and angiotensin II infusion resulted in diastolic dysfunction, fibrosis, and increased oxidative stress (Di Zhang et al., 2008). Diabetes is an increasingly common disease that is associated with poor cardiovascular outcomes and specifically with diastolic dysfunction (Desai and Fang, 2008). In a mouse model of type I diabetes, diastolic dysfunction was demonstrated; however, it appears that changes in fatty acid metabolism, and not fibrosis, is the predominant mechanism for the development of diastolic dysfunction in this model (Basu et al., 2009). In a streptozotocin-induced model of diabetes, diastolic dysfunction was observed, but it was also accompanied by the presence of systolic dysfunction. These changes in cardiac function were attributed to increased oxidative stress and mitochondrial dysfunction (Yu et al., 2007). Finally, several mouse models of FHC have been created by creating single amino acid mutations in a number of different muscle proteins, and these mice develop diastolic dysfunction as well, demonstrating that abnormalities in actin-myosin cross-bridge cycling could contribute to impaired active relaxation and thus diastolic dysfunction (Li et al., 2010; Prabhakar et al., 2001; Spindler et al., 1998; Tardiff et al., 1999). That each of these distinct models develops diastolic dysfunction suggests diastolic dysfunction can develop as a result of hypertension, changes in the RAAS, diabetes, or FHC. Moreover, diastolic dysfunction may or may not be accompanied by fibrosis or oxidative stress depending upon the pathway that causes it, suggesting there are multiple mechanisms for the development of diastolic dysfunction.

While there exist a number of models that demonstrate diastolic dysfunction, and hence implicate a number of different proteins, pathways, and related cardiovascular diseases, there has not thus far been a model that demonstrates spontaneous diastolic

dysfunction. Furthermore, the impact of aging on diastolic dysfunction in mouse models has not been extensively explored. The SAM model is a unique model of spontaneous age-associated diastolic dysfunction, and it is valuable because it develops diastolic dysfunction in the course of normal aging, which more closely recapitulates age-associated diastolic dysfunction observed in humans. Another advantageous feature of the SAM model is that senescence-prone mice develop diastolic dysfunction between 3 and 6 months of age, which is a relatively early time frame in the life cycle of laboratory mice. In contrast to wild-type mice, which may develop diastolic dysfunction at the age of 1 year or older, the SAM model offers a convenient window of time for studying the mechanisms that contribute to diastolic dysfunction.

In the SAM model, SAMP8 mice develop diastolic dysfunction, as measured by echocardiography and invasive hemodynamics, by 6 months of age compared to SAMR1 controls. Using echocardiography, a decrease in the E/A ratio and the E'/A' ratio was observed in SAMP8 mice compared to SAMR1 mice at 6 months of age, indicating decreased early diastolic filling and increased late diastolic filling. A hallmark of diastolic dysfunction is an increased dependence upon late diastolic filling, which is mainly provided by atrial contraction, to maintain adequate filling. The changes observed in these ratios are consistent with this characteristic of diastolic dysfunction. Invasive hemodynamic studies were used to confirm the echocardiography findings, and invasive hemodynamic studies have the advantage of providing more detailed information about which aspect of diastole, i.e. passive stiffness versus active relaxation, is impaired. Using invasive hemodynamics, an increase in the LVEDPVR, which indicates increased passive stiffness of the LV, was observed, which was accompanied by a modest but significant increase in the LVEDP, which is consistent with diastolic dysfunction because it indicates increased filling pressures, which have also been observed in diastolic dysfunction. Nevertheless, no differences in maximal slope of left

ventricular pressure decline during diastole, $-dP/dt_{min}$, the time constant of pressure decay, τ, or time interval of pressure decay to 50% of peak pressure, $t_{1/2}$ were observed. All of these measurements represent different ways of assessing pressure decay. Whereas LVEDPVR is thought to represent passive stiffness, these measurements, and in particular, τ, are thought to be more representative of the active relaxation component of diastole. As illustrated by the wide variety of mouse models that develop diastolic dysfunction, there appears to be more than one path to the development of diastolic dysfunction, and diastolic dysfunction resulting from different underlying mechanisms and pathologies likely manifests somewhat different characteristics. Based on the observations in this aging model, it appears that diastolic dysfunction is primarily related to increased passive stiffness of the LV as opposed to impaired active relaxation, which more likely characterizes models which develop diastolic dysfunction because of sarcomeric protein mutations, for example.

Since diastolic dysfunction independent of hypertension was demonstrated, the potential role of fibrosis in the SAM model was examined. It appears that a primary cause of diastolic dysfunction in the SAM model is LV stiffening, which is directly related to cardiac fibrosis. The elevated LVEDPVR is strong evidence of LV stiffening, and this is further supported by the increases in cardiac collagens 1A1 and 3A as well as fibronectin observed using both qRT-PCR and histology. Nevertheless, there is a discrepancy in the data because while fibrosis and increased TGF-β and CTGF gene expression in the LV of 6-month-old SAMP8 mice using qRT-PCR have been found, increased TGF-β protein in either plasma or LV homogenates using the TGF-β ELISA was not demonstrated. There are several possible explanations for this discrepancy. First, it is possible that while TGF-β mRNA is increased, it does not translate in increased protein expression of TGF-β. Nevertheless, the presence of fibrosis in the LV

suggests that pro-fibrotic cytokines are active in the LV. Perhaps while TGF-β does not increase to statistically significant levels, it does increase other pro-fibrotic cytokines, such as CTGF. It is known that the synergism of these two cytokines is far more pro-fibrotic than either one alone. Originally, experiments aimed to quantify both TGF-β and CTGF using Western blotting, but the method was not sensitive enough to detect quantifiable protein levels, so instead an ELISA was used to measure TGF-β. Future studies could investigate whether CTGF protein expression is increased in this model. Endothelin-1 has also been found to interact synergistically with TGF-β to stimulate ECM production (Horstmeyer et al., 2005; Xu et al., 2004), so this protein could be investigated as well. Another possibility is that while the level of TGF-β protein is not increased in the heart, the expression of the TGF-β receptors is increased, which could explain the fibrosis observed in the LV. TGF-β binds to the a combination of the TGF-β type I and type II receptors, which phosphorylate Smad2 and Smad3, which translocates the nucleus to initiate transcription of fibrosis-associated genes (Zawel et al., 1998). Furthermore, TGF-β receptors could have altered sensitivity to TGF-β as a result of the pro-fibrotic environment that contributes to the cardiac fibrosis observed in the myocardium. In addition to the Smad signaling pathway, TGF-β also signals through the MAPK pathway (Chen et al., 2002b). Therefore, expression and/or phosphorylation of any of these signaling proteins could contribute to fibrosis in this model and represent future experimental directions. A third possibility is that while neither circulating (plasma) or local (cardiac) TGF-β levels are different between SAMR1 and SAMP8 mice, TGF-β has a pronounced pro-fibrotic effect on the LV of SAMP8 mice. While this could affect any number of cells in the LV, the role played by fibroblasts was examined. Because fibroblasts, and their transition to myofibroblasts under the influence of TGF-β, is pivotal in the fibrotic process, isolated cardiac fibroblasts from 6-month-old SAMR1 and SAMP8

mice were characterized to determine how fibroblasts from SAMP8 mice might express more pro-fibrotic markers and/or react more strongly to stimulation with TGF-β.

Since fibroblasts play a pivotal role in fibrosis, the next hypothesis was that cardiac fibroblasts isolated from 6-month-old SAMP8 mice would demonstrate a phenotype more characteristic of activated myofibroblasts, evidenced by increased expression of α-SMA, compared to cardiac fibroblasts isolated from SAMR1 mice. It was also expected that SAMP8 fibroblasts would express increased collagens and fibronectin. In contrast with this hypothesis, no differences were observed in α-SMA, fibronectin 1, collagen 1A1, or collagen 3A at baseline in cardiac fibroblasts isolated from SAMP8 versus SAMR1 mice. There are several possible explanations for this observation. First, it is simply possible that there are no differences in pro-fibrotic markers between fibroblasts isolated from SAMR1 and SAMP8 hearts. One reason for this could be that as the cells were maintained in culture, their phenotype changed such that differences between the two types of fibroblasts were no longer discernible. Although fibroblasts from SAMR1 and SAMP8 mice were harvested at the same time and cultured under identical conditions, the possibility exists that they both changed significantly in culture. Alternatively, it is possible that differences between SAMR1 and SAMP8 cardiac fibroblasts are not observed until the fibroblasts are subjected to some sort of challenge, such as stimulation with a pro-fibrotic or pro-inflammatory cytokine. The hypothesis was refined to account for this possibility, and it was expected that upon stimulation with TGF-β, cardiac fibroblasts from SAMP8 mice would have an exaggerated response and express more pro-fibrotic markers than cardiac fibroblasts from SAMR1 mice subjected to the same conditions. While it was found that TGF-β stimulation markedly increased expression of α-SMA, but it had a similar effect in both groups of fibroblasts. No differences were observed in collagen 1A1 or fibronectin

between SAMR1 and SAMP8 fibroblasts, and there was no increase in these markers in response to TGF-β stimulation, which was unexpected. The most compelling piece of evidence for difference in response to TGF-β stimulation between SAMR1 and SAMP8 fibroblasts is the change in collagen 3A. Somewhat paradoxically, TGF-β treatment decreased collagen 3A in SAMP8, but not SAMR1, fibroblasts. While it might be expected that collagen expression would increase in response to TGF-β stimulation, the decrease in collagen 3A, which is the more elastic, compliant form of collagen, could result in a stiffer LV because the more elastic form is reduced, and hence the stiffer collagen 1A1 isoform predominates. Taken together, these data suggest that there are no differences between cardiac fibroblasts isolated from SAMR1 versus SAMP8 mice at baseline, and differences in the response to TGF-β are modest and so far restricted to decreased expression of collagen 3A in SAMP8 fibroblasts. However, the possibility that the cells changed phenotype significantly in culture exists, so the possibility that differences exist but have been lost in culture cannot be ruled out. To investigate the possibility, an ideal experiment would be one where cardiac fibroblasts are harvested and the pro-fibrotic markers are immediately measured, circumventing the need for cell culture. However, this approach is complicated by the very small quantity of cardiac fibroblasts that can be isolated from a single mouse heart.

Before the role and possible mechanisms of fibrosis were investigated in the SAM model, the original hypothesis stated that oxidative stress would prove to be the main mechanism behind the development of diastolic dysfunction in this model. Oxidative stress has been implicated in aging (Balaban et al., 2005), demonstrated in a variety of cardiovascular diseases (Griendling and FitzGerald, 2003a; Griendling and FitzGerald, 2003b) including diastolic dysfunction (Dai and Rabinovitch, 2009), and has also been demonstrated in the SAM model. In previous studies, senescence-prone mice

have shown increased lipid peroxidation in the skin and increased ROS in the brain (Chiba et al., 2009), impaired aerobic metabolism in liver mitochondria (Nakahara et al., 1998), and prolonged lifespan as a result of administration of a free radical trapping agent (Edamatsu et al., 1995). In cardiac mitochondria, increased lipid peroxidation was accompanied by changes in GSH and GPX, and decreased mitochondrial respiratory capability, indicating the presence of cardiac oxidative stress (Rodriguez et al., 2007a; Rodriguez et al., 2007b). Based on these previous studies, it was hypothesized that accelerated senescence triggers increased ROS production, which may also upregulate compensatory antioxidant systems. Indirect evidence of systemic oxidative stress was observed in 6-month-old SAMP8 mice compared to SAMR1 mice in the form of depleted total cysteine and GSH in the plasma. Next, increased $O_2^{\bullet-}$ was found in the aortas of 6-month-old SAMP8 mice, indicative of vascular oxidative stress. However, there was no difference found in $O_2^{\bullet-}$ in LV tissue samples. There are several possible explanations for this observation. First, it is possible that oxidative stress initially increases in the heart, and in doing so, upregulates compensatory antioxidants. Possible evidence for this idea was found in increased gene expression of cardiac catalase, GPX1, GPX3, and GPX4. Therefore, a net increase in ROS may not be present because of the concomitant increase in antioxidant capacity. A second possibility is that $O_2^{\bullet-}$ is not the dominant ROS in the heart. $O_2^{\bullet-}$ is highly reactive, and in addition to being difficult to measure from an experimental standpoint, it is likely to react quickly. Because of its reactivity, it is a particularly damaging ROS; it is capable of combining with $NO^{\bullet}$ to produce peroxynitrite, which can damage lipids and proteins. $O_2^{\bullet-}$ is dismutated to H_2O_2 by SOD. Unlike $O_2^{\bullet-}$, H_2O_2 is a longer-lived ROS because it is less reactive. As such, it is more likely to function as a signaling molecule. Though these experiments primarily focused on attempting to quantify $O_2^{\bullet-}$, there is a strong possibility that H_2O_2 plays an important role in this model. Evidence for this idea comes from the observation that

Nox4, an NADPH oxidase that primarily produces H_2O_2, is increased in the hearts of 6-month-old SAMP8 mice compared to SAMR1 mice. Furthermore, the fact that the specific antioxidants that were increased, catalase and GPX, detoxify H_2O_2 and not $O_2^{\bullet-}$, suggests that H_2O_2-mediated signaling plays an important role in diastolic dysfunction in this model. A third possibility is that oxidative stress is compartmentalized in one specific subcellular compartment in the heart, so measuring ROS in a homogenized sample of the LV fails to detect the compartmentalized increase. The studies by Rodriguez et al. demonstrated mitochondrial $O_2^{\bullet-}$ in aged SAMP8 mice (Rodriguez et al., 2007a; Rodriguez et al., 2007b); however, these studies of 6-month-old SAM mice failed to demonstrate increased $O_2^{\bullet-}$ in the LV homogenates, and it is possible that subcellular compartmentalization was responsible for this discrepancy. Likewise, it is possible that oxidative stress is increased in one cell type and not another. For example, if ROS are increased in fibroblasts, which make up a relatively small volume of myocardial tissue as a result of their smaller size relative to myocytes, measuring ROS in a tissue homogenate containing many cell types may not reveal the difference. To address this possibility, cultured cardiac fibroblasts isolated from 6-month-old SAMR1 and SAMP8 mice were used. In addition to the aforementioned studies of fibrosis in these cells, H_2O_2 production was also measured. The hypothesis was that cardiac fibroblasts isolated from SAMP8 mice would produce more H_2O_2; however, no difference was detected. It is possible again that culture conditions changed the phenotype of the cells, that differences between the two groups are not evident until stimulation, or that fibroblasts do not produce appreciable amounts of H_2O_2.

While diastolic dysfunction accompanied by cardiac fibrosis and changes in proteins related to oxidative stress has been demonstrated in the SAM model and established the SAM model as a valuable model for the study of age-related diastolic dysfunction, there are several weaknesses inherent to this model. First, the model is

phenotypic in nature; it was developed by a subjective scale assessing mice for general body characteristics such as behavior, coat and skin appearance, and cataracts. In contrast to transgenic mouse models, it is not known which genes are altered and what, mechanistically, is responsible for accelerated senescence in the SAMP strains. Since these mice are somewhat of a “black box” with respect to genetics, the source of the differences observed between SAMR1 mice and SAMP8 mice is unknown, and there exists the possibility that some other characteristic of these mice, which may be unrelated to aging, is responsible for the fibrosis and diastolic dysfunction observed. On the other hand, since these mice are not subject to genetic manipulation and the compensatory changes that often accompany the deletion or overexpression of a specific gene, they are more likely to reflect natural aging. Like many strains of laboratory mice used currently, the SAM model is an inbred strain, so while the reduction of population variability is advantageous in controlled laboratory experiments, results are not fully generalizable. Aside from the animal model itself, there are other limitations in methodology. For example, methods used to measure oxidative stress are well-validated in aorta samples. Techniques such ESR and HPLC depend upon the ability of the spin probe or DHE, respectively, to permeate the tissue. While this occurs predictably in this tissues such as aortas, results can be more varied in LV tissue samples. Therefore, measurement of ROS is not always straightforward. Furthermore, the heart is made up of different types of cells with very different functions, and changes in ROS, cytokines, or fibrosis markers may be highly compartmentalized, making detection difficult. One way to overcome the compartmentalization issue is to culture the different cell types and assess them individually, such as the experiments that were done on isolated cardiac fibroblasts aimed at discerning the specific role of that cell type in cardiac fibrosis. However, this technique is subject to limitations of its own. The main disadvantage of primary cell culture is that cells often change phenotype in culture since

the conditions are not identical to those in the intact organism. An optimal technique would be one that would allow for the separation of cell types and measurement of proteins and ROS immediately. In an alternative approach, pathways could be selectively targeted with pharmacological agents in mice and the physiological effects could be measured. For example, SAM mice could be given a TGF-β inhibitor from 3 to 6 months of age then evaluated for the presence of diastolic dysfunction and cardiac fibrosis to test the hypothesis that this pro-fibrotic cytokine is responsible for fibrosis accompanied by diastolic dysfunction.

The SAM model has been shown to display age-associated diastolic dysfunction accompanied by cardiac fibrosis. This knowledge provides a foundation for further studies into the mechanism of diastolic dysfunction in this model. Two of the most noteworthy patient characteristics of those with diastolic dysfunction are old age and being female, which stands in contrast to the more "classic" form of systolic heart failure, in which the typical patient is more likely to be male, younger, and have a history of ischemia (Aurigemma and Gaasch, 2004). At this point, the SAM model has been used to establish the relationship between aging and diastolic dysfunction, and it is currently being using it to investigate the relationship between female gender and the development of diastolic dysfunction. Based on what is known about the clinical population, it would be reasonable to expect that female SAMP8 mice might develop worse diastolic dysfunction, or develop diastolic dysfunction earlier than their male counterparts. In conjunction with these studies, the role of the extracellular matrix in the development of diastolic dysfunction is also being investigated. These studies will determine whether there are alteration in MMPs and their inhibitors associated with the fibrotic process. Furthermore, plasma analyte profiling is being done to identify possible cytokines and markers in the blood that contribute to fibrosis and diastolic dysfunction.

This high-throughput screening method is particularly useful because it will quickly analyze many molecules and provide refined direction for more directed future studies.

In summary, these data indicate that SAMP8 mice develop age-associated diastolic dysfunction independent of hypertension. This diastolic dysfunction is associated with cardiac fibrosis, which includes deposition of fibronectin and collagen as well as increased gene expression of pro-fibrotic cytokines. Diastolic dysfunction and fibrosis in this model are also accompanied by changes in gene expression of NADPH oxidases as well as antioxidants. Collectively, the data suggest that diastolic dysfunction, fibrosis, and oxidative stress are all linked. However, as is common in many complex scientific projects, this work has raised as many questions as it has answered, and the knowledge gained in the course of these studies has provided a framework for further study into the mechanisms behind diastolic dysfunction in this model. Based on these data as well as the background literature that has guided the development of this project, a refined hypothesis is proposed. As SAMP8 mice undergo accelerated senescence, the mitochondria become damaged and begin to overproduce ROS. The production of ROS activates other signaling pathways. For example, increased ROS results in increased angiotensin II, which in turn stimulates increased production of pro-fibrotic cytokines. Additionally, mitochondrial ROS result in increased expression of NADPH oxidases, such as Nox2 and Nox4. Nox2 produces $O_2^{\bullet -}$ and Nox4 produces H_2O_2, which becomes the predominant ROS in this model. Increased H_2O_2 levels lead to upregulation of compensatory antioxidants such as catalase and GPX. These antioxidants regulate the balance of H_2O_2 enough to prevent overt tissue damage by ROS, but enough H_2O_2 persists to activate signaling pathways, such as those that lead to cardiac fibrosis. Nox4 produces H_2O_2 that increases TGF-β. This pivotal pro-fibrotic cytokine is increased by both H_2O_2 and angiotensin II, and TGF-β in turn results

in an increase in CTGF. These two cytokines work synergistically to activate fibroblasts and promote deposition of ECM. The heart undergoes remodeling, in which MMPs are activated and collagen is deposited, which ultimately stiffens the LV and leads to diastolic dysfunction.

These data have demonstrated age-associated diastolic dysfunction in a mouse model of aging, and have shown cardiac fibrosis to be a likely cause of diastolic dysfunction. Mechanistic studies have aimed to elucidate the molecular mechanisms and pathways behind the fibrotic response, and data indicate increased gene expression of pro-fibrotic cytokines and ECM proteins as well as a potential role for cardiac fibroblasts resulting from their differential response to TGF-β. Finally, data demonstrate increased gene expression of NADPH oxidases as well as compensatory antioxidants. This is accompanied by increased systemic and vascular oxidative stress without a documented increase in myocardial oxidative stress. It is likely that oxidative stress plays a role in diastolic dysfunction and fibrosis and this merits further study and elucidation. Since diastolic dysfunction is a complicated disorder which may result secondarily from a diverse number of primary cardiac diseases, and because it is likely that there is not one single pathway that leads to its development, there are probably other pathways and derangements that could lead to this pathophysiological condition other than oxidative stress and pro-fibrotic cytokines. A recent paper by Cieslik et al. (Cieslik et al., 2011), explores the role of immune-inflammatory dysregulation in age-associated of diastolic dysfunction accompanied by fibrosis. With progressive aging, increased numbers of $CD45^+$ fibroblasts of myeloid origin were found in the hearts of aged C57BL/6 mice, and increased levels of monocyte chemotactic protein-1, interleukin-4, and interleukin-13 were found as well, and these markers all correlated with the areas of most pronounced fibrosis and expression of procollagen in the myocardium. In vitro studies demonstrated that interleukin-13 promoted monocyte and

fibroblast transformation, and that monocyte chemotactic protein-1 caused a shift to a Th2 phenotype that correlated with increased interstitial fibrosis. These data suggest that as animals age, their immune systems may undergo changes that contribute to a pro-inflammatory and pro-fibrotic environment, and this can be a contributing factor to diastolic dysfunction. In future studies, it would likely be fruitful to examine the role of the immune system and its possible dysregulation in contributing to a pro-inflammatory, pro-fibrotic environment that promotes cardiac fibrosis and diastolic dysfunction in the SAM model.

In conclusion, the SAM model is a useful model of age-associated diastolic dysfunction that occurs secondary to cardiac fibrosis. The increasing population of older individuals, coupled with the fact that half of all patients with heart failure have diastolic heart failure, means that diastolic dysfunction represents a major public health concern. Moreover, the available treatment strategies, limited largely by an incomplete understanding of the pathophysiology of this condition, leaves a wide-open field for scientific research and discovery. With the use of animal models like the SAM model, a deeper understanding of the cause and mechanisms of development of diastolic dysfunction can be gained with the hope that this progress paves the way for the betterment of human health.

References

Ahmed MS, Oie E, Vinge LE, Yndestad A, Oystein Andersen G, Andersson Y, Attramadal T and Attramadal H (2004) Connective tissue growth factor--a novel mediator of angiotensin II-stimulated cardiac fibroblast activation in heart failure in rats. *J Mol Cell Cardiol* **36**(3):393-404.

Alvarez-Garcia O, Vega-Naredo I, Sierra V, Caballero B, Tomas-Zapico C, Camins A, Garcia JJ, Pallas M and Coto-Montes A (2006) Elevated oxidative stress in the brain of senescence-accelerated mice at 5 months of age. *Biogerontology* **7**(1):43-52.

Antonozzi I, Carducci C, Vestri L, Pontecorvi A and Moretti F (1988) Rapid and sensitive method for high-performance liquid chromatographic analysis of pterins in biological fluids. *J Chromatogr* **459**:319-324.

Asai K, Kudej RK, Shen YT, Yang GP, Takagi G, Kudej AB, Geng YJ, Sato N, Nazareno JB, Vatner DE, Natividad F, Bishop SP and Vatner SF (2000) Peripheral vascular endothelial dysfunction and apoptosis in old monkeys. *Arterioscler Thromb Vasc Biol* **20**(6):1493-1499.

Aurigemma GP and Gaasch WH (2004) Clinical practice. Diastolic heart failure. *N Engl J Med* **351**(11):1097-1105.

Balaban RS, Nemoto S and Finkel T (2005) Mitochondria, oxidants, and aging. *Cell* **120**(4):483-495.

Basso N, Cini R, Pietrelli A, Ferder L, Terragno NA and Inserra F (2007) Protective effect of long-term angiotensin II inhibition. *Am J Physiol Heart Circ Physiol* **293**(3):H1351-1358.

Basu R, Oudit GY, Wang X, Zhang L, Ussher JR, Lopaschuk GD and Kassiri Z (2009) Type 1 diabetic cardiomyopathy in the Akita (Ins2WT/C96Y) mouse model is characterized by lipotoxicity and diastolic dysfunction with preserved systolic function. *Am J Physiol Heart Circ Physiol* **297**(6):H2096-2108.

Benigni A, Corna D, Zoja C, Sonzogni A, Latini R, Salio M, Conti S, Rottoli D, Longaretti L, Cassis P, Morigi M, Coffman TM and Remuzzi G (2009) Disruption of the Ang II type 1 receptor promotes longevity in mice. *J Clin Invest* **119**(3):524-530.

Billet S, Bardin S, Verp S, Baudrie V, Michaud A, Conchon S, Muffat-Joly M, Escoubet B, Souil E, Hamard G, Bernstein KE, Gasc JM, Elghozi JL, Corvol P and Clauser E (2007) Gain-of-function mutant of angiotensin II receptor, type 1A, causes hypertension and cardiovascular fibrosis in mice. *J Clin Invest* **117**(7):1914-1925.

Blagosklonny MV, Campisi J, Sinclair DA, Bartke A, Blasco MA, Bonner WM, Bohr VA, Brosh RM, Jr., Brunet A, Depinho RA, Donehower LA, Finch CE, Finkel T, Gorospe M, Gudkov AV, Hall MN, Hekimi S, Helfand SL, Karlseder J, Kenyon C, Kroemer G, Longo V, Nussenzweig A, Osiewacz HD, Peeper DS, Rando TA, Rudolph KL, Sassone-Corsi P, Serrano M, Sharpless NE, Skulachev VP, Tilly JL, Tower J, Verdin E and Vijg J (2010) Impact papers on aging in 2009. *Aging (Albany NY)* **2**(3):111-121.

Border WA and Noble NA (1998) Interactions of transforming growth factor-beta and angiotensin II in renal fibrosis. *Hypertension* **31**(1 Pt 2):181-188.

Borlaug BA and Kass DA (2006) Mechanisms of diastolic dysfunction in heart failure. *Trends Cardiovasc Med* **16**(8):273-279.

Brutsaert DL (2003) Cardiac endothelial-myocardial signaling: its role in cardiac growth, contractile performance, and rhythmicity. *Physiol Rev* **83**(1):59-115.

Bujak M, Kweon HJ, Chatila K, Li N, Taffet G and Frangogiannis NG (2008) Aging-related defects are associated with adverse cardiac remodeling in a mouse model of reperfused myocardial infarction. *J Am Coll Cardiol* **51**(14):1384-1392.

Burkhoff D, Mirsky I and Suga H (2005) Assessment of systolic and diastolic ventricular properties via pressure-volume analysis: a guide for clinical, translational, and basic researchers. *Am J Physiol Heart Circ Physiol* **289**(2):H501-512.

Burton AC (1954) Relation of structure to function of the tissues of the wall of blood vessels. *Physiol Rev* **34**(4):619-642.

Busuttil RA, Rubio M, Dolle ME, Campisi J and Vijg J (2003) Oxygen accelerates the accumulation of mutations during the senescence and immortalization of murine cells in culture. *Aging Cell* **2**(6):287-294.

Butterfield DA, Howard BJ, Yatin S, Allen KL and Carney JM (1997) Free radical oxidation of brain proteins in accelerated senescence and its modulation by N-tert-butyl-alpha-phenylnitrone. *Proc Natl Acad Sci U S A* **94**(2):674-678.

Cai H and Harrison DG (2000) Endothelial dysfunction in cardiovascular diseases: the role of oxidant stress. *Circ Res* **87**(10):840-844.

Campbell SE and Katwa LC (1997) Angiotensin II stimulated expression of transforming growth factor-beta1 in cardiac fibroblasts and myofibroblasts. *J Mol Cell Cardiol* **29**(7):1947-1958.

CDC (2007) The State of Aging and Health in America 2007, (Foundation CfDCaPaTMC ed), The Merck Company Foundation, Whitehouse Station, NJ.

Challah M, Nadaud S, Philippe M, Battle T, Soubrier F, Corman B and Michel JB (1997) Circulating and cellular markers of endothelial dysfunction with aging in rats. *Am J Physiol* **273**(4 Pt 2):H1941-1948.

Chen C, Liu Y and Zheng P (2009) mTOR regulation and therapeutic rejuvenation of aging hematopoietic stem cells. *Sci Signal* **2**(98):ra75.

Chen CH, Ting CT, Lin SJ, Hsu TL, Ho SJ, Chou P, Chang MS, O'Connor F, Spurgeon H, Lakatta E and Yin FC (1998) Which arterial and cardiac parameters best predict left ventricular mass? *Circulation* **98**(5):422-428.

Chen MA (2009) Heart failure with preserved ejection fraction in older adults. *Am J Med* **122**(8):713-723.

Chen MM, Lam A, Abraham JA, Schreiner GF and Joly AH (2000) CTGF expression is induced by TGF- beta in cardiac fibroblasts and cardiac myocytes: a potential role in heart fibrosis. *J Mol Cell Cardiol* **32**(10):1805-1819.

Chen Y, Blom IE, Sa S, Goldschmeding R, Abraham DJ and Leask A (2002a) CTGF expression in mesangial cells: involvement of SMADs, MAP kinase, and PKC. *Kidney Int* **62**(4):1149-1159.

Chen Y, Blom IE, Sa S, Goldschmeding R, Abraham DJ and Leask A (2002b) CTGF expression in mesangial cells: involvement of SMADs, MAP kinase, and PKC. *Kidney international* **62**(4):1149-1159.

Cheng XW, Okumura K, Kuzuya M, Jin Z, Nagata K, Obata K, Inoue A, Hirashiki A, Takeshita K, Unno K, Harada K, Shi GP, Yokota M and Murohara T (2009) Mechanism of diastolic stiffening of the failing myocardium and its prevention by angiotensin receptor and calcium channel blockers. *J Cardiovasc Pharmacol* **54**(1):47-56.

Chiba Y, Shimada A, Kumagai N, Yoshikawa K, Ishii S, Furukawa A, Takei S, Sakura M, Kawamura N and Hosokawa M (2009) The senescence-accelerated mouse (SAM): a higher oxidative stress and age-dependent degenerative diseases model. *Neurochem Res* **34**(4):679-687.

Chua CC, Chua BH, Zhao ZY, Krebs C, Diglio C and Perrin E (1991) Effect of growth factors on collagen metabolism in cultured human heart fibroblasts. *Connect Tissue Res* **26**(4):271-281.

Chuva de Sousa Lopes SM, Feijen A, Korving J, Korchynskyi O, Larsson J, Karlsson S, ten Dijke P, Lyons KM, Goldschmeding R, Doevendans P and Mummery CL (2004) Connective tissue growth factor expression and Smad signaling during mouse heart development and myocardial infarction. *Dev Dyn* **231**(3):542-550.

Cieslik KA, Taffet GE, Carlson S, Hermosillo J, Trial J and Entman ML (2011) Immune-inflammatory dysregulation modulates the incidence of progressive fibrosis and diastolic stiffness in the aging heart. *Journal of molecular and cellular cardiology* **50**(1):248-256.

Cigola E, Kajstura J, Li B, Meggs LG and Anversa P (1997) Angiotensin II activates programmed myocyte cell death in vitro. *Exp Cell Res* **231**(2):363-371.

Cleland JG, Tendera M, Adamus J, Freemantle N, Polonski L and Taylor J (2006) The perindopril in elderly people with chronic heart failure (PEP-CHF) study. *Eur Heart J* **27**(19):2338-2345.

Colman RJ, Anderson RM, Johnson SC, Kastman EK, Kosmatka KJ, Beasley TM, Allison DB, Cruzen C, Simmons HA, Kemnitz JW and Weindruch R (2009) Caloric restriction delays disease onset and mortality in rhesus monkeys. *Science* **325**(5937):201-204.

Crawford DC, Chobanian AV and Brecher P (1994) Angiotensin II induces fibronectin expression associated with cardiac fibrosis in the rat. *Circ Res* **74**(4):727-739.

Cucoranu I, Clempus R, Dikalova A, Phelan PJ, Ariyan S, Dikalov S and Sorescu D (2005) NAD(P)H oxidase 4 mediates transforming growth factor-beta1-induced differentiation of cardiac fibroblasts into myofibroblasts. *Circ Res* **97**(9):900-907.

Dai DF and Rabinovitch PS (2009) Cardiac aging in mice and humans: the role of mitochondrial oxidative stress. *Trends Cardiovasc Med* **19**(7):213-220.

Dai DF, Santana LF, Vermulst M, Tomazela DM, Emond MJ, MacCoss MJ, Gollahon K, Martin GM, Loeb LA, Ladiges WC and Rabinovitch PS (2009) Overexpression of catalase targeted to mitochondria attenuates murine cardiac aging. *Circulation* **119**(21):2789-2797.

de Boer RA, Pokharel S, Flesch M, van Kampen DA, Suurmeijer AJ, Boomsma F, van Gilst WH, van Veldhuisen DJ and Pinto YM (2004) Extracellular signal regulated kinase and SMAD signaling both mediate the angiotensin II driven progression towards overt heart failure in homozygous TGR(mRen2)27. *J Mol Med* **82**(10):678-687.

de Souza-Pinto NC, Eide L, Hogue BA, Thybo T, Stevnsner T, Seeberg E, Klungland A and Bohr VA (2001) Repair of 8-oxodeoxyguanosine lesions in mitochondrial dna depends on the oxoguanine dna glycosylase (OGG1) gene and 8-oxoguanine accumulates in the mitochondrial dna of OGG1-defective mice. *Cancer Res* **61**(14):5378-5381.

Demidenko ZN, Zubova SG, Bukreeva EI, Pospelov VA, Pospelova TV and Blagosklonny MV (2009) Rapamycin decelerates cellular senescence. *Cell Cycle* **8**(12):1888-1895.

Desai A and Fang JC (2008) Heart failure with preserved ejection fraction: hypertension, diabetes, obesity/sleep apnea, and hypertrophic and infiltrative cardiomyopathy. *Heart failure clinics* **4**(1):87-97.

Desmouliere A, Geinoz A, Gabbiani F and Gabbiani G (1993) Transforming growth factor-beta 1 induces alpha-smooth muscle actin expression in granulation tissue myofibroblasts and in quiescent and growing cultured fibroblasts. *J Cell Biol* **122**(1):103-111.

Di Zhang A, Nguyen Dinh Cat A, Soukaseum C, Escoubet B, Cherfa A, Messaoudi S, Delcayre C, Samuel JL and Jaisser F (2008) Cross-talk between mineralocorticoid and angiotensin II signaling for cardiac remodeling. *Hypertension* **52**(6):1060-1067.

Ding A, Hwang S and Schwab R (1994) Effect of aging on murine macrophages. Diminished response to IFN-gamma for enhanced oxidative metabolism. *J Immunol* **153**(5):2146-2152.

Ebner R, Chen RH, Lawler S, Zioncheck T and Derynck R (1993) Determination of type I receptor specificity by the type II receptors for TGF-beta or activin. *Science* **262**(5135):900-902.

Edamatsu R, Mori A and Packer L (1995) The spin-trap N-tert-alpha-phenyl-butylnitrone prolongs the life span of the senescence accelerated mouse. *Biochem Biophys Res Commun* **211**(3):847-849.

Eghbali M, Tomek R, Woods C and Bhambi B (1991) Cardiac fibroblasts are predisposed to convert into myocyte phenotype: specific effect of transforming growth factor beta. *Proc Natl Acad Sci U S A* **88**(3):795-799.

Engelmann GL and Grutkoski PS (1994) Coordinate TGF-beta receptor gene expression during rat heart development. *Cell Mol Biol Res* **40**(2):93-104.

Epel ES, Merkin SS, Cawthon R, Blackburn EH, Adler NE, Pletcher MJ and Seeman TE (2009) The rate of leukocyte telomere shortening predicts mortality from cardiovascular disease in elderly men. *Aging (Albany NY)* **1**(1):81-88.

Esler MD, Turner AG, Kaye DM, Thompson JM, Kingwell BA, Morris M, Lambert GW, Jennings GL, Cox HS and Seals DR (1995) Aging effects on human sympathetic neuronal function. *Am J Physiol* **268**(1 Pt 2):R278-285.

Everett THt, Verheule S, Wilson EE, Foreman S and Olgin JE (2004) Left atrial dilatation resulting from chronic mitral regurgitation decreases spatiotemporal organization of atrial fibrillation in left atrium. *Am J Physiol Heart Circ Physiol* **286**(6):H2452-2460.

Fenton M, Huang HL, Hong Y, Hawe E, Kurz DJ and Erusalimsky JD (2004) Early atherogenesis in senescence-accelerated mice. *Exp Gerontol* **39**(1):115-122.

Finkel T (2011) Telomeres and mitochondrial function. *Circ Res* **108**(8):903-904.

Flagg TP, Cazorla O, Remedi MS, Haim TE, Tones MA, Bahinski A, Numann RE, Kovacs A, Schaffer JE, Nichols CG and Nerbonne JM (2009) Ca2+-independent alterations in diastolic sarcomere length and relaxation kinetics in a mouse model of lipotoxic diabetic cardiomyopathy. *Circ Res* **104**(1):95-103.

Fleg JL and Kennedy HL (1982) Cardiac arrhythmias in a healthy elderly population: detection by 24-hour ambulatory electrocardiography. *Chest* **81**(3):302-307.

Fleg JL, O'Connor F, Gerstenblith G, Becker LC, Clulow J, Schulman SP and Lakatta EG (1995) Impact of age on the cardiovascular response to dynamic upright exercise in healthy men and women. *J Appl Physiol* **78**(3):890-900.

Flood JF and Morley JE (1998) Learning and memory in the SAMP8 mouse. *Neurosci Biobehav Rev* **22**(1):1-20.

Forman K, Vara E, Garcia C, Kireev R, Cuesta S, Acuna-Castroviejo D and Tresguerres JA (2010) Beneficial effects of melatonin on cardiological alterations in a murine model of accelerated aging. *J Pineal Res* **49**(3):312-320.

Fraga CG, Shigenaga MK, Park JW, Degan P and Ames BN (1990) Oxidative damage to DNA during aging: 8-hydroxy-2'-deoxyguanosine in rat organ DNA and urine. *Proc Natl Acad Sci U S A* **87**(12):4533-4537.

Franklin SS, Gustin Wt, Wong ND, Larson MG, Weber MA, Kannel WB and Levy D (1997) Hemodynamic patterns of age-related changes in blood pressure. The Framingham Heart Study. *Circulation* **96**(1):308-315.

Fraticelli A, Josephson R, Danziger R, Lakatta E and Spurgeon H (1989) Morphological and contractile characteristics of rat cardiac myocytes from maturation to senescence. *Am J Physiol* **257**(1 Pt 2):H259-265.

Frey RS and Mulder KM (1997) Involvement of extracellular signal-regulated kinase 2 and stress-activated protein kinase/Jun N-terminal kinase activation by transforming growth factor beta in the negative growth control of breast cancer cells. *Cancer Res* **57**(4):628-633.

Galis ZS, Sukhova GK and Libby P (1995) Microscopic localization of active proteases by in situ zymography: detection of matrix metalloproteinase activity in vascular tissue. *FASEB J* **9**(10):974-980.

Gerstenblith G, Frederiksen J, Yin FC, Fortuin NJ, Lakatta EG and Weisfeldt ML (1977) Echocardiographic assessment of a normal adult aging population. *Circulation* **56**(2):273-278.

Gimbrone MA, Jr. (1999) Vascular endothelium, hemodynamic forces, and atherogenesis. *Am J Pathol* **155**(1):1-5.

Griendling KK and FitzGerald GA (2003a) Oxidative stress and cardiovascular injury: Part I: basic mechanisms and in vivo monitoring of ROS. *Circulation* **108**(16):1912-1916.

Griendling KK and FitzGerald GA (2003b) Oxidative stress and cardiovascular injury: Part II: animal and human studies. *Circulation* **108**(17):2034-2040.

Hamilton ML, Van Remmen H, Drake JA, Yang H, Guo ZM, Kewitt K, Walter CA and Richardson A (2001) Does oxidative damage to DNA increase with age? *Proc Natl Acad Sci U S A* **98**(18):10469-10474.

Harman D (1956) Aging: a theory based on free radical and radiation chemistry. *J Gerontol* **11**(3):298-300.

Harrison DE, Strong R, Sharp ZD, Nelson JF, Astle CM, Flurkey K, Nadon NL, Wilkinson JE, Frenkel K, Carter CS, Pahor M, Javors MA, Fernandez E and Miller RA (2009) Rapamycin fed late in life extends lifespan in genetically heterogeneous mice. *Nature* **460**(7253):392-395.

Hartsough MT and Mulder KM (1995) Transforming growth factor beta activation of p44mapk in proliferating cultures of epithelial cells. *J Biol Chem* **270**(13):7117-7124.

Hayflick L (1965) The Limited in Vitro Lifetime of Human Diploid Cell Strains. *Exp Cell Res* **37**:614-636.

Heine UI, Burmester JK, Flanders KC, Danielpour D, Munoz EF, Roberts AB and Sporn MB (1991) Localization of transforming growth factor-beta 1 in mitochondria of murine heart and liver. *Cell Regul* **2**(6):467-477.

Hill JM, Zalos G, Halcox JP, Schenke WH, Waclawiw MA, Quyyumi AA and Finkel T (2003) Circulating endothelial progenitor cells, vascular function, and cardiovascular risk. *N Engl J Med* **348**(7):593-600.

Holzenberger M, Dupont J, Ducos B, Leneuve P, Geloen A, Even PC, Cervera P and Le Bouc Y (2003) IGF-1 receptor regulates lifespan and resistance to oxidative stress in mice. *Nature* **421**(6919):182-187.

Hongo K, Nakagomi T, Kassell NF, Sasaki T, Lehman M, Vollmer DG, Tsukahara T, Ogawa H and Torner J (1988) Effects of aging and hypertension on endothelium-dependent vascular relaxation in rat carotid artery. *Stroke* **19**(7):892-897.

Horstmeyer A, Licht C, Scherr G, Eckes B and Krieg T (2005) Signalling and regulation of collagen I synthesis by ET-1 and TGF-beta1. *The FEBS journal* **272**(24):6297-6309.

Hosokawa M, Abe T, Higuchi K, Shimakawa K, Omori Y, Matsushita T, Kogishi K, Deguchi E, Kishimoto Y, Yasuoka K and Takeda T (1997) Management and

design of the maintenance of SAM mouse strains: an animal model for accelerated senescence and age-associated disorders. *Exp Gerontol* **32**(1-2):111-116.

Inada K, Yokoi I, Kabuto H, Habu H, Mori A and Ogawa N (1996) Age-related increase in nitric oxide synthase activity in senescence accelerated mouse brain and the effect of long-term administration of superoxide radical scavenger. *Mech Ageing Dev* **89**(2):95-102.

Jenkins GM, Crow MT, Bilato C, Gluzband Y, Ryu WS, Li Z, Stetler-Stevenson W, Nater C, Froehlich JP, Lakatta EG and Cheng L (1998) Increased expression of membrane-type matrix metalloproteinase and preferential localization of matrix metalloproteinase-2 to the neointima of balloon-injured rat carotid arteries. *Circulation* **97**(1):82-90.

Junqueira LC, Bignolas G and Brentani RR (1979) Picrosirius staining plus polarization microscopy, a specific method for collagen detection in tissue sections. *Histochem J* **11**(4):447-455.

Kass DA, Bronzwaer JG and Paulus WJ (2004) What mechanisms underlie diastolic dysfunction in heart failure? *Circ Res* **94**(12):1533-1542.

Kim S, Ohta K, Hamaguchi A, Yukimura T, Miura K and Iwao H (1995) Angiotensin II induces cardiac phenotypic modulation and remodeling in vivo in rats. *Hypertension* **25**(6):1252-1259.

Kleinhenz JM, Kleinhenz DJ, You S, Ritzenthaler JD, Hansen JM, Archer DR, Sutliff RL and Hart CM (2009) Disruption of endothelial peroxisome proliferator-activated receptor-gamma reduces vascular nitric oxide production. *Am J Physiol Heart Circ Physiol* **297**(5):H1647-1654.

Koban MU, Moorman AF, Holtz J, Yacoub MH and Boheler KR (1998) Expressional analysis of the cardiac Na-Ca exchanger in rat development and senescence. *Cardiovasc Res* **37**(2):405-423.

Kook H, Lepore JJ, Gitler AD, Lu MM, Wing-Man Yung W, Mackay J, Zhou R, Ferrari V, Gruber P and Epstein JA (2003) Cardiac hypertrophy and histone deacetylase-dependent transcriptional repression mediated by the atypical homeodomain protein Hop. *J Clin Invest* **112**(6):863-871.

Lakatta EG (1993) Cardiovascular regulatory mechanisms in advanced age. *Physiol Rev* **73**(2):413-467.

Lakatta EG (2003) Arterial and cardiac aging: major shareholders in cardiovascular disease enterprises: Part III: cellular and molecular clues to heart and arterial aging. *Circulation* **107**(3):490-497.

Lakatta EG and Levy D (2003a) Arterial and cardiac aging: major shareholders in cardiovascular disease enterprises: Part I: aging arteries: a "set up" for vascular disease. *Circulation* **107**(1):139-146.

Lakatta EG and Levy D (2003b) Arterial and cardiac aging: major shareholders in cardiovascular disease enterprises: Part II: the aging heart in health: links to heart disease. *Circulation* **107**(2):346-354.

Leask A (2007) TGFbeta, cardiac fibroblasts, and the fibrotic response. *Cardiovasc Res* **74**(2):207-212.

Leask A, Holmes A, Black CM and Abraham DJ (2003) Connective tissue growth factor gene regulation. Requirements for its induction by transforming growth factor-beta 2 in fibroblasts. *J Biol Chem* **278**(15):13008-13015.

Lee AA, Dillmann WH, McCulloch AD and Villarreal FJ (1995) Angiotensin II stimulates the autocrine production of transforming growth factor-beta 1 in adult rat cardiac fibroblasts. *J Mol Cell Cardiol* **27**(10):2347-2357.

Lee AC, Fenster BE, Ito H, Takeda K, Bae NS, Hirai T, Yu ZX, Ferrans VJ, Howard BH and Finkel T (1999) Ras proteins induce senescence by altering the intracellular levels of reactive oxygen species. *J Biol Chem* **274**(12):7936-7940.

Li G, Li RK, Mickle DA, Weisel RD, Merante F, Ball WT, Christakis GT, Cusimano RJ and Williams WG (1998) Elevated insulin-like growth factor-I and transforming growth factor-beta 1 and their receptors in patients with idiopathic hypertrophic obstructive cardiomyopathy. A possible mechanism. *Circulation* **98**(19 Suppl):II144-149; discussion II149-150.

Li Y, Charles PY, Nan C, Pinto JR, Wang Y, Liang J, Wu G, Tian J, Feng HZ, Potter JD, Jin JP and Huang X (2010) Correcting diastolic dysfunction by Ca2+ desensitizing troponin in a transgenic mouse model of restrictive cardiomyopathy. *J Mol Cell Cardiol* **49**(3):402-411.

Li Z, Froehlich J, Galis ZS and Lakatta EG (1999) Increased expression of matrix metalloproteinase-2 in the thickened intima of aged rats. *Hypertension* **33**(1):116-123.

Lijnen PJ, Petrov VV and Fagard RH (2000) Induction of cardiac fibrosis by transforming growth factor-beta(1). *Mol Genet Metab* **71**(1-2):418-435.

Lim H and Zhu YZ (2006) Role of transforming growth factor-beta in the progression of heart failure. *Cell Mol Life Sci* **63**(22):2584-2596.

Liu F, Levin MD, Petrenko NB, Lu MM, Wang T, Yuan LJ, Stout AL, Epstein JA and Patel VV (2008) Histone-deacetylase inhibition reverses atrial arrhythmia inducibility and fibrosis in cardiac hypertrophy independent of angiotensin. *J Mol Cell Cardiol* **45**(6):715-723.

Llorens S, de Mera RM, Pascual A, Prieto-Martin A, Mendizabal Y, de Cabo C, Nava E and Jordan J (2007) The senescence-accelerated mouse (SAM-P8) as a model for the study of vascular functional alterations during aging. *Biogerontology* **8**(6):663-672.

Long X, Boluyt MO, O'Neill L, Zheng JS, Wu G, Nitta YK, Crow MT and Lakatta EG (1999) Myocardial retinoid X receptor, thyroid hormone receptor, and myosin heavy chain gene expression in the rat during adult aging. *J Gerontol A Biol Sci Med Sci* **54**(1):B23-27.

Lu T and Finkel T (2008) Free radicals and senescence. *Exp Cell Res* **314**(9):1918-1922.

Luo W, Grupp IL, Harrer J, Ponniah S, Grupp G, Duffy JJ, Doetschman T and Kranias EG (1994) Targeted ablation of the phospholamban gene is associated with markedly enhanced myocardial contractility and loss of beta-agonist stimulation. *Circ Res* **75**(3):401-409.

Maass A and Leinwand LA (2000) Animal models of hypertrophic cardiomyopathy. *Curr Opin Cardiol* **15**(3):189-196.

Maizel J, Six I, Slama M, Tribouilloy C, Sevestre H, Poirot S, Giummelly P, Atkinson J, Choukroun G, Andrejak M, Kamel S, Maziere JC and Massy ZA (2009) Mechanisms of aortic and cardiac dysfunction in uremic mice with aortic calcification. *Circulation* **119**(2):306-313.

Marks AR (2001) Ryanodine receptors/calcium release channels in heart failure and sudden cardiac death. *J Mol Cell Cardiol* **33**(4):615-624.

Maron BJ, Niimura H, Casey SA, Soper MK, Wright GB, Seidman JG and Seidman CE (2001) Development of left ventricular hypertrophy in adults in hypertrophic cardiomyopathy caused by cardiac myosin-binding protein C gene mutations. *J Am Coll Cardiol* **38**(2):315-321.

Marx SO, Reiken S, Hisamatsu Y, Jayaraman T, Burkhoff D, Rosemblit N and Marks AR (2000) PKA phosphorylation dissociates FKBP12.6 from the calcium release

channel (ryanodine receptor): defective regulation in failing hearts. *Cell* **101**(4):365-376.

Massie BM, Carson PE, McMurray JJ, Komajda M, McKelvie R, Zile MR, Anderson S, Donovan M, Iverson E, Staiger C and Ptaszynska A (2008) Irbesartan in patients with heart failure and preserved ejection fraction. *N Engl J Med* **359**(23):2456-2467.

Maurer MS, Shefrin EA and Fleg JL (1995) Prevalence and prognostic significance of exercise-induced supraventricular tachycardia in apparently healthy volunteers. *Am J Cardiol* **75**(12):788-792.

Migliaccio E, Giorgio M, Mele S, Pelicci G, Reboldi P, Pandolfi PP, Lanfrancone L and Pelicci PG (1999) The p66shc adaptor protein controls oxidative stress response and life span in mammals. *Nature* **402**(6759):309-313.

Minamino T, Miyauchi H, Yoshida T, Ishida Y, Yoshida H and Komuro I (2002) Endothelial cell senescence in human atherosclerosis: role of telomere in endothelial dysfunction. *Circulation* **105**(13):1541-1544.

Miyauchi H, Minamino T, Tateno K, Kunieda T, Toko H and Komuro I (2004) Akt negatively regulates the in vitro lifespan of human endothelial cells via a p53/p21-dependent pathway. *EMBO J* **23**(1):212-220.

Mori T, Kawara S, Shinozaki M, Hayashi N, Kakinuma T, Igarashi A, Takigawa M, Nakanishi T and Takehara K (1999) Role and interaction of connective tissue growth factor with transforming growth factor-beta in persistent fibrosis: A mouse fibrosis model. *J Cell Physiol* **181**(1):153-159.

Motwani JG and Topol EJ (1998) Aortocoronary saphenous vein graft disease: pathogenesis, predisposition, and prevention. *Circulation* **97**(9):916-931.

Murphy CT (2006) The search for DAF-16/FOXO transcriptional targets: approaches and discoveries. *Exp Gerontol* **41**(10):910-921.

Nakahara H, Kanno T, Inai Y, Utsumi K, Hiramatsu M, Mori A and Packer L (1998) Mitochondrial dysfunction in the senescence accelerated mouse (SAM). *Free Radic Biol Med* **24**(1):85-92.

Nemoto S and Finkel T (2002) Redox regulation of forkhead proteins through a p66shc-dependent signaling pathway. *Science* **295**(5564):2450-2452.

Nishikawa T, Takahashi JA, Fujibayashi Y, Fujisawa H, Zhu B, Nishimura Y, Ohnishi K, Higuchi K, Hashimoto N and Hosokawa M (1998) An early stage mechanism of the age-associated mitochondrial dysfunction in the brain of SAMP8 mice; an age-associated neurodegeneration animal model. *Neurosci Lett* **254**(2):69-72.

Nishiyama A and Kim-Mitsuyama S (2010) New approaches to blockade of the renin-angiotensin-aldosterone system: overview of regulation of the renin-angiotensin-aldosterone system. *J Pharmacol Sci* **113**(4):289-291.

North BJ and Verdin E (2004) Sirtuins: Sir2-related NAD-dependent protein deacetylases. *Genome Biol* **5**(5):224.

Oliver CN, Ahn BW, Moerman EJ, Goldstein S and Stadtman ER (1987) Age-related changes in oxidized proteins. *J Biol Chem* **262**(12):5488-5491.

Olivetti G, Giordano G, Corradi D, Melissari M, Lagrasta C, Gambert SR and Anversa P (1995) Gender differences and aging: effects on the human heart. *J Am Coll Cardiol* **26**(4):1068-1079.

Owan TE, Hodge DO, Herges RM, Jacobsen SJ, Roger VL and Redfield MM (2006) Trends in prevalence and outcome of heart failure with preserved ejection fraction. *N Engl J Med* **355**(3):251-259.

Parrinello S, Samper E, Krtolica A, Goldstein J, Melov S and Campisi J (2003) Oxygen sensitivity severely limits the replicative lifespan of murine fibroblasts. *Nat Cell Biol* **5**(8):741-747.

Pearl R (1928) *The Rate of Living*. University of London Press, London.
Pellett AA, Tolar WG, Merwin DG and Kerut EK (2004) The Tei index: methodology and disease state values. *Echocardiography* **21**(7):669-672.
Pelouch V, Dixon IM, Golfman L, Beamish RE and Dhalla NS (1993) Role of extracellular matrix proteins in heart function. *Mol Cell Biochem* **129**(2):101-120.
Pena JR, Szkudlarek AC, Warren CM, Heinrich LS, Gaffin RD, Jagatheesan G, del Monte F, Hajjar RJ, Goldspink PH, Solaro RJ, Wieczorek DF and Wolska BM (2010) Neonatal gene transfer of Serca2a delays onset of hypertrophic remodeling and improves function in familial hypertrophic cardiomyopathy. *J Mol Cell Cardiol* **49**(6):993-1002.
Pendergrass KD, Varghese ST, Maiellaro-Rafferty K, Brown ME, Taylor WR and Davis ME (2011) Temporal effects of catalase overexpression on healing after myocardial infarction. *Circ Heart Fail* **4**(1):98-106.
Periasamy M and Janssen PM (2008) Molecular basis of diastolic dysfunction. *Heart Fail Clin* **4**(1):13-21.
Prabhakar R, Boivin GP, Grupp IL, Hoit B, Arteaga G, Solaro JR and Wieczorek DF (2001) A familial hypertrophic cardiomyopathy alpha-tropomyosin mutation causes severe cardiac hypertrophy and death in mice. *J Mol Cell Cardiol* **33**(10):1815-1828.
Quarrie JK and Riabowol KT (2004) Murine models of life span extension. *Sci Aging Knowledge Environ* **2004**(31):re5.
Rebrin I, Zicker S, Wedekind KJ, Paetau-Robinson I, Packer L and Sohal RS (2005) Effect of antioxidant-enriched diets on glutathione redox status in tissue homogenates and mitochondria of the senescence-accelerated mouse. *Free Radic Biol Med* **39**(4):549-557.
Richter C, Park JW and Ames BN (1988) Normal oxidative damage to mitochondrial and nuclear DNA is extensive. *Proc Natl Acad Sci U S A* **85**(17):6465-6467.
Rivard A, Berthou-Soulie L, Principe N, Kearney M, Curry C, Branellec D, Semenza GL and Isner JM (2000) Age-dependent defect in vascular endothelial growth factor expression is associated with reduced hypoxia-inducible factor 1 activity. *J Biol Chem* **275**(38):29643-29647.
Rodeheffer RJ, Gerstenblith G, Beard E, Fleg JL, Becker LC, Weisfeldt ML and Lakatta EG (1986) Postural changes in cardiac volumes in men in relation to adult age. *Exp Gerontol* **21**(4-5):367-378.
Rodriguez MI, Carretero M, Escames G, Lopez LC, Maldonado MD, Tan DX, Reiter RJ and Acuna-Castroviejo D (2007a) Chronic melatonin treatment prevents age-dependent cardiac mitochondrial dysfunction in senescence-accelerated mice. *Free Radic Res* **41**(1):15-24.
Rodriguez MI, Escames G, Lopez LC, Garcia JA, Ortiz F, Lopez A and Acuna-Castroviejo D (2007b) Melatonin administration prevents cardiac and diaphragmatic mitochondrial oxidative damage in senescence-accelerated mice. *J Endocrinol* **194**(3):637-643.
Roger VL, Go AS, Lloyd-Jones DM, Adams RJ, Berry JD, Brown TM, Carnethon MR, Dai S, de Simone G, Ford ES, Fox CS, Fullerton HJ, Gillespie C, Greenlund KJ, Hailpern SM, Heit JA, Ho PM, Howard VJ, Kissela BM, Kittner SJ, Lackland DT, Lichtman JH, Lisabeth LD, Makuc DM, Marcus GM, Marelli A, Matchar DB, McDermott MM, Meigs JB, Moy CS, Mozaffarian D, Mussolino ME, Nichol G, Paynter NP, Rosamond WD, Sorlie PD, Stafford RS, Turan TN, Turner MB, Wong ND and Wylie-Rosett J (2011) Heart disease and stroke statistics--2011 update: a report from the American Heart Association. *Circulation* **123**(4):e18-e209.

Sahin E, Colla S, Liesa M, Moslehi J, Muller FL, Guo M, Cooper M, Kotton D, Fabian AJ, Walkey C, Maser RS, Tonon G, Foerster F, Xiong R, Wang YA, Shukla SA, Jaskelioff M, Martin ES, Heffernan TP, Protopopov A, Ivanova E, Mahoney JE, Kost-Alimova M, Perry SR, Bronson R, Liao R, Mulligan R, Shirihai OS, Chin L and DePinho RA (2011) Telomere dysfunction induces metabolic and mitochondrial compromise. *Nature* **470**(7334):359-365.

Sawada M and Carlson JC (1987) Changes in superoxide radical and lipid peroxide formation in the brain, heart and liver during the lifetime of the rat. *Mech Ageing Dev* **41**(1-2):125-137.

Schocken DD, Benjamin EJ, Fonarow GC, Krumholz HM, Levy D, Mensah GA, Narula J, Shor ES, Young JB and Hong Y (2008) Prevention of heart failure: a scientific statement from the American Heart Association Councils on Epidemiology and Prevention, Clinical Cardiology, Cardiovascular Nursing, and High Blood Pressure Research; Quality of Care and Outcomes Research Interdisciplinary Working Group; and Functional Genomics and Translational Biology Interdisciplinary Working Group. *Circulation* **117**(19):2544-2565.

Seidman CE and Seidman JG (1991) Mutations in cardiac myosin heavy chain genes cause familial hypertrophic cardiomyopathy. *Mol Biol Med* **8**(2):159-166.

Selesniemi K, Lee HJ, Niikura T and Tilly JL (2009) Young adult donor bone marrow infusions into female mice postpone age-related reproductive failure and improve offspring survival. *Aging* **1**(1):49-57.

Serrano M, Lin AW, McCurrach ME, Beach D and Lowe SW (1997) Oncogenic ras provokes premature cell senescence associated with accumulation of p53 and p16INK4a. *Cell* **88**(5):593-602.

Shah RV, Desai AS and Givertz MM (2010) The effect of renin-angiotensin system inhibitors on mortality and heart failure hospitalization in patients with heart failure and preserved ejection fraction: a systematic review and meta-analysis. *Journal of cardiac failure* **16**(3):260-267.

Sharpless NE (2004) Ink4a/Arf links senescence and aging. *Exp Gerontol* **39**(11-12):1751-1759.

Silberman GA, Fan TH, Liu H, Jiao Z, Xiao HD, Lovelock JD, Boulden BM, Widder J, Fredd S, Bernstein KE, Wolska BM, Dikalov S, Harrison DG and Dudley SC, Jr. (2010) Uncoupled cardiac nitric oxide synthase mediates diastolic dysfunction. *Circulation* **121**(4):519-528.

Simpson D, Liu H, Fan TH, Nerem R and Dudley SC, Jr. (2007) A tissue engineering approach to progenitor cell delivery results in significant cell engraftment and improved myocardial remodeling. *Stem Cells* **25**(9):2350-2357.

Skalli O, Schurch W, Seemayer T, Lagace R, Montandon D, Pittet B and Gabbiani G (1989) Myofibroblasts from diverse pathologic settings are heterogeneous in their content of actin isoforms and intermediate filament proteins. *Lab Invest* **60**(2):275-285.

Spindler M, Saupe KW, Christe ME, Sweeney HL, Seidman CE, Seidman JG and Ingwall JS (1998) Diastolic dysfunction and altered energetics in the alphaMHC403/+ mouse model of familial hypertrophic cardiomyopathy. *J Clin Invest* **101**(8):1775-1783.

Stary HC, Blankenhorn DH, Chandler AB, Glagov S, Insull W, Jr., Richardson M, Rosenfeld ME, Schaffer SA, Schwartz CJ, Wagner WD and et al. (1992) A definition of the intima of human arteries and of its atherosclerosis-prone regions. A report from the Committee on Vascular Lesions of the Council on Arteriosclerosis, American Heart Association. *Circulation* **85**(1):391-405.

Stratton R, Rajkumar V, Ponticos M, Nichols B, Shiwen X, Black CM, Abraham DJ and Leask A (2002) Prostacyclin derivatives prevent the fibrotic response to TGF-beta by inhibiting the Ras/MEK/ERK pathway. *FASEB J* **16**(14):1949-1951.

Sun Y, Ratajska A and Weber KT (1995) Bradykinin receptor and tissue ACE binding in myocardial fibrosis: response to chronic angiotensin II or aldosterone administration in rats. *J Mol Cell Cardiol* **27**(2):813-822.

Sun Y, Zhang JQ, Zhang J and Ramires FJ (1998) Angiotensin II, transforming growth factor-beta1 and repair in the infarcted heart. *J Mol Cell Cardiol* **30**(8):1559-1569.

Swinne CJ, Shapiro EP, Lima SD and Fleg JL (1992) Age-associated changes in left ventricular diastolic performance during isometric exercise in normal subjects. *Am J Cardiol* **69**(8):823-826.

Taffet GE, Pham TT and Hartley CJ (1997) The age-associated alterations in late diastolic function in mice are improved by caloric restriction. *J Gerontol A Biol Sci Med Sci* **52**(6):B285-290.

Takeda T (1999) Senescence-accelerated mouse (SAM): a biogerontological resource in aging research. *Neurobiol Aging* **20**(2):105-110.

Takeda T, Higuchi K and Hosokawa M (1997a) Senescence-accelerated Mouse (SAM): With Special Reference to Development and Pathological Phenotypes. *Ilar J* **38**(3):109-118.

Takeda T, Hosokawa M and Higuchi K (1991) Senescence-accelerated mouse (SAM): a novel murine model of accelerated senescence. *J Am Geriatr Soc* **39**(9):911-919.

Takeda T, Hosokawa M, Takeshita S, Irino M, Higuchi K, Matsushita T, Tomita Y, Yasuhira K, Hamamoto H, Shimizu K, Ishii M and Yamamuro T (1981) A new murine model of accelerated senescence. *Mech Ageing Dev* **17**(2):183-194.

Takeda T, Matsushita T, Kurozumi M, Takemura K, Higuchi K and Hosokawa M (1997b) Pathobiology of the senescence-accelerated mouse (SAM). *Exp Gerontol* **32**(1-2):117-127.

Tappel AL (1973) Lipid peroxidation damage to cell components. *Fed Proc* **32**(8):1870-1874.

Tardiff JC, Hewett TE, Palmer BM, Olsson C, Factor SM, Moore RL, Robbins J and Leinwand LA (1999) Cardiac troponin T mutations result in allele-specific phenotypes in a mouse model for hypertrophic cardiomyopathy. *J Clin Invest* **104**(4):469-481.

Thannickal VJ, Lee DY, White ES, Cui Z, Larios JM, Chacon R, Horowitz JC, Day RM and Thomas PE (2003) Myofibroblast differentiation by transforming growth factor-beta1 is dependent on cell adhesion and integrin signaling via focal adhesion kinase. *J Biol Chem* **278**(14):12384-12389.

Treins C, Giorgetti-Peraldi S, Murdaca J and Van Obberghen E (2001) Regulation of vascular endothelial growth factor expression by advanced glycation end products. *J Biol Chem* **276**(47):43836-43841.

Trifunovic A, Wredenberg A, Falkenberg M, Spelbrink JN, Rovio AT, Bruder CE, Bohlooly YM, Gidlof S, Oldfors A, Wibom R, Tornell J, Jacobs HT and Larsson NG (2004) Premature ageing in mice expressing defective mitochondrial DNA polymerase. *Nature* **429**(6990):417-423.

Trinei M, Giorgio M, Cicalese A, Barozzi S, Ventura A, Migliaccio E, Milia E, Padura IM, Raker VA, Maccarana M, Petronilli V, Minucci S, Bernardi P, Lanfrancone L and Pelicci PG (2002) A p53-p66Shc signalling pathway controls intracellular redox status, levels of oxidation-damaged DNA and oxidative stress-induced apoptosis. *Oncogene* **21**(24):3872-3878.

Vaitkevicius PV, Fleg JL, Engel JH, O'Connor FC, Wright JG, Lakatta LE, Yin FC and Lakatta EG (1993) Effects of age and aerobic capacity on arterial stiffness in healthy adults. *Circulation* **88**(4 Pt 1):1456-1462.

Verheule S, Sato T, Everett Tt, Engle SK, Otten D, Rubart-von der Lohe M, Nakajima HO, Nakajima H, Field LJ and Olgin JE (2004) Increased vulnerability to atrial fibrillation in transgenic mice with selective atrial fibrosis caused by overexpression of TGF-beta1. *Circ Res* **94**(11):1458-1465.

Wei JY, Spurgeon HA and Lakatta EG (1984) Excitation-contraction in rat myocardium: alterations with adult aging. *Am J Physiol* **246**(6 Pt 2):H784-791.

Willems IE, Havenith MG, De Mey JG and Daemen MJ (1994) The alpha-smooth muscle actin-positive cells in healing human myocardial scars. *Am J Pathol* **145**(4):868-875.

Xia Y, Lee K, Li N, Corbett D, Mendoza L and Frangogiannis NG (2009) Characterization of the inflammatory and fibrotic response in a mouse model of cardiac pressure overload. *Histochem Cell Biol* **131**(4):471-481.

Xia Y, Tsai AL, Berka V and Zweier JL (1998) Superoxide generation from endothelial nitric-oxide synthase. A Ca2+/calmodulin-dependent and tetrahydrobiopterin regulatory process. *J Biol Chem* **273**(40):25804-25808.

Xu SW, Howat SL, Renzoni EA, Holmes A, Pearson JD, Dashwood MR, Bou-Gharios G, Denton CP, du Bois RM, Black CM, Leask A and Abraham DJ (2004) Endothelin-1 induces expression of matrix-associated genes in lung fibroblasts through MEK/ERK. *The Journal of biological chemistry* **279**(22):23098-23103.

Yagi K, Komura S, Sasaguri Y, Yoshino K and Ohishi N (1995) Atherogenic change in the thoracic aorta of the senescence-accelerated mouse. *Atherosclerosis* **118**(2):233-236.

Yamamoto H, Schoonjans K and Auwerx J (2007) Sirtuin functions in health and disease. *Mol Endocrinol* **21**(8):1745-1755.

Yamasaki R, Berri M, Wu Y, Trombitas K, McNabb M, Kellermayer MS, Witt C, Labeit D, Labeit S, Greaser M and Granzier H (2001) Titin-actin interaction in mouse myocardium: passive tension modulation and its regulation by calcium/S100A1. *Biophys J* **81**(4):2297-2313.

Yamasaki R, Wu Y, McNabb M, Greaser M, Labeit S and Granzier H (2002) Protein kinase A phosphorylates titin's cardiac-specific N2B domain and reduces passive tension in rat cardiac myocytes. *Circ Res* **90**(11):1181-1188.

Yan Z, Winawer S and Friedman E (1994) Two different signal transduction pathways can be activated by transforming growth factor beta 1 in epithelial cells. *J Biol Chem* **269**(18):13231-13237.

Yang B, Larson DF, Beischel J, Kelly R, Shi J and Watson RR (2001) Validation of conductance catheter system for quantification of murine pressure-volume loops. *J Invest Surg* **14**(6):341-355.

Ye X, Meeker HC, Kozlowski PB, Wegiel J, Wang KC, Imaki H and Carp RI (2004) Pathological changes in the liver of a senescence accelerated mouse strain (SAMP8): a mouse model for the study of liver diseases. *Histol Histopathol* **19**(4):1141-1151.

Yin FC, Raizes GS, Guarnieri T, Spurgeon HA, Lakatta EG, Fortuin NJ and Weisfeldt ML (1978) Age-associated decrease in ventricular response to haemodynamic stress during beta-adrenergic blockade. *Br Heart J* **40**(12):1349-1355.

Yoo KH, Thornhill BA, Wolstenholme JT and Chevalier RL (1998) Tissue-specific regulation of growth factors and clusterin by angiotensin II. *Am J Hypertens* **11**(6 Pt 1):715-722.

Yu X, Tesiram YA, Towner RA, Abbott A, Patterson E, Huang S, Garrett MW, Chandrasekaran S, Matsuzaki S, Szweda LI, Gordon BE and Kem DC (2007) Early myocardial dysfunction in streptozotocin-induced diabetic mice: a study using in vivo magnetic resonance imaging (MRI). *Cardiovasc Diabetol* **6**:6.

Yusuf S, Pfeffer MA, Swedberg K, Granger CB, Held P, McMurray JJ, Michelson EL, Olofsson B and Ostergren J (2003) Effects of candesartan in patients with chronic heart failure and preserved left-ventricular ejection fraction: the CHARM-Preserved Trial. *Lancet* **362**(9386):777-781.

Zawel L, Dai JL, Buckhaults P, Zhou S, Kinzler KW, Vogelstein B and Kern SE (1998) Human Smad3 and Smad4 are sequence-specific transcription activators. *Mol Cell* **1**(4):611-617.

Zhu BH, Ueno M, Matsushita T, Fujisawa H, Seriu N, Nishikawa T, Nishimura Y and Hosokawa M (2001) Effects of aging and blood pressure on the structure of the thoracic aorta in SAM mice: a model of age-associated degenerative vascular changes. *Exp Gerontol* **36**(1):111-124.

Zile MR, Baicu CF and Bonnema DD (2005) Diastolic heart failure: definitions and terminology. *Prog Cardiovasc Dis* **47**(5):307-313.

Zile MR and Brutsaert DL (2002a) New concepts in diastolic dysfunction and diastolic heart failure: Part I: diagnosis, prognosis, and measurements of diastolic function. *Circulation* **105**(11):1387-1393.

Zile MR and Brutsaert DL (2002b) New concepts in diastolic dysfunction and diastolic heart failure: Part II: causal mechanisms and treatment. *Circulation* **105**(12):1503-1508.